**Université catholique de Louvain**

Institut de la matière condensée et des nanosciences

Faculté d'ingénierie biologique, agronomique et environnementale

# Heterogeneous surfaces with organized collagen layers for the control of cell behavior

*Thèse soutenue en vue de l'obtention du grade de docteur en sciences agronomiques et ingénierie biologique par*

**Emilienne ZUYDERHOFF**

Composition du jury:

Pr. Christine DUPONT-GILLAIN (UCL/IMCN) - *Promoteur*

Pr. Sophie DEMOUSTIER (UCL/IMCN) - *Président*

Pr. Alain JONAS (UCL/IMCN)

Pr. Claude REMACLE (UCL/ISV)

Dr. Karine GLINEL (UCL/IMCN)

Pr. Jacqueline MARCHAND (UCL/IMCN)

Pr. Joëlle AMEDEE (Université Bordeaux Segalen, France)

November 2012

# Remerciements

Tout d’abord, je souhaite remercier mon promoteur, le professeur Christine Dupont pour m’avoir fait confiance en m’accueillant au sein de son équipe de recherche et avoir mis tous les moyens à ma disposition afin que ce travail et sa finalisation puissent se faire dans les meilleures conditions.

Je souhaite également remercier les membres du jury pour avoir pris le temps de lire ce travail et d’avoir apporté de nombreux et précieux commentaires qui ont permis d’améliorer la qualité de celui-ci. Merci à Sophie Demoustier pour la présidence de ce jury, merci aux professeurs Claude Remacle et Alain Jonas d’avoir accepté de faire partie de mon comité d’encadrement, et merci aux professeurs Jacqueline Marchand, Karine Glinel et Joëlle Amedée de m’avoir fait l’honneur de juger ce travail.

Mes remerciements vont également aux membres de l’unité BANI/Cell biology pour m’avoir accueilli dans leurs locaux et pour m’avoir initiée à la culture cellulaire. Je remercie tout particulièrement Pierre Romanus, Valérie Van der Eecken et Julie Goemaere pour le temps qu’ils m’ont consacré, à transmettre leur savoir et à répondre à mes innombrables questions.

Ma reconnaissance s'adresse ensuite à tous les membres de l'unité CIFA/SURF qui ont rendu ces quelques 7 années agréables et enrichissantes, tant sur le plan scientifique que personnel. Merci à Sylvie, Michel, Yasmine, Françoise et Rose-Anne pour les aspects techniques et logistiques, mais aussi pour leur sympathie, leur soutien et leurs encouragements. Merci à Pierre-Alexis et Marie pour le travail réalisé dans le cadre de leur mémoire de fin d'études. Merci aux chercheurs passés, Caroline, Samuel, Sandrine, Cristèle, Ela, Michaël, Claire, Guillaumes, Jessem, Deepak, Kevin, Vincent et Gregory pour le savoir qu’ils m’ont transmis mais aussi pour la bonne ambiance, les discussions et les activités hors-laboratoire. Merci à Caroline pour m’avoir initiée au monde de la recherche lors de mon mémoire. Merci à Claire, Sandrine et Caroline, pour leur amitié, mais aussi pour leur soutien et leurs encouragements tout au long de cette longue thèse.

Il me tient également à cœur de remercier tous les membres de la jeune équipe de recherche de mon promoteur qui n'a pas cessé de grandir depuis mon arrivée, Kévin, Simon, Marie, Pierre, Yang Hi, Jean-François, Sarah, Gilles, Mireya, Deepak, Guillaume et Jessem. Merci pour l'entraide qu'il y a toujours régné, la bonne ambiance et les amitiés qui s'y sont développées au fur et à mesure des années. Je voudrais remercier tout particulièrement Kévin pour son aide précieuse pendant toutes ces années. Merci pour ton soutien lors des moments difficiles tant sur le plan scientifique que personnel « à chaque problème, il y a une solution ».

A côté de la recherche, l'assistanat, fonction passionnante et prenante. Merci à l'ensemble de mes étudiants. Merci au professeur Christine Dupont pour son dynamisme et son implication dans la gestion et l'amélioration, année après année des travaux pratiques. Merci également à Yasmine, perle de l'organisation et de la gestion des étudiants, pour son indispensable aide lors de la préparation des laboratoires. Merci pour ton amitié et pour tout ce que tu m'as appris.

Finalement, Grand merci à ma famille et mes amis pour leur soutien infaillible dans mes projets, quels qu'ils soient … Plus particulièrement, merci à Catherine, Isabelle et Gaëtan pour leurs relectures. Merci à toi, maman, d'avoir toujours cru en moi et d'être toujours là pour moi. Et, je garde bien sûr le plus beau pour la fin : merci à toi, Nicolas, d'être à mes côtés, de me soutenir et de me faire vivre les plaisirs simples de la vie avec Aline et maintenant Théo.

# Foreword

This dissertation is composed of two parts:

- an overview, including a general introduction, a short presentation of the thesis and a general conclusion (Part I);
- a detailed presentation of the thesis (Part II), consisting in 3 chapters in the form of publications or manuscripts which will be published, and 1 appendix, as follows:

**Chapter 1**: An AFM, XPS and wettability study of the surface heterogeneity of PS/PMMA-r-PMAA demixed thin films. E.M. Zuyderhoff, C.M. Dekeyser, P.G. Rouxhet, C.C. Dupont-Gillain. *Journal of colloid and interface science* 319, 63-71, (2008).

**Chapter 2:** Nano-organized collagen layers obtained by adsorption on phase-separated polymer thin films. E.M. Zuyderhoff and C.C. Dupont-Gillain. *Langmuir* 28, 2007-2014 (2012).

**Chapter 3**: Improvement of preosteoblast adhesion through heterogeneous collagen layers prepared on PS/PMMA thin films. E.M. Zuyderhoff, S. Degand and C.C. Dupont-Gillain. *In preparation*

**Appendix**: A rough morphology of the adsorbed fibronectin layer favors adhesion of neuronal cells. C.M. Dekeyser, E.M. Zuyderhoff, R.E. Giuliano, H.J. Federoff, C.C. Dupont-Gillain. P.G. Rouxhet. *Journal of biomedical and materials research part A 87,* 116-128 (2008).

The author also contributed to the paper:

Optimization of cryo-XPS analyses for the study of thin films of a block copolymer (PS-PEO). M.F. Delcroix, E.M. Zuyderhoff, M.J. Genet, C.C. Dupont-Gillain. *Surface and Interface Analysis,* 175-184 (2012)

# Abstract

Engineering surfaces that mimic the highly structured environment of cells in tissue, has become a key issue in biomaterials science. However, the effect of nanostructured materials on cell behavior has not well been understood yet. In this context, the aim of this thesis is to better understand the cell-material interactions through elaboration of heterogeneous surfaces for the control and modulation of collagen organization and evaluation of pre-osteoblast behavior.

Heterogeneous surfaces were prepared using demixing of polystyrene (PS) and poly(methyl methacrylate) (PMMA) from solutions in different solvents and with different polymer ratios. Substrates with PMMA inclusions in a PS matrix and, conversely, substrates with PS inclusions in a PMMA matrix were elaborated.

A range of different collagen organizations was obtained on the designed PS/PMMA films. Inclusions size was revealed as an important parameter in the control of collagen organization. If the PS domains were above 600 nm wide, a heterogeneous distribution of collagen was found, in agreement with observations made on pure polymers (assemblies of a few collagen molecules on PMMA *vs* bigger assemblies on pure PS). Otherwise, fibrils formed in the PS domains, were longer and thinner compared to the ones observed on pure PS.

Pre-osteoblast cultures on bare and collagen-coated PS/PMMA films revealed two main effects: (i) the developed cell area on heterogeneous films is intermediate between the ones observed on each pure polymer, (ii) a higher cell density is always observed on heterogeneous films compared to the corresponding pure polymers.

Bio-interfaces with chemical heterogeneities at the submicrometer scale thus trigger particular collagen organizations and cell behaviors, which open perspectives for biomaterials science and tissue engineering.

# List of abbreviations

| | |
|---|---|
| $\Theta_w$ | Water contact angle |
| AFM | Atomic force microscopy |
| BSA | Bovine serum albumin |
| ECM | Extracellular matrix |
| IEP | Isoelectric point |
| MOPTMS | Methacryloxypropyltrimethoxy silane |
| PBS | Phosphate buffered saline |
| PEO | Poly(ethylene oxide) |
| PMMA | Poly(methyl methacrylate) |
| PMMA-r-PMAA | Poly(methyl methacrylate)- random-poly(methacrylic acid) |
| PPO | Poly(propylene oxide) |
| PS | Polystyrene |
| PS-b-PEO | Poly(styrene)-block-poly(ethylene) |
| $PS_{XPS}$ | PS surface fraction determined by XPS |
| $PS\text{-}b\text{-}PEO_{XPS}$ | PS-b-PEO surface fraction determined by XPS |
| $R_{RMS}$ | Root mean square roughness |
| XPS | X-ray photoelectron spectroscopy |

**List of abbreviations used for the polymer blends:**

| | |
|---|---|
| *PS/PMMA* | |
| 5/95t | polymer film prepared from a 5% PS/95% PMMA (w/w) toluene solution |
| 30/70t | polymer film prepared from a 30% PS/70% PMMA (w/w) toluene solution |
| 30/70d | polymer film prepared from a 30% PS/70% PMMA (w/w) dioxane solution |
| 90/10d | polymer film prepared from a 90% PS/10% PMMA (w/w) dioxane solution |
| *PS/PMMA-r-PMAA* | |
| 20/80rd | polymer film prepared from a 20% PS/80% PMMA-r-PMAA (w/w) dioxane solution |
| 30/70rd | polymer film prepared from a 30% PS/70% PMMA-r-PMAA (w/w) dioxane solution |
| 80/20rd | polymer film prepared from a 80% PS/20% PMMA-r-PMAA (w/w) dioxane solution |
| 90/10rd | polymer film prepared from a 90% PS/10% PMMA-r-PMAA (w/w) dioxane solution |
| *PS-b-PEO/PMMA* | |
| 40b/60d | polymer film prepared from a 40% PS-b-PEO/60% PMMA (w/w) dioxane solution |
| 60b/40d | polymer film prepared from a 60% PS-b-PEO/40% PMMA (w/w) dioxane solution |
| 80b/20d | polymer film prepared from a 80% PS-b-PEO/20% PMMA (w/w) dioxane solution |
| 40b/60t | polymer film prepared from a 40% PS-b-PEO/60% PMMA (w/w) toluene solution |
| 60b/40t | polymer film prepared from a 60% PS-b-PEO/40% PMMA (w/w) toluene solution |
| 70b/30t | polymer film prepared from a 70% PS-b-PEO/30% PMMA (w/w) toluene solution |

# Part I:

# Overview

# Table of contents

# 1. Introduction

## 1.1. Context of the research

Biomaterials are commonly defined as materials designed to be placed in contact with biological systems. Although biomaterials are primarily used for medical applications (prosthesis, contact lenses, pacemakers,…) they are also used to grow cells in culture, in apparatus for handling proteins in the laboratory, in devices to regulate fertility in cattle, in the aquaculture of oysters,…[1]

A key aim for biomaterials researchers is to elicit specific cell responses using spatial cues. Biomaterial surface properties may stimulate cells through physical forces, chemical interactions or through topography. Traditionally, in the case of medical applications, inert materials have been used, the goal being to simply avoid implant rejection. A major problem is that these 'inert' materials can be encapsulated by the body.[2]

At present, there is a considerable focus on developing next-generation materials. These materials will not only be tolerated by the body, but will also give organized tissue repair. This may be achieved through the use of bioactive compounds immobilized on or delivered by the material. An even more advanced idea consists in, engineering tissues and organs *in vitro* that could be further implanted into the patient to overcome the limitation of organ and tissue transplantation (scarcity of donors and a high risk of rejection after grafting). The strategy consists firstly in performing a biopsy and collecting cells that are cultured in vitro and proliferate. Cells are then transferred onto a scaffold together with growth factors to enhance proliferation and reimplanted into the site of damage of the patient to integrate with the natural tissue. (see Figure 1).

Central to improving tissue engineering is the development of materials that will influence mesenchymal stem cell differentiation into a specific cell type rather than capsule-forming fibroblasts when it is implanted. This will imply three considerations: (i) to isolate the appropriate cell source (proliferation and differentiation, cell-to-cell signaling, biomolecule production and formation of extracellular matrix), (ii) to

provide appropriate environmental conditions (medium, growth factors) for tissue maintenance and (iii) to develop the proper substrates or scaffold for cell survival and differentiation.[3, 4]

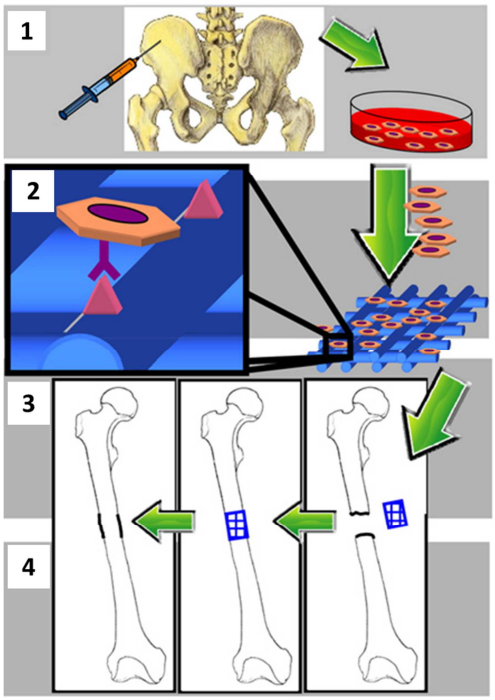


**Figure 1:** The typical tissue engineering approach. (1) Harvest cells from human (or animal) sources and expand them in vitro. (2) Seed cells on scaffolds which may incorporate biomolecules. (3) Implant cells scaffold at injury site. (4) Healing takes place: cells differentiate and form tissue. (adapted from[5])

Finally, the common thread between the diverse biomaterials used is the interaction between biological systems and synthetic (or modified natural) materials. In some cases, biomaterials will need to be modified to enhance migration and attachment of specific cell populations (with a view to repair or replace a damaged tissue), while in other cases, biomaterials will need to be modified to be repellent to cell adhesion and proliferation (contact lenses, blood bags). The control of cell-material interactions then appears to be a critical factor in the development of an appropriate cell response and will be the main focus of the present thesis.

## 1.2. The importance of adhesion proteins in cell behavior

### *1.2.1. Cell adhesion*

For most cell type, adhesion is essential to their survival. Cells in their natural environment are anchored by discrete links to proteins in the extracellular matrix (ECM). The ECM comprises a multitude of different proteins and proteoglycans mixed into an intricate network of macromolecules expressed, secreted, deposited, and processed by, and also fully surrounding, cells within tissues. Similarly, *in vitro*, cell attachment does not take place directly to the naked surface of the material but need to be mediated by ECM proteins recognized by cell receptor. These proteins, which include vitronectin, fibronectin, laminin and collagen, are called adhesion proteins. The substratum can be either coated by these proteins before cell inoculation, or be conditioned by them after inoculation owing to proteins synthesis by the cells themselves or to proteins coming from the serum-supplemented culture medium. The ability of materials to adsorb such proteins in an active form will determine their ability to support cell adhesion and spreading and, hence, is an important aspect of their biocompatibility. For example, it was demonstrated that more cells bind to hydrophilic surfaces than hydrophobic surfaces coated with fibronectin even though more fibronectin is bound to the hydrophobic surface, probably present in a less active form. [6, 7]

After being covered by proteins, the substratum surface is able to support cell adhesion which encompasses two different phenomena. First, an attachment phase will occur rapidly by involving gravitation and sedimentation to up to about 50 nm from the surface whereupon physical and biochemical forces act to close the cell-surface distance gap.[8, 9] Afterwards, cells will attach firmly to the substratum leading to longer term adhesion thanks to various biological molecules: adhesion proteins (as mentioned above), cell membrane proteins and cytoskeleton proteins which will interact together to induce signal transduction and regulation of gene expression.

The ECM adhesion proteins exhibit conserved motifs in their sequences (called adhesion sequences) recognized specifically by cell membrane receptors (called adhesion molecules). The main class of adhesion molecules is the integrin receptor family. The integrin family is composed of heterodimers of two types of sub-units, α and β. So far, 8 β and 18 α different integrin subunits have been found. These integrin subunits associate to form 24 distinct αβ combinations, and each of the resulting integrins has binding characteristics as summarized in Figure 2. Most integrins bind to several types of ECM molecules and conversely, ECM molecules bind to more than one integrin. Integrins can also undergo bidirectional signaling. That is, when ECM binds to the extracellular domain of integrins, it activates intracellular signaling (outside in signaling). Conversely, intracellular signaling can affect the conformation of an integrin, which modulates its affinity to its ligand (inside out signaling).[5]

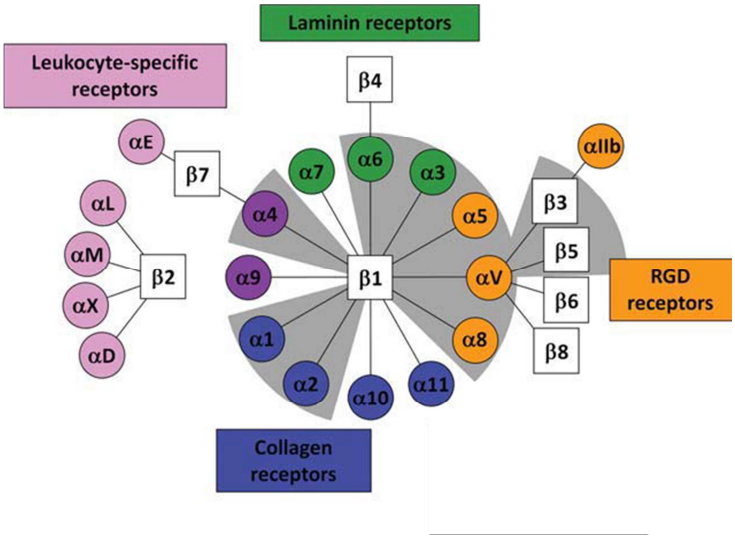


**Figure 2:** Integrin α and β subunits combinations. Biological specificity for adhesion motifs are depicted in colors: collagen receptors in blue, laminin receptors in green, RGD receptors in orange and leukocyte-specific receptors in pink (purple meaning both collagen and leukocyte-specific receptors). (adapted from[10]).

Integrins are approximately 10 nm in diameter[5, 11] and both α and β subunits have large extracellular domains (about 20 nm long)[5] and small cytoplasmic domains. The extracellular domains serve to recognize and bind ECM molecules. Upon ECM molecules binding, integrins can cluster and

their cytoplasmic domains provoke the recruitment of tensin and focal adhesion kinase, their phosphorylation and subsequently the recruitment of talin, vinculin, and α-actinin. Talin, vinculin and α-actinin link the F-actin fibers to the plasma membrane. The rearrangement of F-actin fibers into bundles induces cell shape changes.[8] These clusters of integrins are called adhesion plaque and are often located in the periphery of the cell. In general, they are several square microns in area and can reach 30 µm long on cultured myoblasts.[12, 13]

### *1.2.2. Cell morphology, motility, proliferation and differentiation*

As mentioned above, cell adhesion is the first event in cell behavior and its quality will strongly influence the subsequent responses. By connecting integrin clusters and the nucleus with the actin cytoskeleton, the focal adhesion will induce changes in cell shape which will modify the nuclear matrix and thereby modify gene expression and cell phenotype.[8] Gene and protein expression, as well as phenotypic modulation are also regulated by potent signaling cascades towards the nucleus, set off by transduced signals from outside the cell. These signals are ECM soluble (growth factors, cytokines, hormones) and insoluble (collagen, fibronectin, glycoaminoglycans,…) factors, which are transduced into the cell thanks to cell receptors. They are also mechanical stimuli coming from the local environment. Resulting gene expression regulates normal cell functions such as cell motility, proliferation, cytoskeletal organization, cell survival, and protein production that provides signals to other cells upon release (see Figure 2).[14]

Consequently, the development of appropriate cell morphology, motility, proliferation and differentiation is regulated by a multitude of factors (soluble and insoluble molecules as well as the mechanical environment). In the frame of this thesis, the focus will only be put on the role of adhesion proteins in cell-material adhesion. Cells fate is indeed not only determined by the presence or absence of these adhesion proteins but is also directed by binding to the adhesion sequences and receptor clustering, which are strongly influenced by parameters such as the distribution of

ligands (i.e. the adhesion sequences present on the adhesion proteins) on the substratum, the surface topography and the surface rigidity.

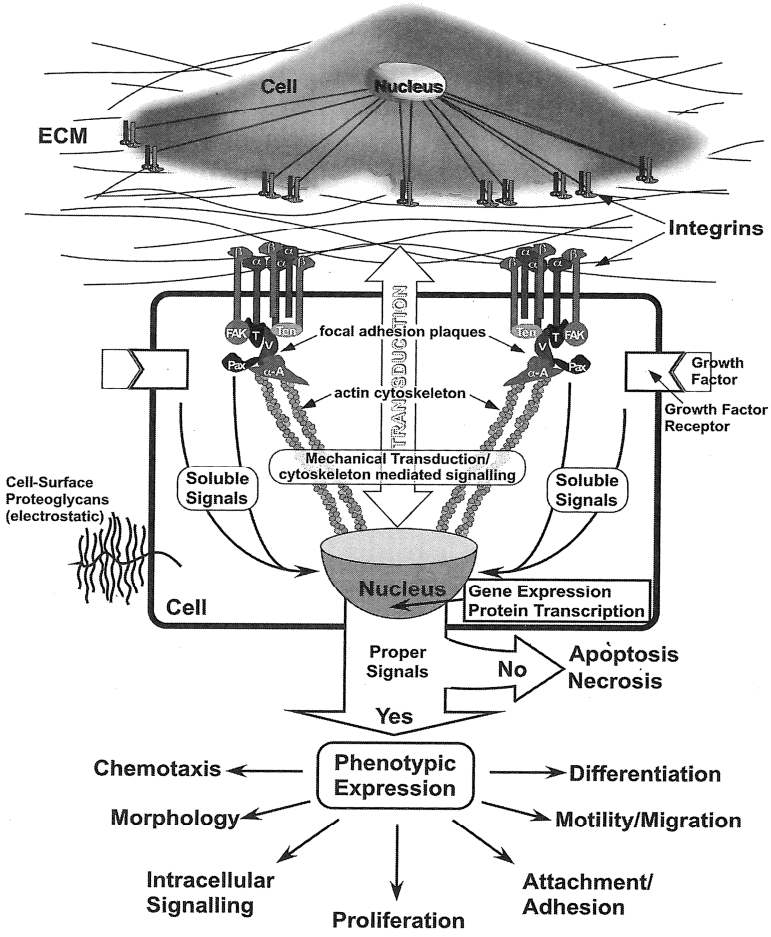


**Figure 3**: Bioactive signals within the extracellular environment and global "outside-in" signaling pathways for a cell interacting with extracellular matrix (ECM). FAK (focal adhesion kinase), T (talin), V (vinculin), Ten (tensin), Pax (paxillin), α-A (α-Actinin).[14]

*Cell response to the distribution of ligands*

The distribution of ligands on substratum and the availability of the appropriate binding sites were seen to be very important in cell adhesion, spreading and subsequent functions.

The optimization of cell function by controlling cell-adhesive ligand spacing was examined and it was suggested that the ligand spacing required for completing cell spreading and focal contacts varied from 10 nm to several hundred of nanometers.[15, 16] Additionally, an increasing number of ligands on substratum was shown to be correlated with increasing cell attachment strength while the average speed of cell migration exhibited a maximal value occurring at an intermediate value of cell-substrate adhesive strength.[17-19] At low ligand densities, cell motility is limited due to the lack of available binding sites, but that at high ligand densities, the surface is too adhesive, so that cell locomotion is severely restricted. In fact, cell migration influences proliferation, and it has been theorized that an optimal ligand density exists for both cell behaviors and ultimately phenotypic expression.[20] Finally, proliferation and differentiation are also dependent on the ability to disengage cell-surface connections, and are thus seen to be dependent on ligand distribution.[21, 22]

In addition to the ligand density, microscale ligand patterning was also shown to be determinant for the control of cell functions. Cell spreading, position and functions can be controlled independently of the amount and density of immobilized integrin ligands by culturing cells on single adhesive islands (surrounded by non-adhesive regions) of different sizes (100 to 200 $\mu m^2$) and shapes (squares, circles, and lines). Islands shape was found to govern cell shapes and whether individual cells grow or die, regardless the type of adhesion protein or integrin used to mediate adhesion.[23, 24] Few studies have also assessed gene expression and differentiation behavior of cells which were confined inside patterns. This gave new insights into the role of cell shape, cytoskeletal tension, and nucleus distortion in cell signaling.[16]

*Cell response to topography*

Altering substratum topography is a noninvasive and nonbiological method to regulate cell function; because textured surfaces serve only as an extracellular physical milieu without involving biomolecules. Topography would act as an “outside in” signal providing biomimetic cell-stimulating cues (like cells *in vivo* contacting textured surfaces of the ECM).[16]

With regards to anisotropic topographies such as ridges and grooves, studies have examined whether cells align along the features main direction, irrespective of micro- or nanoscale (cell contact guidance). Although long-term cell behaviors largely remain unknown, anisotropic topographies induce drastic changes in morphology, cytoskeleton and focal adhesions.[25, 26] Grooved topographies generally induce elongated shapes with cell cytoskeleton directional organization, and the scale of anisotropic cues will determine if cell alignment happens or not. Cell orientation generally increases with increasing groove depth but decreases with increasing groove width or pitch. Additionally, the scale of the cues also determines whether cells bridge between ridges or conform to grooves. With decreasing groove width and increasing grooved depth, cells tend to bridge the ridges without descending into the grooves.[16]

With regards to surfaces uniformly or randomly textured with topographic features (pits, pillars, islands, ribbons…), a control of more general cell functions (such as morphology, proliferation, differentiation,…) would be expected rather than specifically contact guidance expected in the case of anisotropic cues. The topographic scale again determines whether specific cell functions are altered or not. Micro- and nanotextured surfaces can induce positive stimulations in various cell functions. Although the comparison of various isotropic topographies may currently be difficult, because of diversities in topographic size, shape, uniformity, and even chemistry, a tentative trend can be drawn for a limited range of nanotopographic scale such that cell functions are positively stimulated at smaller nanotopographic scale (~10 nm in height or depth) and this effect is less pronounced with increasing nanotopographic scale up to approximately 100 nm.[16]

*Cell response to surface rigidity/mechanical coupling*

In addition to surface architecture, topography, ligand type, density, and accessibility affecting cellular behavior, substrate mechanical properties are now becoming recognized as an important “outside in” parameter as well. In particular, cell focal adhesions associated with integrin cytoplasmic regions act as mechanosensors that convert mechanical forces into

biochemical signaling. Consequently, cells are very tactile, constantly applying forces via mechanically active structures (as cytoskeletal features) by pushing or pulling to actively probe the mechanical properties of their surroundings and respond accordingly via their degree of spreading. It was shown that ligand density and substrate stiffness are significantly coupled variables that together determine average cell behaviors, such as extent of cell spreading, shape and molecular organization. If the substrate is too soft, cells do not respond to increases in adhesion ligand density: pliable or water-swollen, soft substrates (like hydrogels) require substantial ligand densities (~1000 times higher) to elicit similar responses to more rigid substrates. moreover, depending on the elastic properties of the matrix, cells respond by orienting in the direction of the greatest effective stiffness with subsequent strengthening of their adhesion contacts with the cytoskeleton. In essence, cells are guided by elasticity gradients, preferring regions of greater stiffness.[14]

## 1.3. Collagen

One of the major factors affecting cell behavior at material surfaces is thus the distribution of adhesion sequences (ligands) which is strongly dependent on the conformation and supramolecular organization of adhesion proteins. Adhesion proteins are deposited on materials through adsorption which is a spontaneous and often irreversible process that occurs when almost any foreign surface is exposed to a protein solution. Initial adsorption occurs rapidly, effectively preventing direct interactions between cells and the substratum surface. Adsorption may be promoted or opposed by a number of potential enthalpic and entropic changes within the surface-water-protein system which will severely differ in function of the involved protein. In the present work, we decided to focus on type I collagen, an important adhesion protein.

### *1.3.1 Collagen structure*

Collagen molecule are composed of three polypeptide chains (α chains) that fold together to form the characteristic triple helical collagenous domain (see Figure 4). Several types of collagen exist, which contain either

three identical α chains (homotrimers) or a mixture of two or three genetically distinct chains (heterotrimers). The sequence required to form a collagenous domain are Glycine-X-Y repeats in which the X and Y positions are frequently proline and hydroxyproline, respectively. Glycine is required every third residue as it is the only amino acid small enough to pack into the central core of the triple helix. Amino acids with larger side groups cannot fit into the available space in the core of the helix and hence disrupt or prevent folding of the helix during trimer assembly. The hydroxyproline residues stabilise the triple helical domain by hydrogen bonding along the helix.[27]

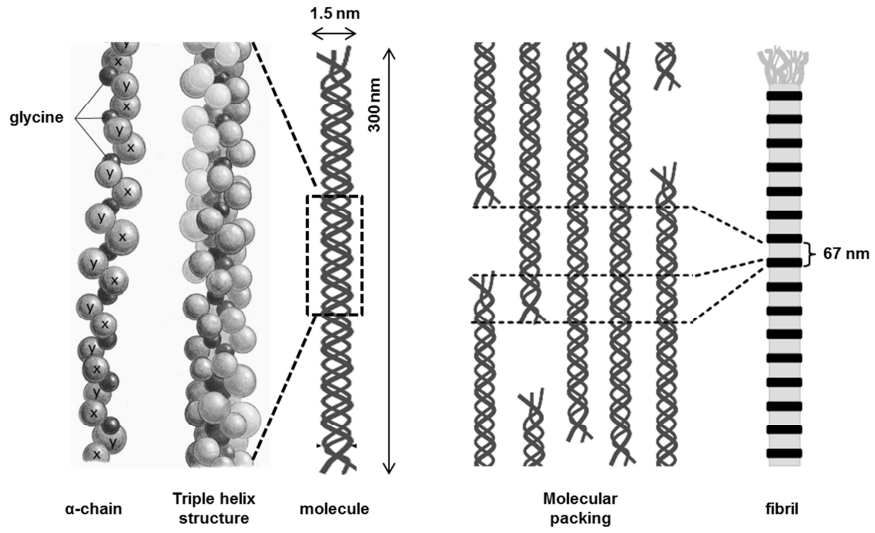


**Figure 4 :** Collagen molecule structure and self-assembly. (adapted from [28, 29])

More than 20 genetically distinct collagens exist in animal tissues. The fibrillar forms comprise collagen types I, II, III, V, XI, XXIV and XXVII.[30] Depending on the tissue, fibrils are arranged with different suprafibrillar architectures and with diameters up to 500 nm. Small-diameter fibrils (~20 nm) are found in cartilage and also in cornea, whereas in the latter the highly ordered arrangement of fibrils within orthogonal lamellae is essential for optical transparency.[31]

Type I collagen is quantitatively the most abundant fibrillar collagen in the body and is the major structural protein of bone and teeth as well as of many other tissues.[27] The collagen type I molecules (the triple chains) are semiflexible rods of approximately 300 nm in length and 1.5 nm in diameter and have the ability to self-assemble. A widely accepted model of collagen axial and lateral molecular packing involves five molecules which fold together. These five molecules packing serves as a basis for the formation of microfibrils which can further grow into larger fibers which show a characteristic band pattern, called D-period. D-periodicity is the result of a 67 nm axial shift between the molecules in parallel array (see Figure 4). The self-assembly/polymerization of collagen molecules into fibers is a thermally driven process implying water-mediated intra- and interbridges between the polypeptide helices[32], hydrophobic interactions between adjacent molecules[33], electrostatic interactions[34], as well as interactions with specific binding sites for fibril formation in different regions of the collagen monomers.[35] Fibrils have been shown to form *in vitro* as well as *in vivo.*[27, 36]

As mentioned before, ***in vivo***, collagen fibrils are assembled into matrices with a variety of organizations and ultrastructures, which range from parallel bundles in tendons and ligaments, to orthogonal lattices in cornea, and interlocking weaves in blood vessels, skin, and bone. Despite the extensive amount of research on the details of collagen self-assembly, the process through which this high order of organization is produced *in vivo* and during development has not been clarified yet. Even if collagen molecules have the ability to self-assemble, *in vivo,* fibrils will not form in the absence of fibronectin, fibronectin-binding and collagen-binding integrins, and collagen type V. Fibrillar collagens have in fact ~50 known binding partners *in vivo.* Consequently, faced with so many potential binding partners, collagen molecules might easily be sequestered into dead-end molecular interactions, which would lower the effective concentration of collagen monomers available to form fibrils by self-assembly/polymerization process. This number of binding partners is presumably required to generate the diversity of fibril patterns. It was then suggested that cells use collagen type V to nucleate collagen fibrils, and fibronectin and integrins to specify their site of assembly. By localizing fibril formation close to the plasma

membrane, the cell maintains tight regulatory control of collagen fibrillogenesis, which is clearly essential for the formation of long-range packing assemblies of collagen fibrils in different tissues.[37]

On the other side, ***in vitro***, purified collagen spontaneously assembles into fibrils because collagen molecules are free to bind to other collagen molecules, and only collagen molecules. However, collagen polymerization in solution may still be influenced by some parameters, namely, the collagen extraction process and the solution properties (pH, ionic strength and temperature). Collagen solutions are extracted from vertebrate tissues and brought into solution without denaturation. ***Collagen extraction*** may be performed in three different ways: (i) dissolution in cold neutral salt solution, (ii) dissolution in low ionic strength acidic solution or (iii) by limited enzyme digestion. The first two techniques lead to collagen solutions with more aggregates than the third one.[38, 39] However, the use of solution extracted with the third technique will lead to less collagen polymerization. The solubilization of collagen by enzyme digestion proceeds with the cleavage of the telopeptides (non-helical end) of collagen monomers which decreases collagen self-assembly. Regarding the ***pH*** dependence of the collagen polymerization, level aggregation tends to increase when the pH approaches the isoelectric point (iep). Around the iep, the surface charge of the collagen monomers is reduced, which would minimize electrostatic repulsion and favor collagen molecule aggregation.[34] However, there is no consensus in the literature regarding the iep value of collagen. This may be partly due to the extraction process which leads to variation in the length of the non-helical domains of the molecule and in the level of aggregation, affecting the $pH_{iep}$. This may also result from the very anisotropic shape of collagen molecules, which affects the electrokinetic measurements. Experimental values of $pH_{iep,}$ of 6.0[40] and 9.3[41] were reported for type I collagen. It was also demonstrated that the ***ionic strength*** and the nature of the salt could influence the $pH_{iep}$ and thereby influence the level of aggregation. The $pH_{iep}$ of collagen was found to be 9.2 in 12 mM NaCl and 7.4 in 12 mM NaCl and 10 mM $Na_2HPO_4$.[34] Collagen fibril formation in solution also depends on ***temperature***. Polymerization is, in fact, known to be initiated by warming. However, temperature of fibril formation can

coincide with temperature of denaturation of monomeric collagen. This is an opposite process consisting in a melting of the triple helix leading to the rupture of hydrogen bonds and to a rearrangement into a random chain configuration.[42] The melting point of collagen as well as his thermal stability increase slightly with increasing pH, and aggregate denaturation occurs at higher temperature compared to monomeric molecules.[43, 44] The melting point of the collagen monomer ranges from 32°C-33°C at pH 2 to 39°C-40°C at pH 7; newly formed fibrils melt at 52°C.[44] It was suggested that the increase in the inherent stability of the collagen helix with pH was partially related to stability conferred to collagen by aggregation.[44]

### *1.3.2 Control of collagen layers organization at solid interfaces*

Owing to its rather rigid structure, collagen is not easily deformable upon adsorption. Then, rearrangement in the protein structure should not greatly contribute to the driving force of adsorption, contrarily to the behavior of most globular proteins. The nearly independence of collagen adsorption with respect to ionic strength and pH leads to the conclusion that ionic and electrostatic interactions do not control collagen adsorption either.[45] The main driving force for collagen adsorption should thus be a gain of entropy due to a change in the hydration state of the sorbent and of the protein surface, involving hydrophobic interactions and van der Waals forces.[36]

Collagen adsorption has been studied for more than 30 years and many factors were then identified as critical in controlling the supramolecular organization of collagen at solid interfaces. Those factors can be classified into three categories: (i) the collagen solution properties, (ii) the adsorption conditions and (iii) the substratum properties.

*Influence of the collagen solution state:*

Collagen solutions contain mainly collagen monomers (triple helix) and some aggregates. The proportion of aggregates depends on extraction conditions and on solution properties (as discussed in the previous section) but also on tissue age and organ from which collagen is extracted. Pure monomer solutions are, indeed, difficult to obtain.[39] The proportion of

aggregates in solution will strongly influence the self-assembling at interface. It was demonstrated that more aggregated solutions behave like less concentrated solutions and lead to a lower adsorbed amount and less fibril formation at the interface. This is explained by a competitive adsorption process between monomers and aggregates of the solution, turning at the advantage of monomers.[46]

Accordingly, collagen solutions are generally stocked in such condition that collagen self-assembly is limited, with the monomeric form mainly (considered as soluble), that is to say in cold and acid solutions. For adsorption experiments, if the purpose is to study collagen self-assembly at solid interface, collagen solutions properties need to favor the aggregation. It has been found that conditions for the formation of native type fibrils are in the pH range of 5.0–8.5, ionic strength between 0.1 and 0.8, and temperatures between 15 and 37 °C.[47, 48]

*Influence of the adsorption procedure*

Besides the conditions and methods used to prepare collagen solutions (discussed deeply in the previous section), the duration of adsorption as well as drying conditions after the adsorption time will greatly influence the obtained collagen organization at interfaces.

The evolution of the adsorbed collagen layer in function of the duration of adsorption was studied in terms of adsorbed amount and organization. At a collagen concentration of 40 µg/mL, the adsorbed amount was seen to increase sharply up to 2 h, after which a plateau was reached. However changes in the organization of the collagen layer are still present between 2 h and 24 h, at almost constant adsorbed amount and imply the formation of fibrils. These reorganizations may be explained either by exchanges between adsorbed collagen and collagen molecules in solution, or by reorganization of adsorbed collagen at interface.[49, 50]

The rate of drying has also a striking effect on the organization of the adsorbed layer obtained at low concentration and short adsorption times. A smooth layer is formed after fast drying while slow drying produced a net-like structure.[49, 51] The formation of such net-like structure is attributed to the rupture of the liquid film by dewetting, collagen being displaced by the

water meniscus.[52] The formation of the net-like structure did not occur when increasing collagen concentration in the solution used for adsorption. The increased intermolecular collagen associations are thought to prevent the displacement of collagen along the surface plane.[53] Note that applying fast drying with a nitrogen flow after collagen adsorption preserves the structures formed under water. Since atomic force microscopy (AFM) images obtained in contact mode in water, in tapping mode in water and in contact mode in air are consistent with each other, the observed structures in air are not artifacts. Nitrogen flow, then, preserves the structures while giving them a sharper contrast, which indicates that the adsorbed layer would be swollen in water.[46]

*Influence of the properties of the substratum*

As it was briefly mentioned at the beginning of this introduction, material properties, such as surface topography and crystallinity, hydrophobicity, roughness, and chemical composition can drastically affect the organization of the adsorbed protein layer and its subsequent biological activity. Many material properties are also shown to influence collagen organization at interfaces.

A number of studies have examined the effect of **substrate surface chemistry** on the adsorption of collagen from solution and have concluded that both the amount of adsorbed collagen and its structure mainly depends on the surface wettability. Elliott *et al.* studied the effect of a range of homogeneous surfaces with different wettabilities on collagen fibril formation, using self-assembled $CH_3$-, COOH-, $NH_2$- and OH-terminated alkylthiolate monolayers. They then compared these results with substratum of varying surface energy by using mixtures of OH- and $CH_3$- terminated thiols. Their results showed that the formation of large fibrils did not occur on the charged and hydrophilic surfaces. This leads to the conclusion that hydrophobicity of the material surface was the significant factor in controlling the supramolecular structure of adsorbed collagen. They also mentioned a water contact angle limit of 63° below which large fibril assembly would not form.[54]

In our laboratory, the organization of collagen on **hydrophobic and hydrophilic surfaces** has been studied thoroughly for many years. The combination of the information brought by AFM in its different operating modes together with the data from radioassays and quartz crystal microbalance lead to a model of the organization of collagen adsorbed layers, as illustrated by Figure 5.

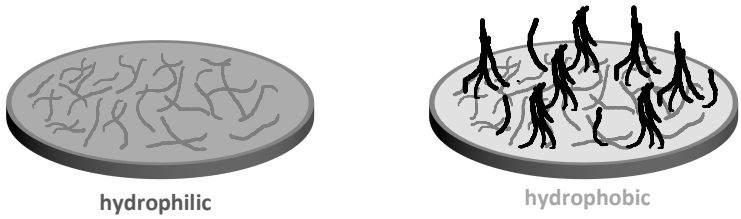


**Figure 5:** Schematic representation of the organization of adsorbed collagen layers on hydrophobic and hydrophilic substrates. (adapted from [55])

On hydrophobic substrates, if the concentration is high enough, collagen molecules are in contact with the substrate only through some segments, leaving part of the molecules dangling in solution. This would explain the higher reversibility of adsorption. Fibrillar structures are thought to be bundles formed by self-assembly of these mobile segments. On hydrophilic substrates or at low concentration, the collagen molecules tend to lie along the surface plane and are intermingled into a felt, which is more compact, less compressible, and more mechanically resistant. The adsorbed molecules may reorganize slowly with time, finally also producing fibrillar structures as a result of the tendency to self-assemble.[55, 56]

Besides the hydrophobicity of the substratum, the collagen layer morphology was seen to clearly depend on the **substratum topography**. Substrates with the same chemical composition, either smooth or nanostructured, were created and collagen was observed on them. The presence of nanometer-scale protrusions hindered the formation of collagen fibrous structures. This effect was attributed to differences in the protein mobility: while the collagen molecules would be relatively free to move and

assemble on smooth surfaces, the nanoscale protrusions of rough substrata would inhibit the collagen mobility.[57]

Finally, the **surface crystalinity** of the substratum was also shown to be determinant for collagen organization. Studies performed on mica have shown that the crystallographic orientation of the mica surface could influence collagen alignment. On muscovite mica, unidirectionally aligned layer of collagen were formed, while on phlogopite mica, collagen assembled into a novel triangular network. The mica lattice was thus seen as leading the growth direction of fibrils during the nucleation step of collagen fibril formation.[58]

## 1.4. Heterogeneous surfaces

In their natural environment, cells are confronted to nanostructured surfaces since extracellular matrix is a highly structured environment. Cells are then highly sensitive to surfaces which are heterogeneous at the nanoscale. Engineering surfaces that closely mimic the complexity and functionality of the ECM has currently become one of the challenging aims in biomaterials science.

### *1.4.1. Case of bone tissue engineering applications*

Bone tissue is a nanocomposite that consists of a protein-based soft hydrogel template (i.e., collagen, non-collagenous proteins (laminin, fibronectin, vitronectin) and water) and hard inorganic components (hydroxyapatite). Bone is then a self-assembled nanostructured ECM that closely surrounds and affects mesenchymal stem cell, osteoblast, osteoclast and fibroblast adhesion, proliferation and differentiation.[59] The design of novel nanomaterials which not only possess excellent mechanical properties but are also biomimetic in terms of their nanostructure, has become a key issue in biomaterials and tissue engineering fields. Therefore, in the case of bone tissue engineering applications, various nanophase ceramics, metals, polymers and composite scaffoldds have been designed by controlling surface properties.

***Ceramics,*** such as hydroxyapatite (HA) (native constituent of bone), are popular bone substitutes due to their ability to promote mineralization. *In vitro* studies demonstrated that nanophase-HA significantly enhanced osteoblast adhesion and osteoclast-like function, and strikingly inhibited competitive fibroblast adhesion compared to conventional grain size HA.[60, 61] ***Nanophase metals*** have been extensively investigated for orthopedic applications due to their higher surface roughness, energy, and presence of more particle boundaries at the surface compared with conventional metals. For example, nanophase titania (Ti), Ti-6Al-4V and CoCrMo alloys significantly enhanced osteoblast adhesion compared to respective conventional metals.[62] ***Synthetic and natural polymers*** (e.g., polyglycolic acid (PGA), poly(lactic-co-glycolic acid) (PLGA), poly(L-lactic acid) (PLLA), polylactic acid (PLA), polycaprolactone (PCL), gelatin, collagen, chitosan) are excellent candidates for bone tissue engineering applications due to their biodegradability and ease of fabrication. Nanoporous or nanofibrous polymer matrices can be fabricated via electrospinning, phase separation, salt leaching, chemical etching and 3-D printing techniques.[63] A large number of studies report the promises of biomimetic 3-D nanostructured polymer scaffolds based on ***nanocomposite polymers***, which encapsulate stem cells and/or osteoblasts. The results demonstrated for example that osteoblast proliferation, alkaline phosphatase activity and mineralization were higher on the highly flexible PCL/HA/gelatin nanocomposite when compared to other PCL nanofibrous scaffolds.[64]

Since materials presenting nanoroughness appeared to improve osteoblast adhesion and differentiation, numerous scaffolds prepared with such roughness and/or porosity resulted in successful clinical outcomes and are eventually expected to enter the commercial market.[65] The positive effect of nanoroughness was suggested to be due to an increase of the surface energy or wettability which would induce a higher adsorption of proteins such as vitronectin (a protein well-known to promote osteoblast adhesion) on nanophase materials compared to conventional materials. This would explain the subsequent enhanced osteoblast adhesion on these materials.[60, 62]

### *1.4.2. Nanopatterning of proteins*

Nanoscale control of ECM-derived peptides and proteins has primarily been used for non-regenerative medicine applications, including biosensing, drug delivery and for model systems in order to study cell functions such as adhesion and spreading. However, since the positive effect of nanoroughness observed for bone applications would be due to a particular protein distribution, and since integrins and focal adhesions are set off by a particular protein distribution on submicron-size scales, there is a compelling rationale for also studying the effect of nanopatterned proteins in bioadhesive tissue engineering applications.

Success in nanopatterning proteins in predefined locations is principally achieved through two approaches (direct or indirect). Proteins were disposed either onto homogeneous surfaces through nanoscale physical contact or selectively onto nanoscale chemical patterns from solution.

In the first case, the nanometer-scale size of the physical contact was controlled by use of scanning probes, direct writing methods using pins or tips, or elastomeric stamps. These approaches can allow immobilization of proteins at the desired positions with high resolution (i.e. tens of nanometers). However, they are less suitable for patterning sensitive biological species, since these methods can induce dehydration which could lead to protein denaturation and loss of biological activity.[66]

In the second case, selective protein deposition was induced by specific or covalent bonds toward domains defined by one surface chemistry and/or by the relative inertness of the other surface chemistry.[66] These approaches have been developed using various lithographic techniques, typically microcontact printing, photolithography and nanoimprint lithography. These lithographic techniques are powerful techniques to obtain regular motifs with highly controlled size. For example, owing to this kind of techniques, the design of anisotropic, flat, surface chemical nanopatterns (alkyl-terminated tracks drawn in an oligo(ethylene glycol)-terminated matrix) was achieved and allowed spontaneous adsorption and accumulation of collagen on the hydrophobic tracks.[67] However these methods are very slow and expensive. Moreover, the elaboration of samples with large surface

area (required for cell culture for example) at the nanoscale, is difficult to achieve. Therefore, more direct and easier approaches were also investigated, such as polymer-assisted patterning, even if less regular motifs with less control in the obtained sizes can be achieved. Block copolymers (giving patterns with nanometer-size scale) or polymer blends (giving patterns in submicron-size scale) phase-separated films are thus now widely used in protein patterning. For example, PS/PMMA blends were studied as templates for albumin patterning. After short adsorption time, albumin was found to adsorb preferentially on PS and at PS/PMMA interfaces.[68]

## 1.5. Aim and research strategy

The general aim of this research is to contribute to the development of model biointerfaces with a view to better understand and control the cell-protein-material interactions. More particularly, our research aims at developing heterogeneous (submicron scale) surfaces for the control and modulation of collagen distribution. This will allow the evaluation of the impact of the obtained surfaces on cell behavior. Adhesion protein organization is one of the major factors influencing cell adhesion. Furthermore, heterogeneity in their distribution could affect the ligand availability and interfere with the formation of focal adhesion. This work is expected to bring novel information that will be interesting for the design of new biomaterials dedicated to tissue engineering applications, resulting in the future in successful clinical outcomes.

A strategy in three steps (as illustrated in Figure 6) was set up to meet this objective:

(i) preparation of the heterogeneous surfaces;

(ii) protein adsorption;

(iii) cell culture.

These three steps are developed here under.

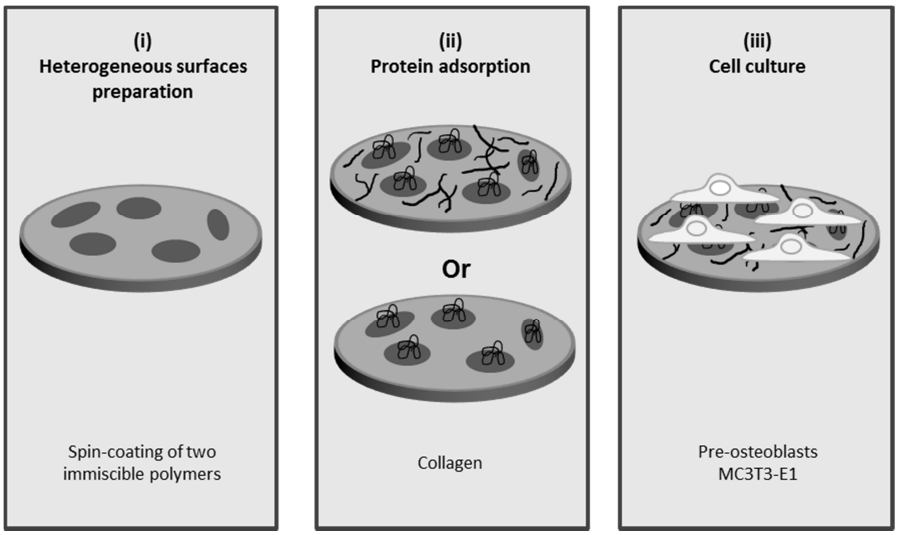


**Figure 6:** Schematic representation of the strategy of the thesis involving three steps.

### *1.5.1. Preparation of the heterogeneous substrates*

Since collagen adsorption and supramolecular organization depends mainly on surface wettability, it was decided to create heterogeneous substrates in term of chemical composition, with surfaces containing hydrophobic inclusions in a more hydrophilic matrix, or conversely. Polymer demixing via spin-coating is a rapid and effective way to generate heterogeneous surfaces. The combination of chemical and/or topographical features of the heterogeneities can be chosen according to the conditions used and consequently, a broad range of different heterogeneities can be easily obtained. Since most polymers are immiscible, the combination of polymers that can be used to generate the heterogeneous surfaces is very broad as well. In this study, the immiscible polymers used for demixing were mainly polystyrene (PS) and poly(methyl methacrylate) (PMMA). These polymers are commonly used in contact with biological systems (bone cement, dental fillings or intraocular lenses in the case of PMMA, and Petri dishes or multi-well plates in the case of PS). Variations in the chemical composition of the heterogeneities were also introduced by the use of two copolymers: a random copolymer derived from PMMA, poly(methyl

methacrylate)-r-poly(methacrylic acid) (PMMA-r-PMAA) and a block copolymer derived from PS, polystyrene-b-poly(ethylene oxide) (PS-b-PEO). These four polymers, whose molecular formulas and properties are presented in Table 1, were used to generate three kinds of blends leading to different heterogeneous substrates:

- blends of PS and PMMA
- blends of PS and PMMA-r-PMAA
- blends of PS-b-PEO and PMMA

**Table 1:** Polymers used to generate the heterogeneous surfaces by spin-coating

| Name | Abbreviation | Molecular formula | Information given by the supplier | Supplier |
|---|---|---|---|---|
| **Polystyrene** | **PS** | 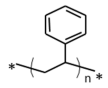 | ***Homopolymer*** $\overline{M}_n$ = 140 000 $\overline{M}_w$ = 230 000 | Merck |
| **poly(methyl methacrylate)** | **PMMA** | 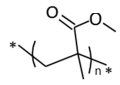 | ***Homopolymer*** $\overline{M}_w$ = 996 000 | Aldrich |
| **polystyrene-b-poly(ethylene oxide)** | **PS-b-PEO** | 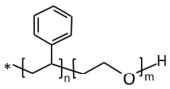 | ***Block copolymer*** PI: 1.06 PS block: $\overline{M}_n$ = 20 000 PEO block: $\overline{M}_n$ = 6500 | Polymer source |
| **poly(methyl methacrylate)-r-poly(methacrylic acid)** | **PMMA-r-PMAA** | 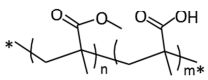 | ***Random copolymer*** $\overline{M}_w$ = ~$10^6$ 80% PMMA 20% PMAA | Polysciences |

$\overline{M}_n$ : Number average molecular weight
$\overline{M}_w$ : Weight average molecular weight
PI: Polydispersity

The morphologies and compositions of the different investigated films were characterized by different surface analysis techniques. X-ray photoelectron spectroscopy (XPS) was used to determine the surface chemical composition. Wettability was evaluated using water contact angle

measurements ($\theta_w$) (in static conditions). Atomic force microscopy (AFM) was performed in contact (height scanning) or tapping (height and phase scanning) modes. Height scanning allows evaluation of surface roughness and film topographies while phase scanning allows evaluation of films mechanical properties which could lead to identifying chemical contrast in certain case.

### *1.5.2. Protein adsorption*

The focus was put on collagen which is the main structural protein found in ECM. As it can assemble into matrices with a variety of heterogeneous organizations and ultrastructures, the control and understanding of its distribution on synthetic material and its subsequent influence on cell behavior appear to be of great interest. However, only a few studies dedicated to the analysis of the impact of heterogeneous distribution of proteins on cell behavior are devoted to collagen, most of the studies on that subject being devoted to fibronectin.

As mentioned in the previous section, we decided to control collagen distribution by using surfaces that are heterogeneous in terms of wettability. Heterogeneous protein distributions can be obtained either by trying to confine proteins in the domains constituted by one of the polymers (matrix or inclusions), or by modulating the supramolecular organization between polymer inclusions and the surrounding polymer matrix. Our purpose, here, was to identify adsorption conditions leading to one of these cases.

In both approaches (illustrated in Figure 7), optimization of adsorption conditions was only investigated under physiological conditions which will be prevalent for cell culture. In the first approach, our strategy for the elaboration of heterogeneous collagen layers was first to determine the concentration leading to a contrast of supramolecular organization between homogeneous surfaces of PS and PMMA. Then, this concentration was used to study collagen organization on heterogeneous surfaces. In the second approach, our strategy for protein confinement within domains of a given polymer involved the use of poly(ethylene oxide) (PEO) for the other domains. PEO strongly binds water and is known to prevent protein adsorption.[69, 70] On the one hand, PEO was introduced in PS/PMMA blends

by interchanging PS by a PS-b-PEO block copolymer. On the other hand, a triblock copolymer of poly(ethylene oxide)-b-poly(propylene oxide)-b-(poly(ethylene oxide) (PEO-b-PPO-b-PEO) (known as Pluronic) was added to the protein solution to be used as a competitor during adsorption. The Pluronic F68 ($PEO_{80}$-b-$PPO_{30}$-b-$PEO_{80}$) from BASF was used. This Pluronic has a weight average molecular weight, $\overline{M}_w$, of 8350 g/mol. Reduction of protein adsorption generated by the use of Pluronic was found to be dependent on the substrate wettability, the reduction being much more pronounced on substrate with higher hydrophobicity.[71] The idea here was then to benefit from the hydrophobicity difference existing between PS and PMMA.

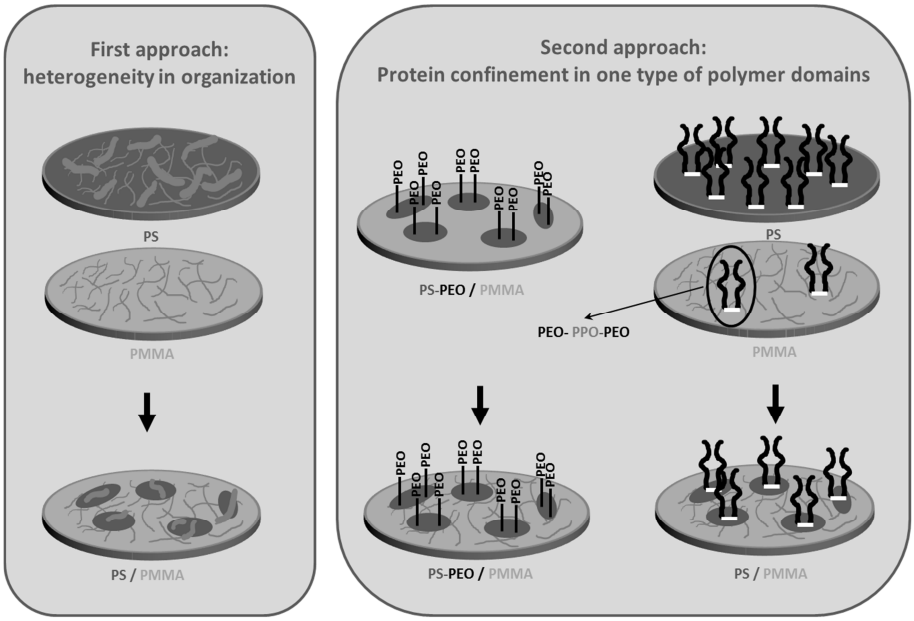


**Figure 7:** Different approaches used for the design of collagen layers showing an ideal heterogeneous distribution.

Protein organization layers were investigated by XPS. This technique was used to determine nitrogen molecular fractions of the protein layers,

related to the detected amount of proteins. Additionally, AFM in tapping height mode was used to investigate the protein organization on the films.

### *1.5.3. Cell culture*

Cell culture experiments were performed with a view to evaluate the impact of the obtained collagen heterogeneous surfaces on cell behaviors. MC3T3-E1 (subclone 14) was chosen for these experiments. It is a robust cell line derived from newborn mouse calvaria osteoblasts and immortalized by Sudo *et al*.[72] Cells of this clonal line are considered as an osteogenic cell line, having the capacity to differentiate into osteoblasts and deposit minerals in vitro.[72] Osteoblast-like cell lines have showed their ability to adhere to fibronectin, collagen types I, IV, and vitronectin through the binding of integrin heterodimers such as $\alpha_1\beta_1$, $\alpha_2\beta_1$, $\alpha_3\beta_1$, $\alpha_5\beta_1$, $\alpha_v\beta_3$, and $\alpha_v\beta_5$.[73-76]

In this thesis, the focus was put on short time experiments (3 h, 24 h and 6 days). General morphologies as well as cell areas developed by the cells were examined by immunofluorescence microscopy. Three fluorescent dyes were used: (i) TRITC-conjugated phalloidin (in order to stain actin cytoskeletons in red), (ii) 4,6 diamidino-2-phenylindole (DAPI) (in order to stain nucleus in blue) and (iii) mouse anti-vinculin monoclonal antibody (in order to stain vinculin, a focal adhesion protein in green). Besides cell morphology, cell activity (thanks to alamar blue test) and cell density (thanks to counting of DAPI stained cells) were also investigated. After that, long term experiments (1, 2, 3 and 4 weeks) were also broached with a view to study cell differentiation on our substrates. However, we were never been able to obtain a differentiate state of our cell line on glass control. Long term experiments were thus not performed on polymer films. Accordingly, results on glass were not presented in this thesis.

# 2. Summary of main results

## 2.1. Elaboration of the heterogeneous surfaces

The heterogeneous surfaces were generated by spin-coating of a pair of immiscible polymers in solution in a common solvent. In most case, polymers in a blend are actually thermodynamically immiscible. Polymers have very small entropies of mixing due to their high molecular weight. Therefore, even a slightly positive enthalpy due to endothermic mixing is sufficient to produce incompatibility. Spin-coating of polymer solutions is used to produce thin homogeneous and smooth films of reproducible thickness. This deposition technique consists in placing drops of polymer solution on the center of an inert substrate, which is then rotated at a fixed speed of several thousand rpm. The solution flows radially outwards, thus reducing the fluid layer thickness and the evaporation of the solvent results in a film of uniform thickness.[77]

In thin films produced by spin-coating, the phase morphology of immiscible blends can consist in distinct phase structure, with one phase dispersed in a matrix of the other, or in a bi-continuous system, with no well-defined dispersed phase. The obtained morphology is governed by the complex interplay between phase separation processes and the interactions of the polymer phases with air (the system will tend to lower its surface energy by enriching its surface with the component of lower surface energy) and substrate (the substrate surface will tend to be cover by the blend component of higher affinity). The relative solubility of each polymer for the solvent used is crucial as well. During the rapid evaporation of the solvent, the less soluble phase will be more quickly depleted of the solvent and will turn solid earlier than the other phase. Subsequent evaporation of remaining solvent will lead to a further collapse of the more soluble phase, which will be thus finally less elevated than the other one.[78]

Three blends were investigated (PS/PMMA, PS-b-PEO/PMMA, PS/PMMA-r-PMAA) and they were dissolved in two different solvents (dioxane and toluene), prior to spin-coating. Before tackling the

investigations of these blends, the following sections will first begin with two technical problems linked to the elaboration of films by spin-coating.

### 2.*1.1. Spin-coating and polymer films adhesion to inert substrate*

In order to prevent any interference of the substrate with the polymer film during the spin-coating process, inert substrates are often desired. Therefore, inorganic substrates such as glass, metals and mineral substrates are generally chosen.

However, the adhesion of organic layers on inorganic substrates may not be very strong and not very stable under liquid conditions. For example, we observed that 50% of the PS films spin-coated on native glass were detached from the substrate after 24h of immersion in a phosphate buffer saline (PBS). After 3 days of immersion, most of the films were detached. Glass is hydrophilic and can attract water at the film/substrate interface which can generate film detachment. This would make cell culture experiments very difficult and limited in time.

Two methods were investigated to solve this problem. Firstly, we tried to improve the adhesion of films on glass by the use of silane coupling agents which can be grafted on glass. They are silicon-based compounds that contain both inorganic and organic reactive function in the same molecule, e.g. $(RO)_3SiCH_2CH_2CH_2$-X (where X is an organofunctional group). Coupling agents act at the interface between inorganic and organic substrates to bind the two dissimilar materials together. The bonding of a coupling agent to an organic polymer is complex. The simplest way to choose an effective silane for a polymer is to match the properties of the organic function with the properties of the organic polymer (an epoxysilane will bond to an epoxy resin and a methacryle silane will bond to an unsaturated polyester resin).[79] In order to help to choose the better coupling agent for one application, manufacturers provide lists of coupling agents compiled on the basis on previous works. In our study, we had to find a coupling agent matching for PS as well as PMMA since blends of these two polymers were prepared. For this application, the use of methacryloxypropyltrimethoxy silane (see Figure 9Figure 8A) as coupling agent was suggested (SIM6487.4, ABCR). Secondly, in order to solve the problem of organic films adhesion

on inorganic substrates, the use of organic substrates was also investigated. Instead of using modified glass as substrate, we decided to use PMMA plates. These were created by compression molding of PMMA powder. As the substrates have to be inert, a PMMA of high molecular mass ($\overline{M_w}$ 996, 000) was chosen to limit PMMA dissolution of these plates during the spin-coating time frame. These two methods are illustrated in Figure 8.

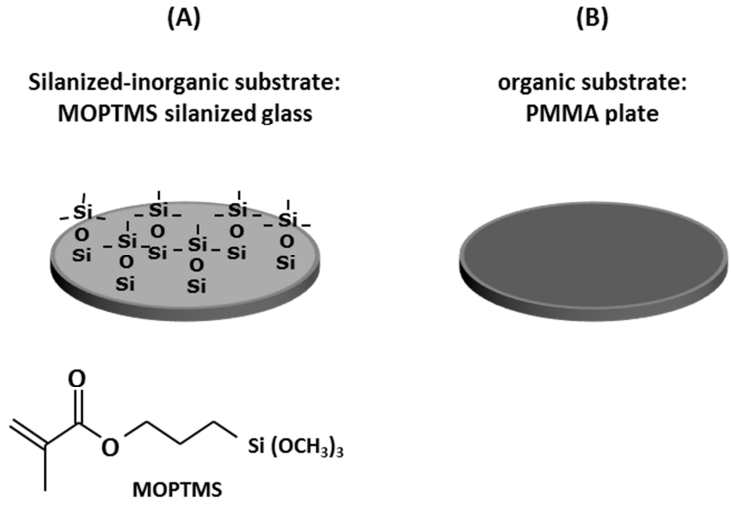


**Figure 8 :** Types of spin-coating substrates investigated in this thesis. (A) inorganic substrate (glass silanized with a methacryloxypropyltrimethoxy silane (MOPTMS)) and (B) organic substrate (PMMA plate)

In order to check the stability of these two substrates, the spin-coating of two PS/PMMA blends (prepared from 30/70 and 90/10 polymer ratios (w/w) and dissolved in dioxane) were investigated. It appeared that adhesion of polymer films on MOPTMS-treated glass and PMMA plates was improved drastically as most films did not detach after 4 weeks of immersion in PBS. Films spin-coated on PMMA plates still appeared to detach less than on MOPTMS-treated glass.

Additionally, the nature of the substrate was shown to influence the morphology of spin-coated polymer blends. Figure 9 presents AFM images of polymer films spin-coated on native glass, MOPTMS-treated glass and on PMMA plates. The use of 30/70 polymer solutions leads to morphologies

showing islands of PS surrounded by a PMMA matrix while 90/10 polymer solutions generate morphologies with inclusions (mostly holes) of PMMA surrounded by a PS matrix. MOPTMS-treated glass substrates lead to less elevated inclusions with a more irregular shape than the others and PMMA plates generate more defaults in the polymer films.

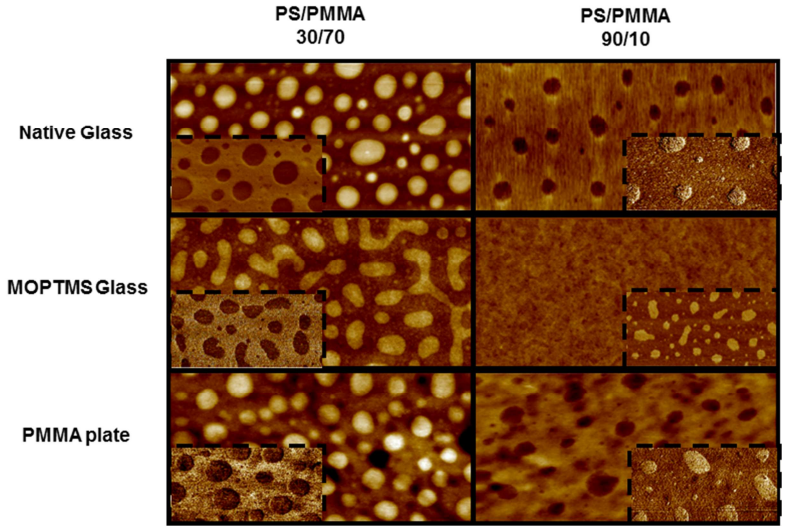


**Figure 9 :** AFM height images (2.5 x 5 µm², z =10 nm; surrounded by solid line) and phase images (1.25 x 2.5 µm², z = 10°; surrounded by hatched line) obtained after spin-coating of 10 g/L PS/PMMA solutions (30/70 and 90/10) in dioxane on three different substrates (native glass, MOPTMS-treated glass and PMMA plates)

The type of substrate also influences the film composition. Table 2 presents the water contact angles and carbon and oxygen molar surface fractions measured by XPS on homogeneous PS and PMMA films spin-coated on the same three substrates (native glass, MOPTMS-treated glass and PMMA plates). Similar results were obtained for the three PMMA films while in the case of PS, films spin-coated on PMMA plates show a higher oxygen molar fraction and a lower water contact angle. This is probably due to the partial dissolution of the substrate upon spin-coating despite the use of high molecular mass PMMA.

**Table 2:** Carbon ($C_{XPS}$) and oxygen ($O_{XPS}$) molar fractions obtained from XPS analyses and water contact angles ($\Theta_w$)of PS and PMMA films spin-coated on three different substrates (native glass, MOPTMS-treated glass and PMMA plates)

| | **PS** | | | **PMMA** | | |
|---|---|---|---|---|---|---|
| | **glass** | **MOPTMS** | **PMMA** | **glass** | **MOPTMS** | **PMMA** |
| **$C_{XPS}$ (%)** | 99.8 | 99.9 | 97.3 | 74.8 | 75.3 | 74.5 |
| **$O_{XPS}$ (%)** | 0.2 | 0.1 | 2.7 | 25.2 | 24.7 | 25.5 |
| **$\Theta_w$[a] (°)** | 92.0 ± 0.4 | 90.2 ± 0.6 | 85.0 ± 2.9 | 73.0 ± 0.5 | 71.8 ± 0.5 | 72.3 ± 0.8 |

[a] Contact angle is given with confident interval at 95% (between 8 and 11 measurements)

In summary, PMMA plates are partially dissolved upon spin-coating and led to polymer films with small defects while MOPTMS-treated glass does not interfere with spin-coating and leads to smoother films. Accordingly, even if adhesion of the film to the substrate is a little bit better on PMMA plates compared to MOPTMS-treated glass, MOPTMS-treated glass was considered as the best substrate to use in liquid conditions. The elaboration of blend polymer films presented in the following sections will not be always performed with MOPTMS-treated glass as this choice was made over the course of the thesis.

### *2.1.2. Spin-coating and reproducibility*

At certain periods of the year, especially during summer, the reproducibility of the spin-coated films morphologies appeared to be limited. This lack of reproducibility appeared to be more important with polymer solutions and with polymer solutions in dioxane containing PS-b-PEO. As an example, Figure 10A presents AFM images showing the poor reproducibility observed for PS-b-PEO/PMMA (60/40 (w/w) ratio in dioxane) films. The ambient humidity during spin-coating seemed to be involved since the problem could be solved by flushing the spin-coating chamber with nitrogen for at least 10 min before spin-coating. However, when ambient humidity raised 60%, this nitrogen flushing step was not sufficient. Above 70%, macroscopic artifacts appeared (see Figure 10B and C). The O-ring which maintains the sample in contact with the spin-coater support seemed to print

his shape on the film. Beyond 90 % of humidity, this latter artifact even appeared on solutions on PS films prepared from a solution in toluene.

Accordingly, whatever the solvent or polymer used, we decided to always perform spin-coating with a nitrogen flushing step and only if ambient humidity was below 50 %. However, since this problem was solved over the course of the thesis, these precautions were only followed for the elaboration of PS/PMMA films. The two other systems were prepared by trying to avoid macroscopic artifacts (films with macroscopic artifacts being always discarded).

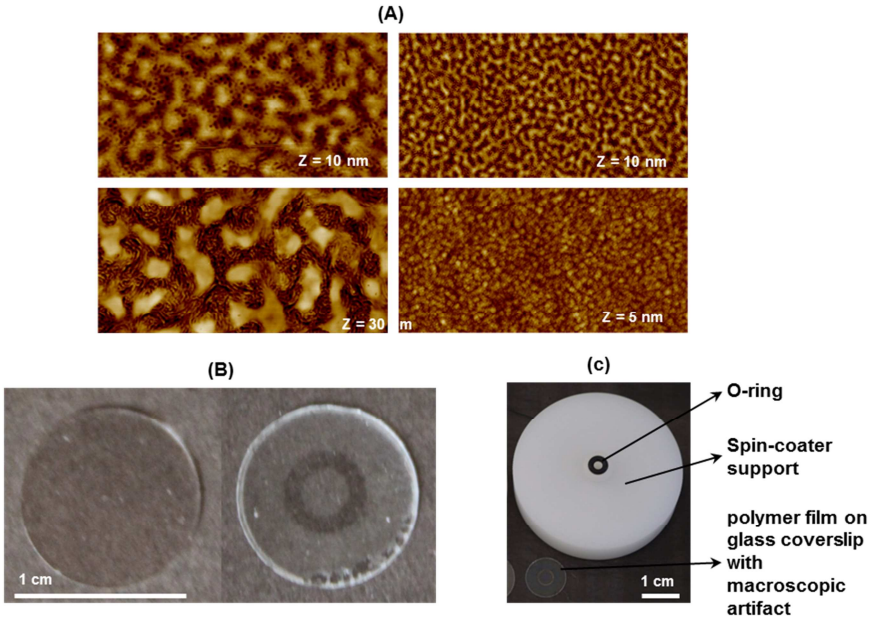


**Figure 10:** (A) AFM height images (2.5 x 5 µm²) of different zones imaged from one PS-b-PEO/PMMA film prepared with a polymer ratio of 60/40 dissolved in dioxane. (B) Glass coverslips (substrate) with spin-coated polymer films, without artifact (left) and with macroscopic artifact (right). (C) polymer film spin-coated on glass substrate showing artifact with a shape similar to the O-ring of the spin coater support.

Besides this problem of reproducibility upon polymer films production, when spin-coated, film morphologies appear to be very stable in time. PS/PMMA and PS/PMMA-r-PMAA films morphologies remain stable at least for one year.

### *2.1.3. Film morphologies and compositions*

*PS/PMMA blends* (details are presented in chapter 2, p119)

Blends of PS and PMMA dissolved in a common solvent (either dioxane or toluene) were prepared with different PS/PMMA polymer ratios: 30/70 (w/w) and 90/10 (w/w) in dioxane, and 30/70 (w/w) and 5/95 (w/w) in toluene (hereafter noted as 30/70d, 90/10d, 30/70t and 5/95t). The total polymer concentration was always 10 g/L. Spin-coating of these blends as well as of pure PMMA and PS solutions was performed onto MOPTMS-treated glass. AFM images of these blends recorded in tapping mode and giving information on topography (height image) and chemical contrast (phase image) are presented in Figure 11. A phase contrast was recorded for each blend indicating that each film displays inclusions of one polymer surrounded by a matrix of the other one. Except for the 90/10d film, which seems to present no topography, these phase contrasts are correlated with a topographic contrast (shown on the height images) revealing holes or islands morphologies which are less than 10 nm in depth or height. Combining this information with the PS fractions detected in surface (see chapter 2 for computing details), we were able to assign each phase to PS or PMMA. Thereby, these films can be classified into two categories: films presenting PS inclusions (being either holes or islands) in a PMMA matrix (5/95t and 30/70d) and films presenting PMMA inclusions (being islands or not correlated with a specific topography) surrounded by a PS matrix (30/70t and 90/10d). The contact angle of the surfaces presenting a PMMA matrix is closer to the one obtained on pure PMMA matrix is closer to the one obtained on pure PMMA, while a $\theta_w$ close to the one of PS is recorded where that polymer forms the matrix.

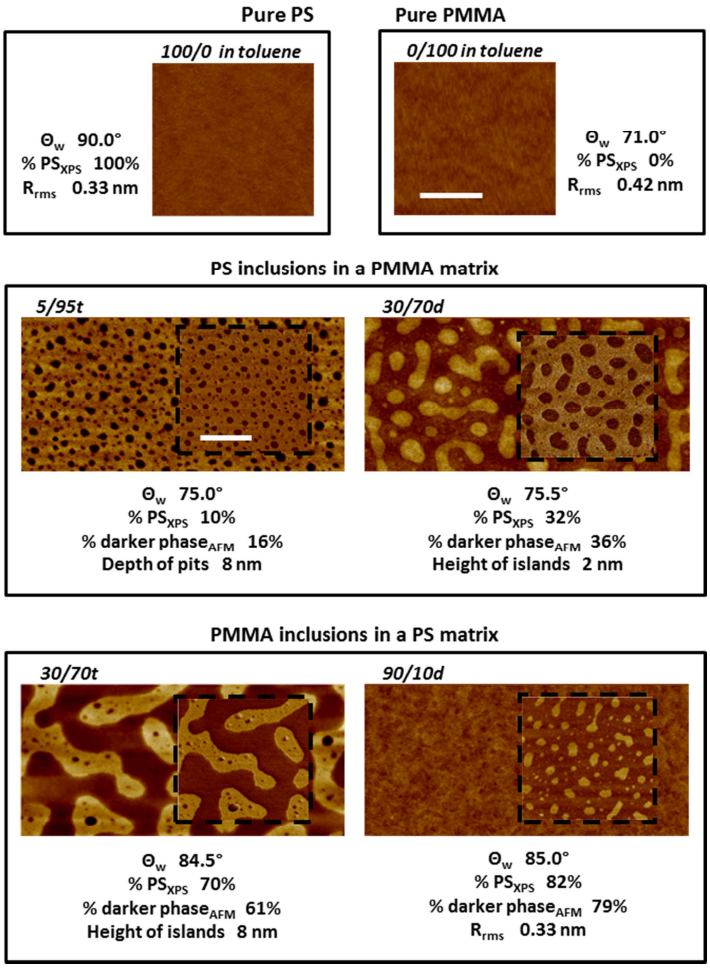


**Figure 11:** Characteristics of films prepared from PS/PMMA solutions. AFM height images (scale bar = 1 µm; z scale = 10 nm) and phase images (scale bar = 1 µm; z=10°; surrounded by hatched line); water contact angle values ($\theta_w$); PS fraction in surface computed from XPS analyses ($PS_{XPS}$) (see chapter 2 for computing details); darker phase surface fraction extracted from AFM phase images; root mean square roughness ($R_{rms}$) and height or depth inclusions extracted from AFM height images.

*PS/PMMA-r-PMAA blends* (details are presented in chapter 1, p99)

Surfaces were also prepared with blends of PS and PMMA-r-PMAA dissolved in dioxane solely, with a total polymer concentration of 10 g/L. The PS/PMMA-r-PMAA polymer ratios investigated in this case were: 20/80 (w/w), 30/70 (w/w), 80/20 (w/w) and 90/10 (w/w) (hereafter noted as 20/80rd, 30/70rd, 80/20rd and 90/10rd). These blends as well as pure

polymer solutions were spin-coated onto PMMA plates. AFM images of these blends, recorded in contact mode, are presented in Figure 12. Pure PS and pure PMMA-r-PMAA films appear to be rather flat with a higher roughness than those observed on pure PS and PMMA spin-coated on silanized glass (Figure 11). This is mainly due to the use of PMMA plates as substrates which was seen to generate films with more defaults (see 2.1.1). In the case of pure PMMA-r-PMAA, however, this is also due to the copolymer itself, which had a roughness of 0.87 nm on films spin-coated on native glass (image not shown). Regarding the blend films, inclusions, either under the form of pits or islands, were observed on all films with a more regular shape and with a higher depth or height (20-40 nm) than those observed on PS/PMMA films (less than 10 nm). Regarding the chemical composition of these films, PS fractions detected in surface were seen to be correlated with the PS fraction in blend solutions: the more the solution contains PS, the higher the PS fraction in surface is. Moreover, surface fractions covered by elevated phases (islands in the case of 20/80rd and 30/70rd, and matrix in the case of 80/20rd and 90/10rd) have been estimated and follow the same trend. Thereby, we were able to assign the elevated phase to PS. This was further confirmed by selective dissolution of PS (see chapter 2). Classification of our films in two categories can also be done: films presenting PS islands in a PMMA-r-PMAA matrix (20/80rd and 30/70rd), and films presenting PMMA-r-PMAA pits in a PS matrix (80/20rd and 90/10rd).

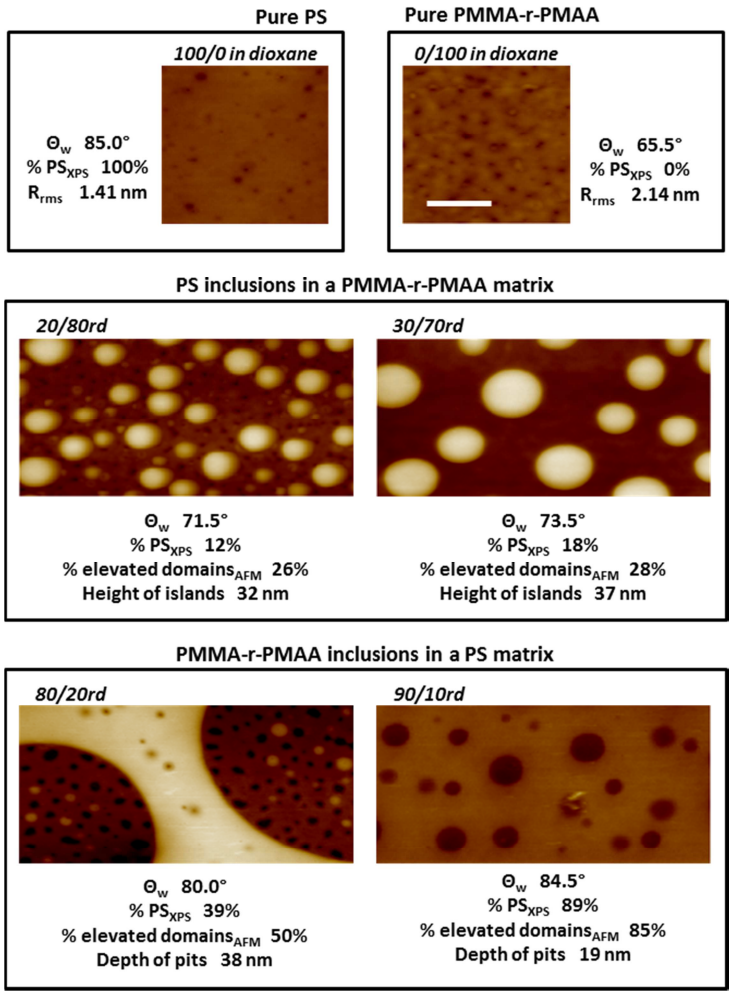


**Figure 12:** Characteristics of films prepared from PS/PMMA-r-PMAA solutions in dioxane. AFM height images (scale bar = 1 µm; z scale = 40 nm) ; water contact angle values ($\theta_w$); PS fraction in surface computed from XPS analyses ($PS_{XPS}$); surface fraction of elevated domains extracted from AFM height images; root mean square roughness ($R_{rms}$) and height or depth of inclusions extracted from AFM height images.

*PS-b-PEO/PMMA blends*

Finally, with the help of Marie Delcroix during her master thesis, we also prepared blends of PS-b-PEO and PMMA dissolved in either dioxane or toluene, still with a total polymer concentration of 10 g/L. The PS-b-

PEO/PMMA polymer ratios investigated in this case were: 80/20 (w/w), 60/40 (w/w) and 40/60 (w/w) in dioxane, and 70/30 (w/w), 60/40 (w/w) and 40/60 (w/w) in toluene (hereafter noted as 80b/20d, 60b/40d, 40b/60d, 70b/30t, 60b/40t and 40b/60t). Spin-coating of these blends as well as of pure PMMA and PS-b-PEO solutions were performed onto native glass. AFM images of these blends recorded in tapping mode (height and phase images are presented in Figure 13). Pure PS-b-PEO films (prepared from dioxane and toluene solutions) show typical microdomains showing a network, attributed to lying down cylinders[80, 81]. These observed cocontinuous morphologies suggest a heterogeneous repartition of the two blocks at the outermost surface. This was confirmed by XPS measurements which showed that both blocks of the copolymer were present in the surface layer.[82] Regarding heterogeneous films, it appeared that blends in dioxane present a phase separation unlike those obtained from blends in toluene. With both solvents, PS-b-PEO and PMMA would be present in surface (as deduced from XPS data, not shown).

Regarding films prepared from solutions in dioxane, a topographic contrast was correlated with the phase contrast. The 80b/20d and 60b/40d films present elevated inclusions surrounded by a matrix showing a network, while the 40b/60d film presents inclusions made of a similar network surrounded by an elevated matrix. This would suggest that the elevated domains would be PMMA while the domains showing the network would be PS-b-PEO. However, if we compare the fraction of the lighter domains (extracted from phase AFM images), presumed to be PMMA domains, with the PS-b-PEO fractions in surface (computed from XPS measurements), it seems that PS-b-PEO fraction in surface is three times higher when computed from AFM than when computed with XPS. Furthermore, water contact angle measurements do not vary much from one blend to another, and remain always close to that of pure PMMA, indicating that all surfaces would be covered by PMMA.

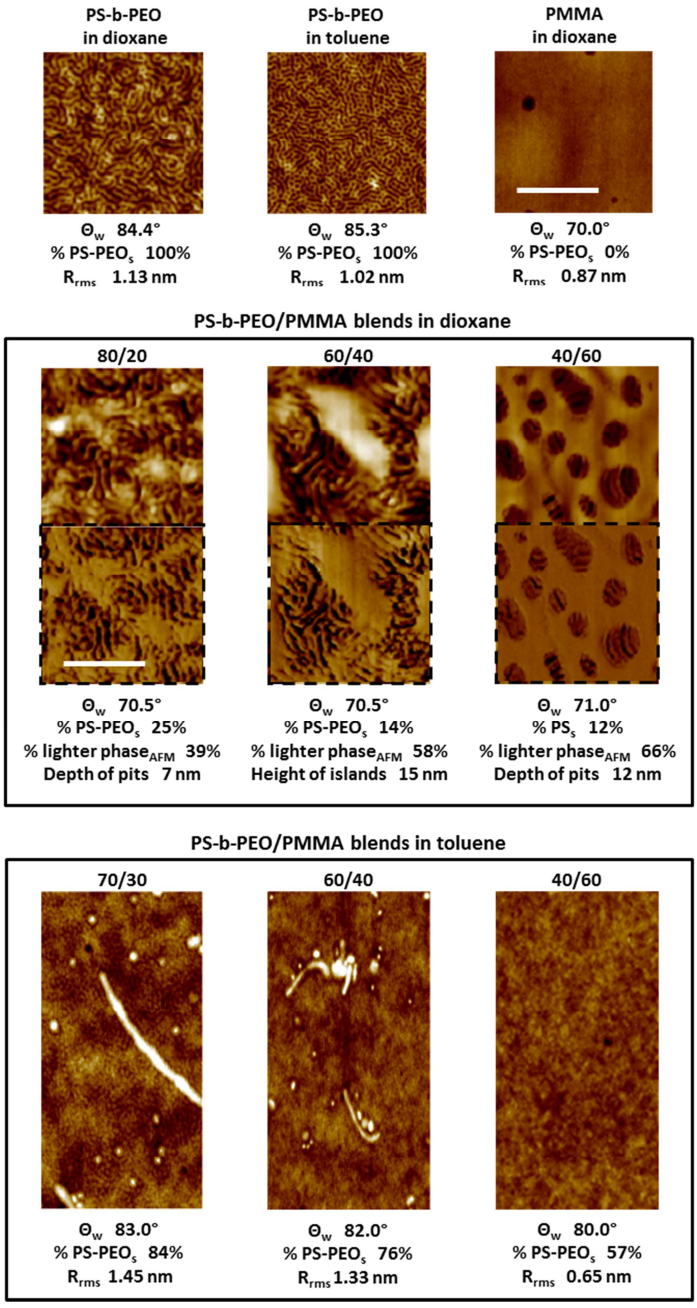


**Figure 13:** Characteristics of films prepared from PS-b-PEO/PMMA solutions. AFM height images (scale bar = 500 nm ; z scale = 10 nm) and AFM phase images (scale bar = 500nm ; z scale =~5°; surrounded by hatched line); water contact angle values ($\theta_w$); PS fraction in surface computed from XPS analyses ($PS_{XPS}$); lighter phase surface fraction extracted from phase AFM images; root mean square roughness ($R_{rms}$) and height or depth inclusions extracted from height AFM images.

These inconsistent results can be combined together by taking into account the layer probed by each technique: contact angle measurements probe the extreme surface (last molecular layer, thickness < 1 nm if water cannot penetrate into the subsurface), AFM probes the surface and subsurface (the distance probed depend on the tapping parameters and can be up to 80 nm with elastomer[83]), while XPS probes a thickness of about 10 nm. Therefore, the morphologies observed on AFM images, attributed to PS-b-PEO, would actually be covered by a PMMA thin layer, as illustrated in Figure 14.

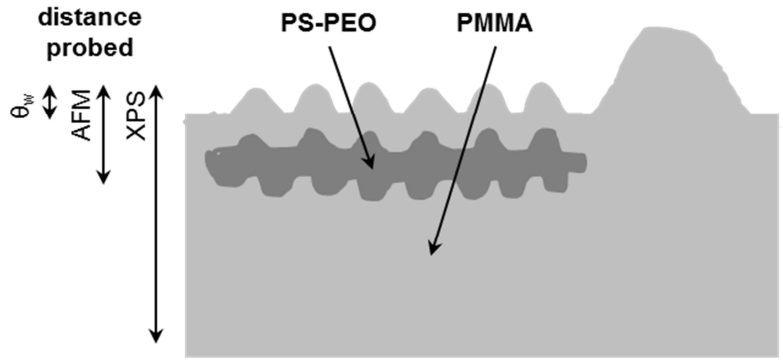


**Figure 14:** Schematic representation of a cross-section through a PS-b-PEO/PMMA thin film prepared from a dioxane solution, along with typical distance probed by each surface analysis technique.

Regarding films prepared from toluene solutions, no specific contrast indicating a possible phase separation was observed (neither on height nor on phase (not shown) images). Contact angle values were intermediate between those of the pure components of the blends, and closer to that of pure PS-b-PEO meaning that the surface would be covered mainly by that component. PS-b-PEO fractions in surface (computed by XPS) show the same trend, suggesting that both components would be present in surface. Now, it is difficult to say if, at the extreme surface, PS-b-PEO covers partially PMMA or if both components are partially blended (as PMMA could be miscible with PEO (negative Flory-huggins parameter, $\chi_{12}$, were

found for PEO/PMMA blends),[84, 85] which was normally limited by the choice of a high molecular mass).

However, one must be aware that XPS works under ultrahigh vacuum condition and AFM analyses are performed in air condition, while protein adsorption or cell culture will be executed under water. Since amphiphilic copolymers materials have the capacity to undergo macromolecular reorientation or changes of conformation in response to environmental modifications, results obtained with these techniques must be carefully related to hydrated structures. For example, it was shown that for a diblock copolymer of polystyrene-poly(acrylic acid) (PS-PAA) with a large PAA block, PS was preferentially exposed to the air or vacuum environment while PAA was preferentially exposed to a pH 11 aqueous solution.[86] In the case of PS-b-PEO copolymers, the control of the humidity condition during spin coating was shown to influence the obtained morphologies (well-defined cylindrical microdomains oriented normal to the surface were induced under high humidity condition).[87] The water-induced surface reorganization of PS-PEO, was also studied by cryogenic X-ray photoelectron spectroscopy (cryo-XPS), and a more pronounced exposure of the PEO block at the outermost surface in hydrated compared to dry environment was revealed.[82]

### *2.1.4. Comparison of the three investigated blends*

*Composition in solution vs at interface*

For most of studied blends, the fraction of PS or PS-b-PEO formed in surface was seen to be correlated positively with the fraction of that component in solution. However, the fraction in surface does not necessary corresponds to the fraction in solution and is sometimes lower or higher. Figure 15 presents the comparison of observed fractions in surface with corresponding fractions in solution. Note that the densities of PS and PS-b-PEO are close to 1 (1.05 for PS).[88]

Except for PS/PMMA blends in dioxane, all the blends deviate from the line of equal composition in surface and solution (dashed line). Blends in toluene (squares) tend to deviate above this line (meaning a surface enrichment of PS or PS-b-PEO) while those in dioxane (diamonds) tend to

deviate below it (meaning a surface enrichment of PMMA or PMMA-r-PMAA). If surface composition was driven by surface energy, which is lower for PS than for PMMA, a surface enrichment in PS (or PS-b-PEO) would be expected.

The spin-coating process does however not generate an equilibrium state, and the surface may be enriched by the component of highest solubility in the solvent. Toluene is, in fact, a better solvent for PS while dioxane is a better solvent for PMMA. PS/PMMA blends in dioxane do not deviate from the equal composition line, probably because of the high molecular mass of PMMA which reduces its solubility in dioxane. Furthermore, this decrease in solubility implies a higher difference of solubility between PS and PMMA in toluene and a lower one in dioxane, explaining why the elevated phase in PS/PMMA blends in toluene are higher than those prepared in dioxane (see chapter 2, supporting information for more details). Unlike PS/PMMA blends in dioxane, PS/PMMA-r-PMAA blends prepared in the same solvent deviate clearly from the equal composition line. This is probably because PMMA-r-PMAA has a higher solubility in dioxane than PMMA, which is also confirmed by the higher elevated phase of those blends (about 40 nm for PS/PMMA-r-PMAA films compared to 2 nm for PS/PMMA films).

In the case of PS-b-PEO/PMMA blends, films prepared from a solution in toluene deviate less than PS/PMMA blends prepared in the same solvent, probably because PEO blocks decrease the solubility of PS-b-PEO in toluene. The evolution of blends elaborated using dioxane are difficult to interpret since PS-b-PEO fractions in surface computed from XPS data do not seem to reflect the situation of the extreme surface, which was found to be covered by a thin PMMA layer (as deduced from contact angle measurements). Note that surface enrichment with PMMA is particularly strong for PS-b-PEO/PMMA films prepared from dioxane solutions, for which a solution containing only 20 % of PMMA leads to a PMMA content of about 75 % in the surface layer probed by XPS.

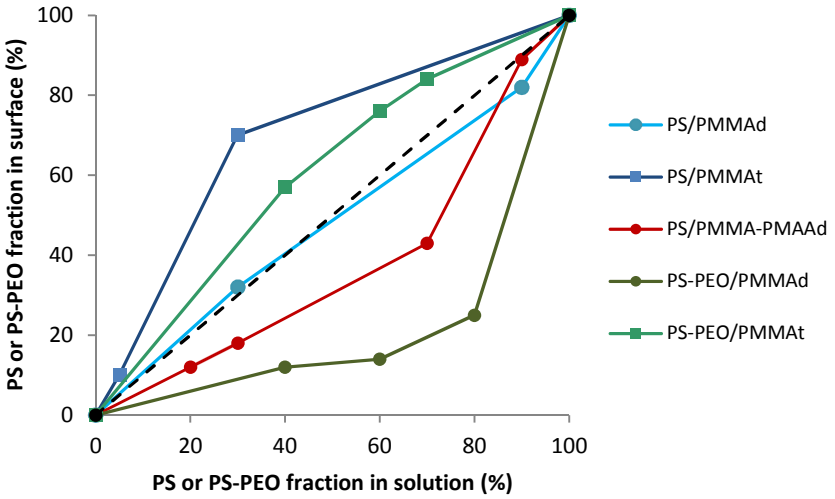


**Figure 15:** Evolution of the PS or PS-b-PEO fraction in surface (computed from XPS data) in function of the PS or PS-b-PEO fraction in solution for all types of blend studied (squares: toluene, circles: dioxane, blue: PS/PMMA blends, green: PS-b-PEO/PMMA blends and red: PS/PMMA-r-PMAA).

*Influence of the film composition on wetting measurements*

Additionally, the influence of film composition on surface wettability was investigated. The water contact angles of all the heterogeneous substrates were observed to be intermediate between the angles measured on the pure components of the blend. For heterogeneous surfaces, the Cassie's law predicts that the cosine of the water contact angle is the average of the cosine of the contact angles of the pure phases weighted by their respective surface fraction.[89] For the three types of investigated blends (PS/PMMA, PS/PMMA-r-PMAA and PS-b-PEO/PMMA), the evolution of the cosine of the water contact angle with the PS or PS-b-PEO fraction in surface is presented in Figure 16 (A, B and C, respectively).

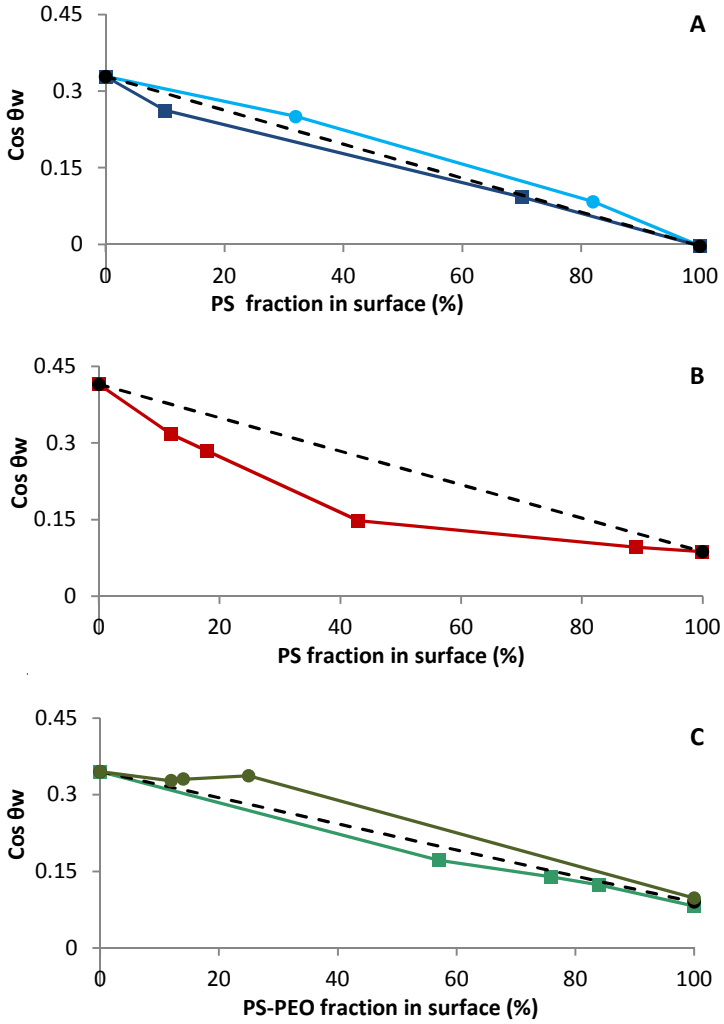


**Figure 16:** Evolution of the water contact angle ($\theta_w$) of thin films in function of the PS or PS-b-PEO fraction in surface evaluated by XPS. (A) PS/PMMA films, (B) PS/PMMA-r-PMAA films and (C) PS-b-PEO/PMMA films. The dashed lines show the trend predicted by Cassie's law.

These evolutions appear to be quite close to the Cassie's law for PS/PMMA (Figure 16A) and PS-b-PEO/PMMA (Figure 16C) blends, while it is clearly not linear for PS/PMMA-r-PMAA (Figure 16B). Contact angle values for that blend appear to be higher, i.e. the surface is more hydrophobic, than expected. Such a deviation can be observed for systems presenting large heterogeneities (> 100 nm). In that case, the evolution of the static contact angle would be mainly governed by the more hydrophobic

phase.[90] However, PS/PMMA and PS/PMMA-r-PMAA blends both present heterogeneities larger than 100 nm, while such deviation is only observed for PS/PMMA-r-PMAA. The surface roughness can also interfere with contact angle values according to Wenzel's law or Cassie-Baxter's law, but none of them can explain the increased hydrophobicity observed here.[89, 91] However, an explanation could still be given by combining the Cassie's law and Wenzel's law. PS/PMMA-r-PMAA films present, in fact, larger inclusions than PS/PMMA films, but more importantly, they display higher elevated phases (about 40 nm *vs* less than 10 nm). Higher elevated phases (being PS in PS/PMMA-r-PMAA films) would imply a higher real surface of the elevated phases than the surface calculated from its projection. However, PS fractions determined by XPS correspond to the surface projection of the elevated phase and would then induce an underestimation of the real PS fraction of the film.

Accordingly, the water contact angle can give indications but precise information on the surface nature are difficult to extract, as most of theoretical laws apply to regular and default-free surfaces, which is rarely the case.

In summary, three polymer blends were investigated, PS/PMMA, PS/PMMA-r-PMAA, PS-b-PEO/PMMA, with a view to create heterogeneous surfaces in terms of chemical composition. Such a chemical contrast at the extreme surface was only successfully obtained with PS/PMMA and PS/PMMA-r-PMAA blends. In the case of PS-b-PEO/PMMA, none of the techniques used to characterize these films, in the chosen conditions, allow us to identify a sufficient chemical contrast. However, these blend films remain interesting for deeper investigations, since promising results were still obtained for films prepared from dioxane solution.

## 2.2. Protein adsorption

Heterogeneous surfaces in terms of wettability were thus successfully elaborated. The focus is now put on protein adsorption (mainly collagen and briefly fibronectin, another adhesion protein), with a view to obtain a

heterogeneous distribution of proteins. Therefore, collagen and fibronectin adsorption onto pure polymers used for the heterogeneous films preparation was first investigated in order to isolate conditions leading to different behaviors depending on the polymer. Collagen and fibronectin adsorption was then performed on heterogeneous surfaces in the conditions identified on the pure polymers.

### *2.2.1. Protein adsorption on pure polymer films*

Collagen adsorption was investigated on the pure polymers to identify adsorption conditions leading either to different protein supramolecular organizations depending on the polymer or to a preferential adsorption (whatever the organization) on one polymer rather than the other. This section will end with a brief comparison of collagen layers organization on the pure polymer films with the organization of layers of another adhesion protein, fibronectin.

*Study of conditions leading to a contrast of collagen organization*

Since PS ($\theta_w$: 90°), PMMA ($\theta_w$: 72°) and PMMA-r-PMAA ($\theta_w$: 66°) show different wettabilities, different adsorbed collagen layer organizations could be expected. Parameters for the adsorption procedure were partially fixed on the basis on previous experiments performed on a hydrophobic/hydrophilic model which was deeply investigated: PS ($\theta_w$: ~90°)[92] and oxidized PS ($\theta_w$: ~20°)[92]. The use of type I collagen in solution at physiological pH and ionic strength and at a temperature of 37°C was chosen, since self-assembly was seen to happen *in vitro* in these conditions. An adsorption time of 2 h was selected, as it was showed that after that time, collagen adsorption reaches a plateau on both hydrophilic and hydrophobic substrates.[49] Even if it was shown that collagen organization can still evolved between 2 h and 24 h of adsorption, a short time was preferred to limit adsorption of aggregates from the solution.

Regarding collagen concentration, since PS and PMMA do not differ (in terms of wettability) as much as PS and oxidized PS, instead of directly selecting the concentration on the basis of these previous experiments, the effect of collagen concentration on its adsorption on PS and PMMA was

investigated. Three different concentrations (8, 25, 100 µg/mL) were then tested with a view to find the concentration leading to the best contrast of organization. Figure 17 presents nitrogen levels detected by XPS on PS and PMMA after collagen adsorption at these 3 concentrations. The value obtained for PMMA-r-PMAA at a collagen concentration of 25 µg/mL is reported as well. The nitrogen level increased with increasing collagen concentration, and for all concentrations a clearly higher nitrogen level was observed for PS compared to PMMA. This could be attributed to the more hydrophobic character of PS. However, collagen adsorption performed on PMMA-r-PMAA led to similar nitrogen level compared to PS, while this polymer has a lower water contact angle than PMMA. This suggests that another parameter than wettability would mainly contribute to adsorption in this case.

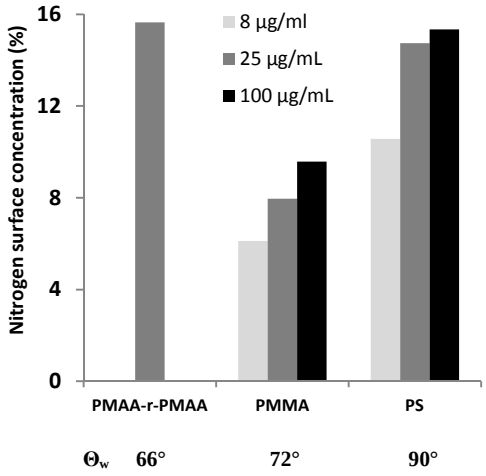


**Figure 17:** Nitrogen surface concentrations determined by XPS after 2 h of collagen adsorption, on PMMA, PMMA-r-PMAA and PS films spin-coated on PMMA plates from dioxane solutions. Adsorption was performed from collagen solutions at different concentrations as indicated. Water contact angle values ($\theta_w$) obtained on bare substrates are reported under the graph.

Figure 18 presents the supramolecular organization of the obtained collagen layers as investigated on AFM height images acquired in tapping mode. The polymer nature as well as the collagen concentration used were seen to generate distinct collagen organizations. On PS and PMMA, smooth

layers were observed at a concentration of 8 µg/mL. When the concentration increased up to 25 µg/mL, small fibrils appeared on PMMA while bigger ones were generated on PS. Finally, when the concentration reached 100 µg/mL, bigger fibrils appeared on PMMA, but in fewer amounts than on PS. Collagen layers on PMMA-r-PMAA appeared to be very different. Whatever the concentration studied, no fibrils were observed. An increase of the roughness with concentration was still detected, which could be attributed to an increase of adsorbed collagen amount. This behavior could not be attributed to electrostatic interactions due to the carboxyl-carboxylate functions conferred by the PMAA segments, as driving forces for collagen adsorption was shown to be poorly influenced by electrostatic interactions (as mentioned before in section 1.3.2). The higher roughness of bare PMMA-r-PMAA films compared to the other polymer films (see 2.1.3.) is probably the reason for the development of the observed organization as it was demonstrated that substrate roughness prevents fibril formation by decreasing protein motility at the interface.[57]

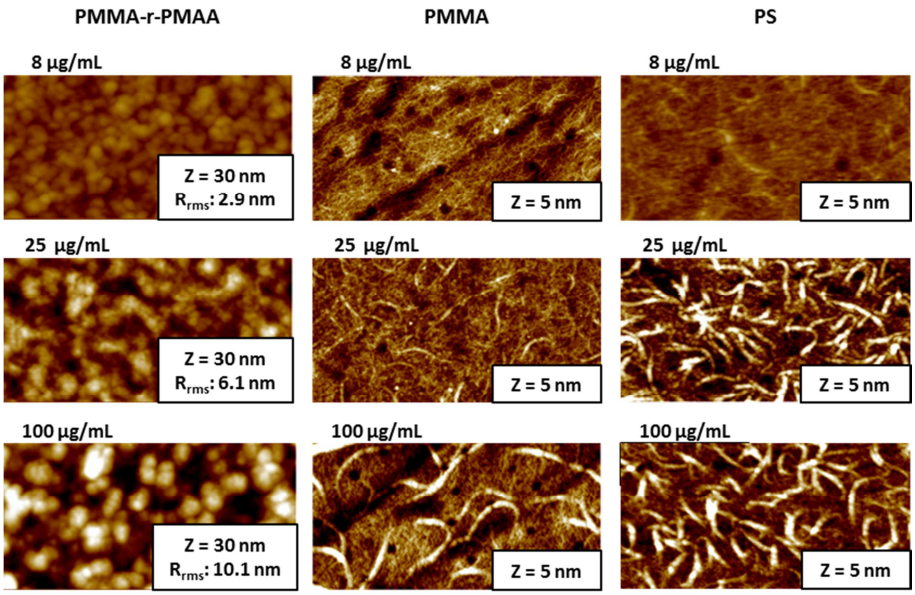


**Figure 18:** AFM height AFM images (2 x 1 µm², z scale indicated on each image) obtained after collagen adsorption on PMMA, PS and PMMA-r-PMAA films spin-coated on PMMA plates from dioxane solutions. For each polymer, three collagen concentrations are investigated: 8, 25 and 100 µg/mL. The root mean square roughness ($R_{rms}$) calculated from AFM images are given for collagen layers obtained on PMMA-r-PMAA films.

Combining XPS and AFM results, it appears that the best contrast in terms of collagen organization is formed between PS and PMMA for a collagen concentration of 25 µg/mL or between PS and PMMA-r-PMAA whatever the concentration used.

The PS and PMMA films used for collagen adsorption for these experiments were prepared onto PMMA plates, which explained the defects observed on the films. Figure 19 shows collagen layers obtained after adsorption for 2 h at a concentration of 25 µg/mL on PS and PMMA films spin-coated on MOPTMS-treated glass. The contrast in terms of collagen organization is similar to the one observed when PMMA plates were used as substrate for spin-coating, with however less defects on polymer films. The collagen layer appears to be quite smooth on PMMA, with collagen assemblies of a few molecules, while on PS, the collagen assemblies are composed of several arms of about 300 nm in length, associated together in an anchoring knot.

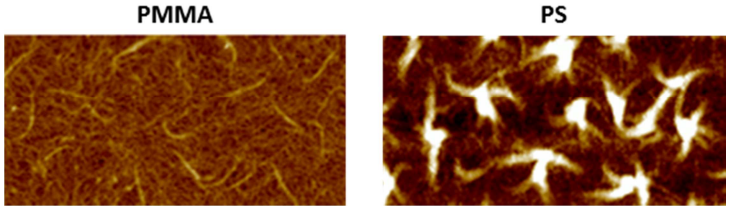


**Figure 19:** AFM height images (2 x 1 µm², z =10 nm) obtained after adsorption of a 25 µg/mL collagen solution on PMMA and PS films. The polymer films were spin-coated from toluene solutions on MOPTMS-treated glass.

*Study of conditions leading to a preferential adsorption on one polymer*

We tried to induce a preferential adsorption of collagen on PS or PMMA, either by interchanging PS by PS-b-PEO in the polymer blend, or by adding Pluronic (PEO-b-PPO-b-PEO) in the collagen solution.

First, collagen adsorption was investigated on PS-b-PEO films prepared from dioxane or toluene solutions. Protein repulsion was expected, owing to the presence of PEO blocks at the interface. Nitrogen levels

extracted from XPS analyses as well as AFM images are presented on Figure 20. Nitrogen levels appeared to be higher on films prepared from dioxane compared to those prepared from toluene, suggesting better antifouling properties for films prepared from a solution in toluene. Additionally, AFM images showed collagen organized into fibrils on films produced from dioxane while a smooth collagen layer seemed to completely cover the films produced from toluene. Even if surface analyses (XPS, $\theta_w$ and AFM) on bare films did not allow to discriminate these films prepared from different solvents, it appears here that their extreme surfaces would be different, leading to different collagen organizations after adsorption. We cannot completely rule out a problem related to reproducibility of sample preparation, as those films were not prepared at the same moment. In summary, contrarily to films produced from dioxane, the use of PS-b-PEO films produced from toluene appears to drastically reduce collagen adsorption without preventing it completely.

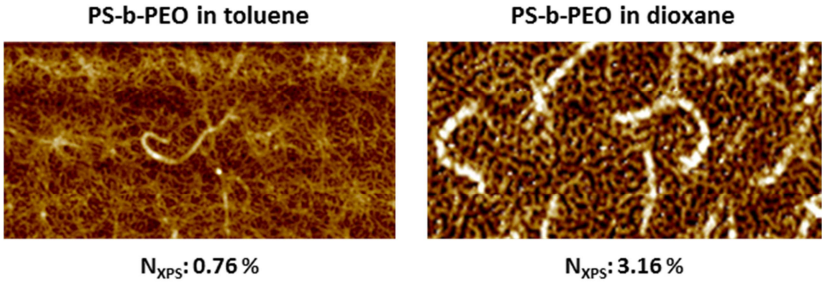


**Figure 20 :** AFM height images (2 x 1 µm², z =10 nm) obtained after adsorption of a 25 µg/mL collagen solution on PS-b-PEO films. The films were obtained by spin-coating from 10g/L dioxane or toluene solutions on MOPTMS-treated glass. The nitrogen molar fraction detected by XPS is reported under the images.

Second, Pluronic was added to the collagen solution before adsorption, in order to induce a competitive adsorption between these two components on PS and PMMA films. Pluronic adsorption was found to be dependent on the substrate wettability, the reduction in protein adsorption being more pronounced on substrates with a higher hydrophobicity. Our aim was to find conditions leading to complete protein repulsion on PS but still allowing adsorption on PMMA.

A large range of Pluronic concentrations (1, 10 and 100 µg/mL) was investigated for three collagen concentrations (8, 25 and 100 µg/mL). Resulting layers were analyzed by XPS. Figure 21 presents nitrogen levels obtained for each combination tested. None of them presents a clear difference of collagen adsorbed amount between PS and PMMA. The more pronounced differences are actually observed in absence of Pluronic. Differences were still observed for collagen concentrations of 100 µg/mL, leading to more collagen on PMMA for Pluronic concentration of 1 µg/mL and more collagen on PS for Pluronic concentrations of 10 and 100 µg/mL. Preferential adsorption on PMMA was thus not always observed. However, these observed differences are probably not significant, and these experiments were only performed one time. The wettability difference existing between PS and PMMA is probably not high enough to induce an interesting contrast of adsorption between these two polymers in presence of Pluronic.

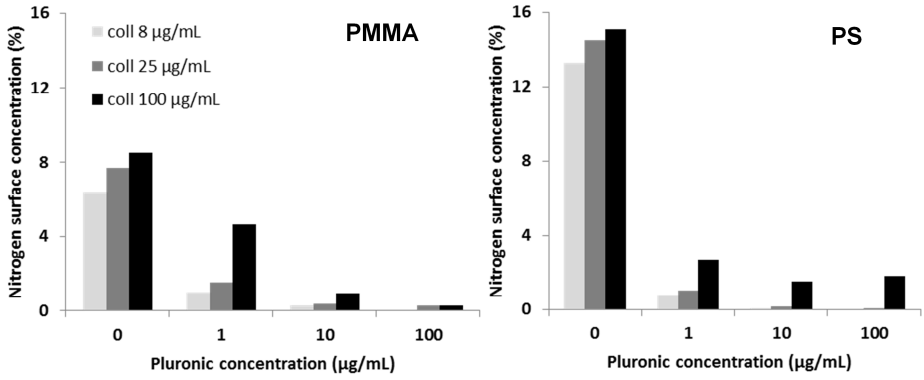


**Figure 21 :** Nitrogen surface concentrations determined by XPS after competitive adsorption of Pluronic and collagen on PS and PMMA. The polymer films were spin-coated on PMMA plates from dioxane solutions. Several concentrations were tested as indicated (Pluronic: 0, 1, 10 and 100 µg/mL; collagen (coll): 8, 25 and 100 µg/mL).

*Protein organization on polymer films: collagen vs fibronectin*

The behavior of another adhesion protein, fibronectin, on the pure polymer films as well as on glass, was also briefly investigated and compared with the one of collagen. Fibronectin is a dimeric protein composed of two nearly identical ~250 kDA subunits, covalently linked by a pair of disulfide bridges near their C-termini.[93] Additionally, unlike collagen, fibronectin cannot self-assemble *in vitro* as its polymerization was shown to be a cell-dependent process.[37]

Figure 22 reports nitrogen levels extracted from XPS data after collagen and fibronectin adsorption (25 µg/mL solutions for 2 h) on pure polymer films and on glass. PS-b-PEO (prepared from a toluene solution) similarly reduces collagen and fibronectin adsorption. For the four other surfaces, in the case of collagen, the nitrogen level appeared to increase with the hydrophobicity (except for PMMA-r-PMAA films as discussed above), while, in the case of fibronectin, nitrogen levels were similar for all the surfaces. These results contradict the trend observed previously in the literature, showing that the amount of adsorbed fibronectin was higher on hydrophobic compared to hydrophilic surfaces.[6, 7, 94]

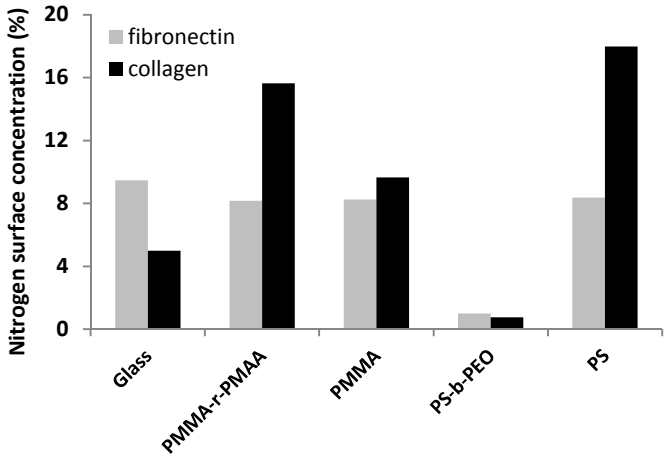


**Figure 22 :** Nitrogen surface concentrations determined by XPS after 2 h of collagen or fibronectin adsorption, on glass, PMMA, PMMA-r-PMAA, PS and PS-b-PEO films spin-coated from dioxane solutions on native or MOPTMS-treated glass.

As XPS is a surface analysis technique probing a depth of about 10 nm, the nitrogen level extracted XPS data is strongly dependent on the protein organization and may not always be directly linked to the exact amount of the protein present on a surface. If the protein layer is thicker than 10 nm or presents aggregates larger than 10 nm, the amount of protein can be underestimated.

The protein organization was also investigated by AFM in tapping mode on the same substrates after collagen and fibronectin adsorption (see Figure 23).

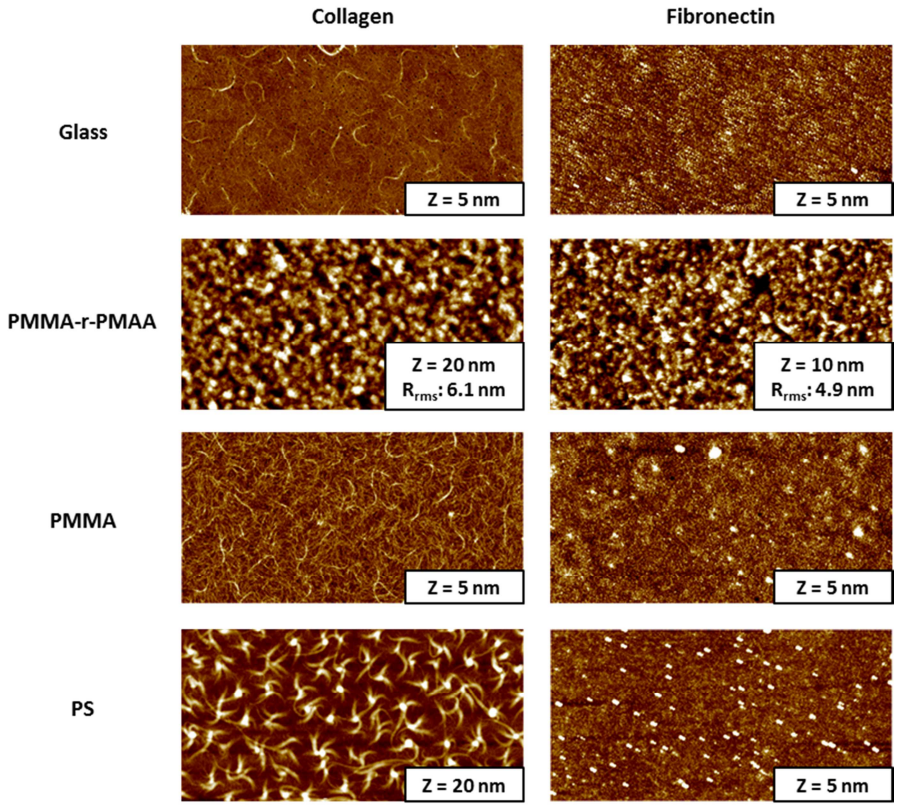


**Figure 23:** AFM height images (5 x 2.5 µm², z scale indicated on each image) obtained after 2 h of collagen or fibronectin adsorption on glass, PMMA, PMMA-r-PMAA and PS films spin-coated on native or MOPTMS-treated glass. The root mean square roughness ($R_{rms}$) calculated from AFM images are given for collagen and fibronectin layers obtained on PMMA-r-PMAA films.

While collagen and fibronectin developed similar rough layers on PMMA-r-PMAA films, both proteins developed extremely different organization on the other substrates. As already discussed here above, collagen organized into fibrils with a number and size increasing in function of the wettability. A few thin fibrils were observed on glass, the density of fibril increased significantly on PMMA and a lot of big fibrils were developed on PS. Regarding fibronectin layers organization, the layer appeared to be quite smooth on glass, with some aggregates on PMMA and with more aggregates on PS. The presence of aggregates could partially explain why nitrogen levels acquired by XPS were similar for all substrates while real amounts are probably not. The AFM images indeed suggest a higher amount on PS.

To conclude this section focused on protein adsorption on homogeneous polymer films, we can say that conditions leading to a contrast of collagen distribution between PS and PMMA (or PMMA-r-PMAA) could be identified. A contrast of collagen organization was indeed obtained for 2 h of adsorption with a collagen solution of 25 µg/mL on these films. A contrast was also highlighted between PS and PMMA-r-PMAA films after fibronectin adsorption. However, fibronectin layers obtained on PS and PMMA did not show as much contrast as collagen layers on these polymers. Additionally, conditions leading to a preferential adsorption of collagen on PMMA could be identified by the use of PS-b-PEO films prepared from toluene solutions which reduce drastically collagen adsorption. However, such a contrast could not be found by the use of Pluronic which did not generate enough contrast.

### *2.2.2. Protein adsorption on heterogeneous films*

Taking into account the investigations performed on homogeneous films, it was decided to study collagen adsorption on heterogeneous PS/PMMA films. Fibronectin adsorption on PS/PMMA-r-PMAA films was also briefly examined. However, even if PS-b-PEO and PMMA prepared from toluene solutions have shown an interesting contrast, collagen adsorption was not investigated on PS-b-PEO/PMMA films since no specific contrast indicating a possible phase separation could be highlighted for the elaboration of these films.

*Collagen adsorption on PS/PMMA films* (details are presented in chapter 2, p119)

PS/PMMA films were elaborated as discussed in section 2.1.3. In that section, we identified four interesting heterogeneous films: films with PMMA inclusions in a PS matrix (30/70t and 90/10d), and conversely, films with PS inclusions in a PMMA matrix (5/95t and 30/70d), the inclusions being either under the form of pits, islands or not correlated with a specific topography. Additionally, we could classify them in function of their PS fraction in surface evaluated by XPS ($PS_{XPS}$): in ascending order, 05/95t < 30/70d < 30/70t < 90/10d.

These four phase-separated films were characterized by AFM in tapping mode after collagen adsorption (see Figure 24). We observe that the higher the $PS_{XPS}$ on the bare film, the more large fibrils developed on the film, which is in good agreement with what was observed on pure polymer films. Large fibrils were indeed observed on PS but not on PMMA. Furthermore, adsorbed collagen organization seems to depend on the polymer forming the matrix (PS or PMMA). On the films presenting a PS matrix, assemblies with morphologies closer to those observed on pure PS and pure PMMA were found in the PS matrix and the PMMA inclusions, respectively (e.g. on the 30/70t film, big fibrils appear to avoid PMMA inclusions). On the other side, longer assemblies than those observed on pure PS, were obtained on films presenting a PMMA matrix. It seems, in fact, that the size of inclusions greatly influences the developed fibril size. On the 30/70d and 5/95t films, the PS inclusions appear to be too small (< 600nm) to allow collagen organization in arms of 300 nm as observed on pure PS. On 90/10d and 30/70t films, the PS matrix present domains larger enough (PS domains > 600 nm) to allow collagen organization similar to those observed on pure PS.

The nitrogen molar fraction was measured by XPS on these heterogeneous collagen layers. To investigate the influence of the $PS_{XPS}$ (determined on bare polymer films) on the obtained collagen layers, $PS_{XPS}$ was platted as a function of the detected nitrogen level measured after collagen adsorption (see Figure 25).

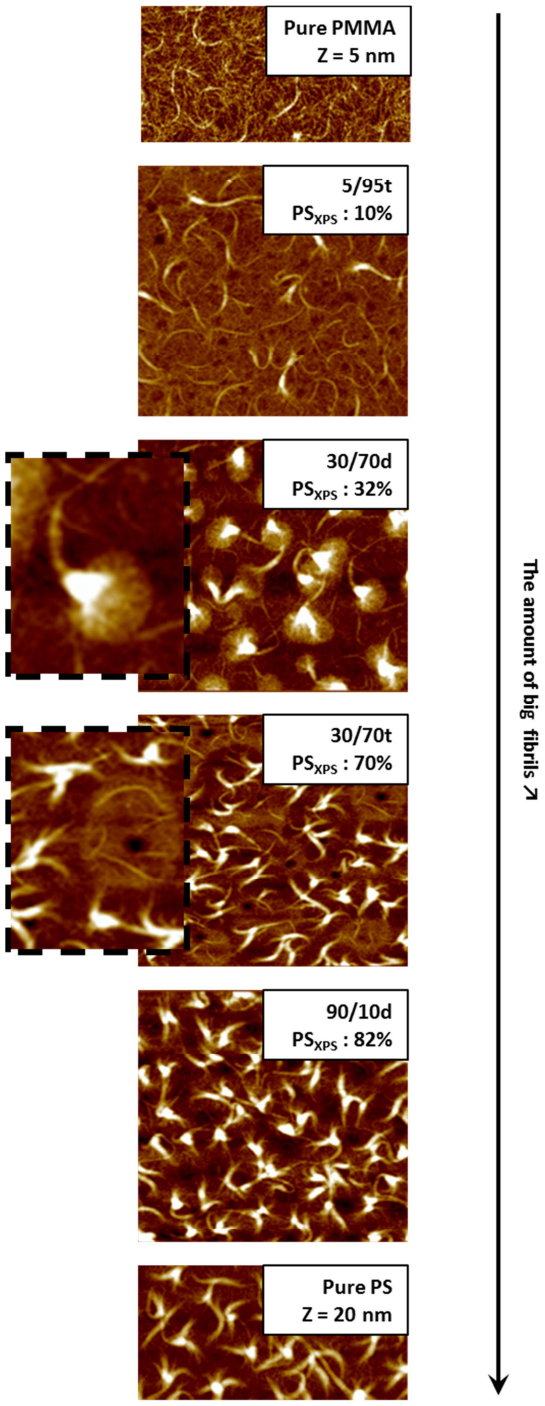


**Figure 24:** AFM height images obtained on heterogeneous PS/PMMA films (2.5 x 2.5 µm²; inserts,3.2 x 4 µm²; z = 30 nm) and on pure PS and PMMA films (2.5 x 1.25 µm²), (spin-coated on MOPTMS-treated glass) after 2 h of collagen adsorption.

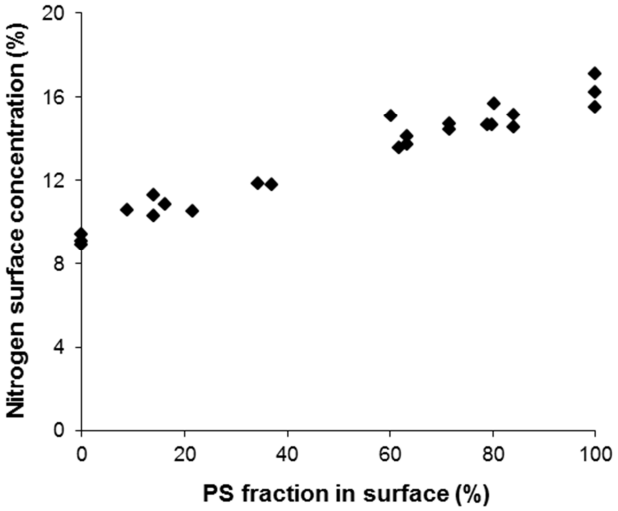


**Figure 25:** Evolution of the nitrogen surface concentration determined by XPS after collagen adsorption as a function of the PS surface fraction determined by XPS on PS/PMMA films before adsorption.

A linear correlation was found between these two parameters, suggesting that the higher the $PS_{XPS}$, the higher the adsorbed collagen amount. This shows that the amount of collagen adsorbed on heterogeneous PS/PMMA surfaces can be described as a combination of that observed on the pure polymers, weighed by their surface fraction.

*Fibronectin adsorption on PS/PMMA-r-PMAA films* (see appendix 1 for details, p173)

Fibronectin adsorption was briefly investigated on 90/10rd and 30/70rd PS/PMMA-r-PMAA films spin-coated on PMMA plates. AFM images of these films before and after adsorption are shown in Figure 26.

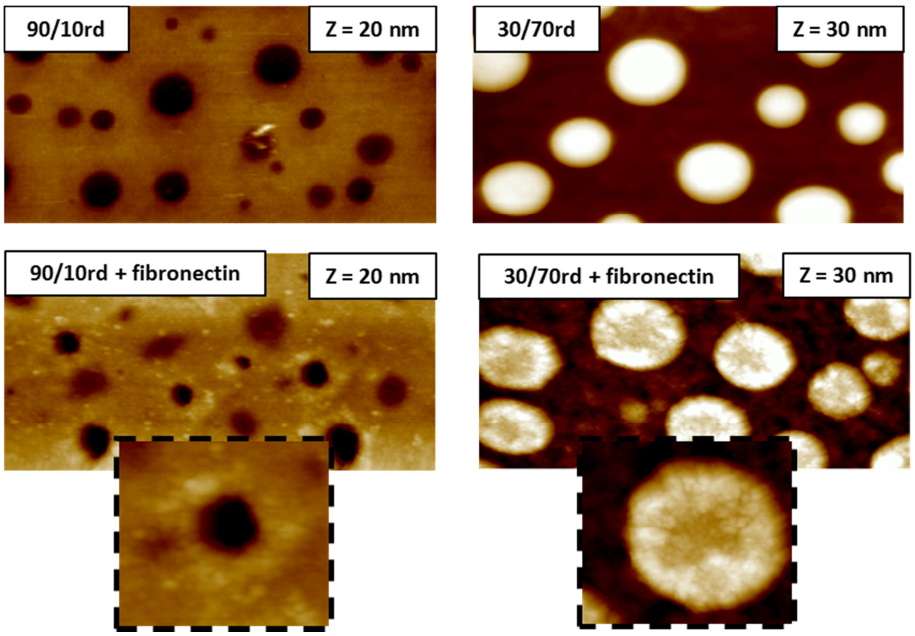


**Figure 26:** AFM height images (5 x 2.5 µm$^2$, z scale is indicated on each image) obtained on PS/PMMA-r-PMAA films (90/10rd and 30/70rd) (spin-coated on PMMA plates), before and after fibronectin adsorption (30 µg/mL for 2 h). (zoom images are 2 x 2µm²)

Whereas the matrix and inclusions (pits or islands) are originally extremely smooth, the surface becomes much rougher after fibronectin adsorption. Two observations can be made: (i) fibronectin seems to accumulate at the edges of inclusions, inducing a decrease in the pits width or an increase in the islands width, and (ii) around the inclusions, in the PS matrix for 90/10rd films and inside the PS inclusions for 30/70rd films, fibronectin forms a much smooth layer. Accordingly, it seems that, as observed on the corresponding homogeneous surfaces (see previous section 2.2.1), fibronectin formed a much smoother layer on PS compared to PMMA-r-PMAA domains. Protein accumulation on inclusion edges was previously observed with albumin on PS/PMMA films. The explanation given for that observation was that the difference in surface energy between PS and PMMA being significant, adsorption at interfaces would allow the binding of more hydrophobic regions of albumin to the PS domains as well as the binding of its more hydrophilic regions to the PMMA domains.[68]

## 2.3. Cell culture (details are presented in chapter 3, p147)

Finally, the focus was put on cell culture experiments, which were performed on the PS/PMMA films with and without collagen coating. The polymer films were first sterilized in ethanol for 30 min, and coated with a sterile collagen solution, before inoculating MC3T3-E1 cells in serum-supplemented medium. Cell culture was first performed on pure PS and PMMA polymer films prior to and after collagen adsorption and finally, heterogeneous films were investigated.

### *2.3.1. Cell culture on pure polymer films*

MC3T3-E1 cells were cultured on pure PS and PMMA polymer films as well as on glass (used as a positive control). The morphology of cells developed on these substrates was examined by immunofluorescent microscopy: nuclei were colored in blue, actin cytoskeleton was stained in red and vinculin was revealed in green. The results are presented in Figure 27. In absence of collagen coating, MC3T3-E1 cells appeared to adhere poorly on polymer films compared to glass. While cells already began to spread on glass after 4 h, cells with poor cell areas adhered on PS and PMMA (note that scale bars are not the same for these three pictures). When collagen was adsorbed on the substrates prior to cell inoculation, the observed morphologies were dramatically different. Cells on glass still developed a well spread rounded morphology, but more pronounced than without collagen coating. On PMMA, cells presented spider-shape morphology, and were less spread than the elongated cells developing on PS. After 24 h of culture on collagen coated-surfaces (see Figure 28), cell morphology continued to evolve on all surfaces. Cells on glass became cuboid, as expected for pre-osteoblasts. The initially elongated cells observed on PS became triangular-shaped, while the spider-shaped cells observed on PMMA became elongated.

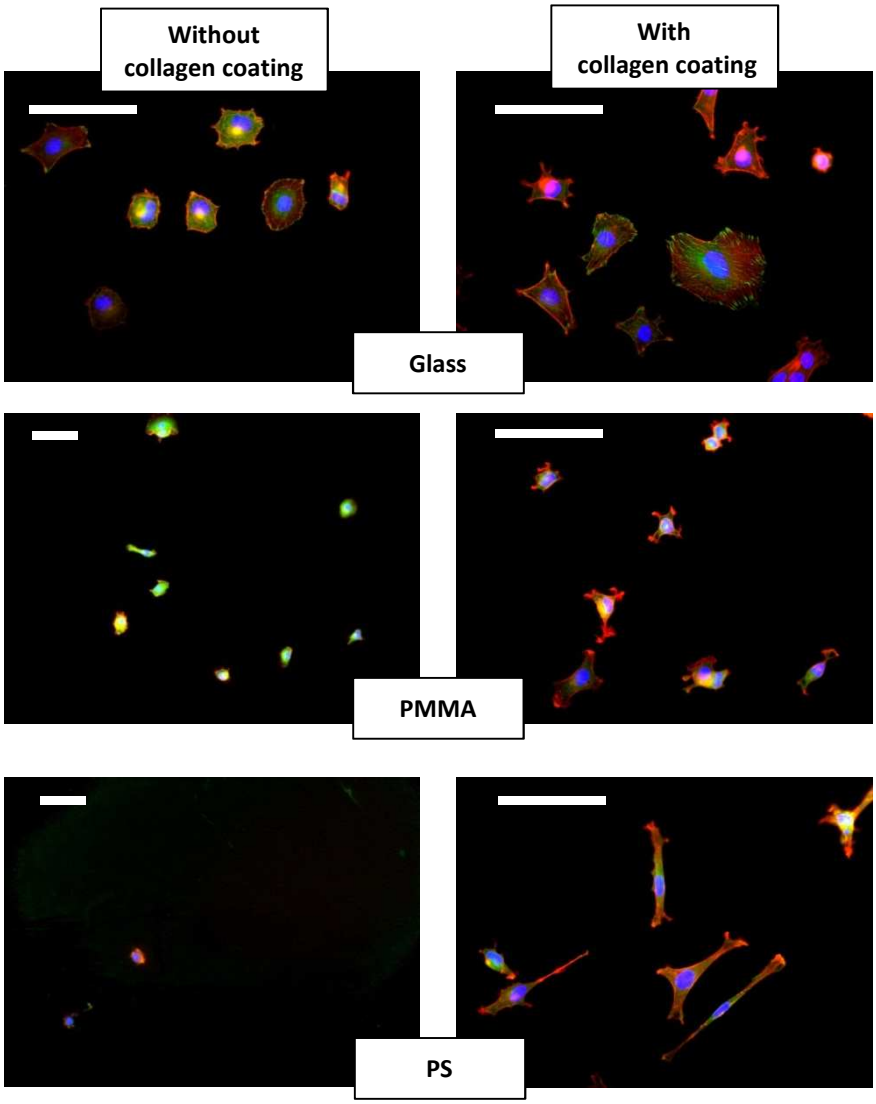


**Figure 27:** Actin (red), vinculin (green) and nucleus (blue) staining for MC3T3-E1 cells cultured for 4 h on glass and pure PMMA and PS polymer films, with and without collagen coating (white scale bar = 100 µm).

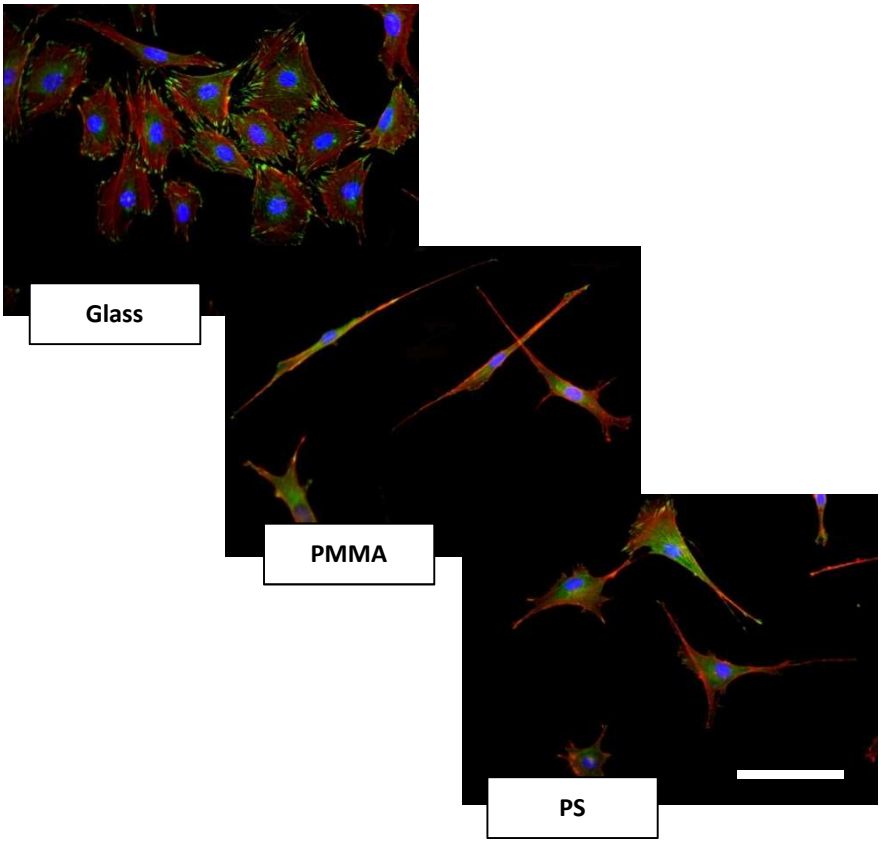


**Figure 28:** Actin (red), vinculin (green) and nucleus (blue) staining for MC3T3-E1 cells cultured for 24 h on glass and pure PMMA and PS polymer films, with collagen coating (white scale bar = 100 µm).

Additionally, the attachment strength of cells on each surface can be examined through the analysis of vinculin (stained in green on pictures) organization in the cell. The number of vinculin aggregates found on pictures reflects the extent of focal points formation. The more cells are attached to the substrate, the more cells present vinculin aggregates. After 4 h, vinculin appeared homogeneously dispersed in cells, except on collagen-coated glass surfaces where several cells already presented vinculin under the form of aggregates. After 24 h of culture on collagen-coated surfaces, cells on glass presented bigger vinculin aggregates than after 4 h. Small aggregates were observed in several cells on PS while vinculin was still homogeneously dispersed on the cells grown on PMMA.

These results show a drastic effect of the nature of substrate and of collagen precoating on cell adhesion. This can be explained by the use of serum-supplemented medium for cell culture. Serum contains a high concentration of albumin, which will cover bare substrates. This could prevent the further adsorption of adhesion proteins present in serum, and thereby, the cell adhesion itself. Actually, it is well known that albumin is more easily displaced by adhesion proteins on hydrophilic compared to hydrophobic substrates.[95-97] When collagen is adsorbed on substrates prior to cell seeding, we know that its organization varies depending on the nature of the substrate (see section 2.2). It is not surprising that this strongly influences the developed cell morphology. On glass, collagen forms a few amounts of small fibrils. This generates strongly attached cuboid cells. A lot of small collagen fibrils are formed on PMMA films. This induces adhesion of a few poorly attached spider-shaped (to elongated-shape) cells. Finally, a lot of large collagen fibrils are formed on PS films. Moderately attached elongated-shape (to stellate-shape) cells develop on such large assemblies.

Collagen organization will certainly influence the exposure of ligands available for cells. In a previous study, it was shown that large fibrils as well as collagen monomers or smaller assemblies induced cell attachment to the substrate by means of the same integrins ($\alpha1\beta1$ and $\alpha2\beta1$).[98] However, the activity of other cell receptors for collagen, including the discoidin receptor, was only detected on fibrillar collagen.[99] Additionally, different protein organizations could generate different mechanical stimuli for the cell. It has been shown that different types of collagen organization (fibrils *vs* monomers) generated layers with different mechanical properties: on PMMA, the collagen layer would be more compact, less compressible, and more mechanically resistant than on PS, where collagen appeared to form a stable but still flexible matrix.[55] Both explanations, or their combination, could potentially explain why cell behaviors strongly varies with collagen organization.

### *2.3.2. Cell culture on heterogeneous polymer films*

Cell culture experiments were then performed on PS/PMMA films. For each PS/PMMA and corresponding homogeneous film, cell densities

and cell areas were determined on the basis of fluorescent microscope images, after 4 h and 6 days of culture.

Figure 29 presents cell densities obtained for the polymer films which were named in function of their $PS_{XPS}$ (0%, 15%, 21%, 64%, 78% and 100%, correspond to PMMA, 5/95t, 30/70d, 30/70t, 90/10d and PS respectively). After 4 h of culture (Figure 29 in blue), cell densities were higher on polymer films with collagen coatings than in absence of such coating. In the case of collagen coated films, the cell density was moreover higher on any heterogeneous PS/PMMA films compared to pure polymer films, while in the case of films without collagen, the highest densities was observed for films with $PS_{XPS}$ of 15% and 21% (5/95t and 30/70d). After 6 days of culture (Figure 29 in red), the measured densities on films with or without collagen coatings were generally similar, and were presenting maximum for films of $PS_{XPS}$ of 15% and 21% (5/95t and 30/70d).

The corresponding developed average cell areas are presented in Figure 30. After 4 h of culture (in blue), cells grown on PMMA presented similar areas on films with and without collagen coatings, while in the case of PS, larger areas were measured on collagen-coated films. On heterogeneous films, intermediate values between the ones formed on pure PS and PMMA were observed. Thus, in the case of collagen-coated films, the higher the PS fraction in surface, the higher the cell spreading, while in the case of films without collagen, cell spreading seemed to be inversely proportional to $PS_{XPS}$. After 6 days (in red), cell areas were generally higher on collagen films. In both cases (coated and non-coated) however, a similar trend was observed, cell spreading being roughly inversely proportional to $PS_{XPS}$. Accordingly, even if after 4 h, collagen-coated PS films appeared to be better in terms of cell spreading, after 6 days, collagen-coated PMMA films appeared to promote cell spreading the best.

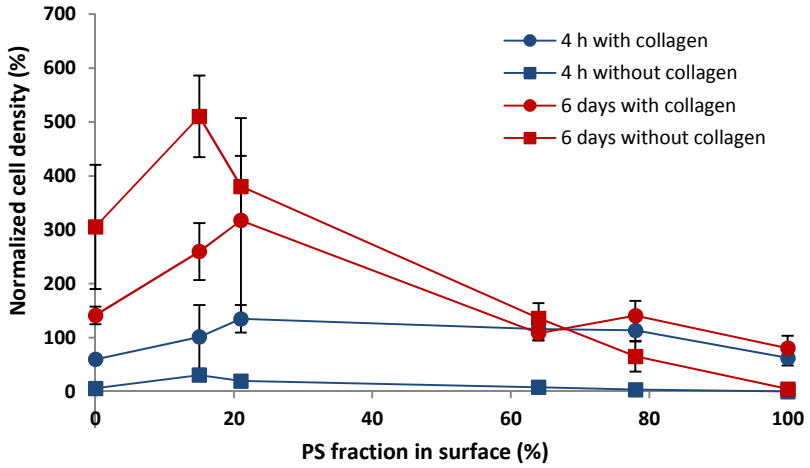


**Figure 29:** Evolution of the cell density after 4 h (blue) and 6 days (red) of culture, in function of the PS fraction in surface ($PS_{XPS}$) determined by XPS on bare PS/PMMA polymer films. Cell density was calculated from the number of DAPI stained nucleus present on the polymer film: circles represent evolution of culture on films with collagen while squares symbolize evolution on films without collagen. Densities are expressed in percentage of the density found on glass with collagen coating after 4 h of culture. Error bars report confidence intervals (95 % level of confidence).

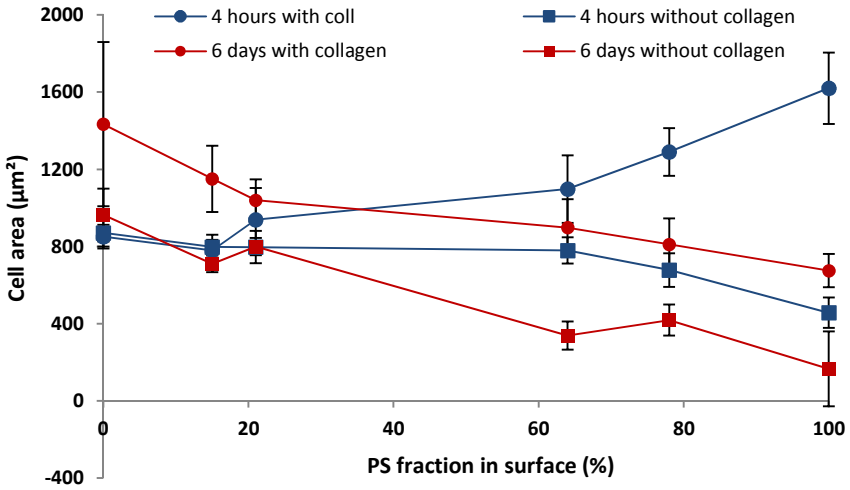


**Figure 30:** Evolution of the cell area in function of the PS fraction in surface ($PS_{XPS}$) determined by XPS on bare PS/PMMA polymer films. The cell area was calculated from images obtained by merging the signal from the 3 dyes (DAPI, Phalloïdin and vinculin). Evolution are presented for culture of 4 h (in blue) or of 6 days (in red). Culture were performed on films with (circles) or without (square) collagen. Error bars report confidence intervals.

To summarize, cell areas and densities observed after 4 h differed significantly from those observed after 6 days. It was surprising to observe that, after 4 h, films coated with collagen seemed be to better than those without, while after 6 days, the opposite was observed. Furthermore, it appeared that cell areas were always higher on collagen-coated homogeneous films (on PS after 4 h and on PMMA after 6 days), while the highest cell density was always obtained on heterogeneous films (any PS/PMMA films with collagen after 4 h and films with $PS_{XPS}$ of 15% and 21% without collagen after 6 days).

As discussed in point 2.3.1, the difference observed between PS and PMMA could be explained by the different supramolecular organization and mechanical properties of collagen layers of these films. Cell areas observed on PS after 4 h are maybe higher than on PMMA, but the morphology observed was however far from that observed on glass positive control. The cells on PS were more stellate than on glass, which indicates a higher motility. This may be a sign of good adhesion but of low proliferation.[100, 101] The fibrillated and flexible collagen layer developed on PS would induce high adhesion of stellate-shaped cells, which could have a low proliferation rate. This would finally lead to a low cell density and to poorly spread cells, as observed after 6 days.

It was also interesting to note that MC3T3-E1cells behavior on our films was not only a question of $PS_{XPS}$, since the density was found to be higher on heterogeneous films compared to the corresponding pure polymers, suggesting that heterogeneity would be an important parameter for the control of cell density. Heterogeneity arises from the chemical composition and topography of the film as well as from the collagen layer organization. The trend observed on films without collagen coatings (maximum at $PS_{XPS}$ 15 % and 21 %) must be directed by heterogeneity of polymer film itself. However, in the case of films with collagen coatings, the trend is not similar after 4 h and after 6 days of culture. The trend observed after 4 h would be directed by the organization of the collagen layer. Accordingly, after 4 h, a heterogeneous collagen layers (whatever the amount of small or large fibrils) could induce an increase of cell density. On the other hand, the trend observed after 6 days, being similar to those

observed on films without collagen coating, would suggest that collagen layers would not be stable after 6 days in culture medium and would reorganize in a layer close to that observed on films without collagen. Cells are continuously synthesizing and excreting proteins and other ECM constituents which can clearly modify the protein layer present on the surface at the very beginning of the cell culture.

# 3. Conclusions

## 3.1. Main achievements

### *3.1.1. Elaboration of heterogeneous films*

The preparation of heterogeneous surfaces in terms of chemical composition was achieved by polymer demixing of immiscible polymers, using spin-coating. Even if three polymer blends were investigated (PS/PMMA, PS/PMMA-r-PMAA, PS-b-PEO/PMMA), such a chemical contrast at the extreme surface was only successfully obtained with PS/PMMA and PS/PMMA-r-PMAA blends. In the case of PS-b-PEO/PMMA, none of the conditions used led to a sufficiently interesting contrast.

**Regarding PS/PMMA blends,** four interesting heterogeneous films were identified: films with PMMA inclusions in a PS matrix (30/70t and 90/10d), and conversely, films with PS inclusions in a PMMA matrix (5/95t and 30/70d), the inclusions being either under the form of pits, islands or not correlated with a specific topography.

**Regarding PS/PMMA-r-PMAA/PS blends**: a series of heterogeneous films were produced, and can be classified in two categories: films presenting PS islands in a PMMA-r-PMAA matrix (20/80rd and 30/70rd), and films presenting PMMA-r-PMAA pits in a PS matrix (80/20rd and 90/10rd).

In both cases, heterogeneities generated by spin-coating were not only chemical but also topographical. However, PS/PMMA films appeared to be more suitable since PS/PMMA-r-PMAA films present inclusions which are higher or deeper. Moreover, the corresponding homogeneous substrates are rougher. This brings additional parameters into the system which are unwanted for the future protein adsorption and cell studies.

### *3.1.2. Protein adsorption*

Collagen adsorption was first examined on the pure polymer films and conditions leading to a different collagen distribution depending on the

polymer could be found. Even if two types of potentially interesting behaviors were investigated (preferential adsorption on one phase vs different supramolecular organization depending on the phase), we were only able to identify conditions leading to an interesting contrast between two polymers in term of collagen supramolecular organization. A contrast of collagen organization was indeed obtained between PS and PMMA (or PMMA-r-PMAA) for 2 h of adsorption with a collagen solution at 25 µg/mL. Large collagen assemblies were found on PS while a layer of collagen monomers or very small assemblies covered the surface of PMMA. A contrast was also observed between PS and PMMA-r-PMAA films after the adsorption of fibronectin, another adhesion protein. In that case fibronectin formed much more globular aggregates on PMMA-r-PMAA compared to PS.

Adsorption was then investigated on heterogeneous films in the promising conditions identified on the pure polymers:

A range of **different collagen organizations** was obtained on **PS/PMMA** films. **Inclusions size** was revealed as **an important parameter** in the control of the supramolecular organization on these blend films. It appeared that, if the PS domains, either surrounding or surrounded by the PMMA phase, were above 600 nm wide, a heterogeneous distribution of collagen was found, in agreement with observations made on pure polymers. Otherwise, the formed fibrils in the PS domains were longer and thinner compared to the ones observed on pure PS. The nitrogen molar fraction determined by XPS suggested however that the amount of collagen detected on all PS/PMMA films is a combination of the ones obtained on the pure polymers.

On the other hand, **heterogeneous fibronectin organizations** were obtained on **PS/PMMA-r-PMAA** films: the morphology of adsorbed fibronectin layers obtained on heterogeneous films **was a combination** of th e ones observed **on the pure polymers,** (i.e. rougher layer on PMMA-r-PMAA compared to PS), along with an effect of accumulation at the interface between the two polymers (edges of inclusions).

### *3.1.3. Cell culture*

The impact of **bare and collagen-coated PS/PMMA films** on cell behavior, after short culture times (4h and 6 days), was finally studied. We were able to **identify positive effects of heterogeneities** (in terms of film surface chemical composition and of collagen organization) on **cell morphology, developed cell area and cell density.**

**Collagen adsorption** prior to cell inoculation was shown to **affect cell behavior mainly after 4 h**. This is attributed to **the organization of collagen,** which would **induce** a combination of **2 effects**:

(i) collagen organization **direct the exposure ligands** available for the cells. Different amount and type of ligand may lead to different cell behavior

(ii) collagen organization **generates specific mechanical environments** for the cells which again may lead to different cell behavior.

A longer time in culture (6 days) would induce a reorganization of the protein layer, which would lead to protein layers giving similar cues to the cells in absence or presence of collagen precoating. After 4 h, cells with high cell area and high density were found on heterogeneous films with a high PS surface content, while after 6 days, such behavior is rather obserevd on heterogeneous films with a high PMMA surface content.

Finally, both in absence or presence of collagen precoating and after 4 h or 6 days in culture, two other effects were revealed:

(i) the **developed cell area** on heterogeneous films is a linear contribution of the behaviors observed on the pure polymers.

(ii) cell **density** is positively affected by the **heterogeneity** of the surface, a higher cell density being observed on heterogeneous films compared to the corresponding pure polymers.

This part of the work emphasizes the importance of the study of adsorbed proteins on chemically heterogeneous surfaces. The cell behavior cannot only be explained by the nature and amount of adsorbed proteins.

Their organization is here identified as a crucial factor, which could be controlled by the underlying surface chemical composition. Our results represent then a new point of knowledge in the interaction of cells with protein organization and surface chemical composition heterogeneities.

Our findings give also two main requirements for future research. The first is to identify the scope of the response, specifically which cell types react to these cues. Previous studies have clearly highlighted that one cell type could response positively to a specific cue while others could react oppositely. This also needs to be observed at a molecular level so as to further elucidate the mechanisms of cell reaction. The second is to investigate differentiation with longer time in culture. Previous studies have indeed shown that initially, cell could be highly responsive to substrates heterogeneities, while, with time, the same cues could lead to a negative response. The important challenge here is to be able to induce appropriate cell response which will lead to the desired differentiation pathway depending on the application.

The future of cell and tissue engineering depends on the development of next-generation biomaterials. These materials must either provide culture supports to ensure the proliferation of the cells collected through biopsy, or provide control over cell attachment and development into tissues. On the one hand, our results could be used to design new culture supports to enhance the proliferation of cells collected from bone biopsy and thereby would improve the speed of the process. These new culture supports would be, first, covered by a PS/PMMA polymer blend layer which will be made with PS/PMMA optimum ratio for cell proliferation on which collagen layers would be deposited. On the other hand, our results could be used in the design of new implants or scaffolds. The idea would be to use metals, ceramics, polymers or composites which possess the right mechanical properties end to modify them so that they would be able to induce the collagen organization of interest.

## 3.2. Future prospects

### *3.2.1. Strategy chosen for the design of protein layers with a heterogeneous distribution*

The aim of this thesis was to evaluate the impact of protein distribution on cell behavior. A heterogeneous protein organization was obtained by protein adsorption on chemically heterogeneous substrates. As explained above, another possible strategy which was only partially exploited here consists in preparing heterogeneous surfaces on which one phase inhibits protein adsorption. The use of Pluronic could be investigated further, by understanding Pluronic conformation and assembly in solution as well as its interaction with collagen, and by examining the effect of the type of Pluronic used or by using sequential (i.e. Pluronic adsorption prior to collagen adsorption) instead of simultaneous adsorption.

Instead of trying to create domains with or without proteins, with a view to further create zones allowing or preventing cell adhesion, another strategy could also have been conceived. Instead of examining the protein layer in depth prior to performing cell experiments, we could first culture cells on homogeneous films, treated with adhesion protein, and based on the results, select couples of one polymer allowing cell adhesion with one polymer preventing cell adhesion, in a given condition, to finally focus on the elaboration of blend polymer films.

Cell cultures on all the polymers investigated in this thesis (not only PS and PMMA) were actually briefly carried out to implement such strategy. After three days of culture, Coomassie dye was used for cell staining to globally see how cell had proliferated. The results are presented in Table 3 and are expressed in terms of very good proliferation (+), moderate proliferation (+/-) and very poor to no adhesion (-). These results already allow us to identify other potentially interesting systems that could be investigated to achieve our goal: fibronectin on PS (or PS-b-PEO)/PMMA-r-PMAA or collagen on PS/PMMA-r-PMAA and on PS-b-PEO/PMMA films.

**Table 3: Qualitative observation of MC3T3-E1 cells cultured for 3 days on pure polymer films and on glass after incubation of the substrate in PBS, fibronectin or collagen. Cells proliferation was observed after Coommassie blue staining.**

| | PBS | Fibronectin | collagen |
|---|---|---|---|
| **Glass** | + | + | + |
| **PS** | - | + | +/- |
| **PMMA** | +/- | + | +/- |
| **PS-b-PEO** | - | + | - |
| **PMMA-r-PMAA** | - | - | - |

### *3.2.2. Blend films elaboration*

The results obtained here on PS-b-PEO and PMMA films suggest again the investigation of cell culture on blends films (with a collagen coating or not). However, we were not able to elaborate films exposing both polymers at the extreme surface. Even if films prepared from dioxane solutions seemed to phase-separate better than those prepared from toluene, they were still covered by a thin PMMA layer. We could investigate other solvents, annealing procedures (solvent, temperature) or modify the spin-coating conditions (always kept at 5000 rpm) in order to try to modify the extreme surface and reach the exposure of both components at the interface.

### *3.2.3. Protein adsorption*

We observed a drastic difference of nitrogen level detected by XPS on the pure polymer films after fibronectin or collagen adsorption. It could be interesting to clarify these behaviors by means of other techniques such as radiolabeling or Quartz Cristal Microbalance.

### *3.2.4. Cell culture experiments*

**On films without collagen precoating**, we found that the cell density was influenced by the surface chemical heterogeneity, leading to a higher cell density on heterogeneous films with a high PMMA content. Since cell cultures were performed under serum condition, it is obvious that adhesion

proteins from the serum cover the polymer film prior to cell adhesion and therefore, the observed effect would also be directed by the heterogeneous distribution of those serum proteins. We could repeat the same experiment in absence of serum to confirm this hypothesis.

**On films with collagen precoating**, we also found an effect of heterogeneity on cell density. This effect was attributed to a combination of the exposure of ligands and of mechanical properties of the protein layer. The study of cell density on the same films with fibronectin precoating would be interesting in order to determine if this effect is due to the presence of adhesion ligands whatever their nature, or if it is a specific behavior generated by collagen. Additionally, different cell morphologies were observed between pure PS and PMMA. These differences would be a cumulative effect of collagen organization along with chemical composition of the films. To free oneself of the chemical composition, the investigation of cell culture on PMMA precoated with a collagen solution at 100 µg/mL (leading to the formation of large fibrils), and on PS precoated with a collagen solution at 8 µg/mL (leading to the formation of small assemblies only) should help us better understanding the different behaviors observed between PS and PMMA in this thesis.

Finally, the main perspective of the work of this thesis is the investigation of cell differentiation. Even if it is very important to understand very well the cell behavior after short time in cell culture before investigating differentiation after longer times, behaviors appearing to be excellent after short time could prove to be not appropriate for differentiation after a longer time. We attempted to evaluate cell differentiation in the course of the present thesis. We could highlight the differentiation of MC3T3-E1 cells on glass through alkaline phosphatase assay (generally used as short term tag of differentiation). However, an increase of osteocalcin concentration or the formation of a mineralized matrix (generally used as longer term tag of differentiation) was never observed with our MC3T3-E1 cells. We assume that our cell line lost its ability to differentiate. We believe that the series of collagen layers that was elaborated here is highly interesting to investigate differentiation. Therefore, submitting the

heterogeneous films to the culture of more stable osteoblast lines would be relevant.

# 4. References

[1] Ratner, B., In *Biomaterials science: an introduction to materials in medecine*, Ratner, B.; Hoffman, C.; Schoen, A.; Lemons, F., Eds. San Diego, **1996;** 1.

[2] Castner, D. G.; Ratner, B. D., Biomedical surface science: Foundations to frontiers. *Surf. Sci.* **2002,** *500*, 28-60.

[3] Petreaca, M.; Martins-Green, M., In *Principles of tissue engineering*, Lanza, R.; Langer, R.; Vancanti, J., Eds. **2007**; 81.

[4] Chapekar, M. S., Tissue engineering: challenges and opportunities. *J Biomed Mater Res* **2000,** *53*, 617-20.

[5] Shekaran, A.; Garcia, A. J., Nanoscale engineering of extracellular matrix-mimetic bioadhesive surfaces and implants for tissue engineering. *Biochim Biophys Acta* **2011,** *1810*, 350-60.

[6] Grinnell, F., Fibronectin adsorption on material surfaces. *Ann N Y Acad Sci* **1987,** *516*, 280-90.

[7] Grinnell, F.; Feld, M. K., Fibronectin adsorption on hydrophilic and hydrophobic surfaces detected by antibody binding and analyzed during cell adhesion in serum-containing medium. *The Journal of biological chemistry* **1982,** *257*, 4888-93.

[8] Anselme, K., Osteoblast adhesion on biomaterials. *Biomaterials* **2000,** *21*, 667-681.

[9] Liu, X.; Lim, J. Y.; Donahue, H. J.; Dhurjati, R.; Mastro, A. M.; Vogler, E. A., Influence of substratum surface chemistry/energy and topography on the human fetal osteoblastic cell line hFOB 1.19: Phenotypic and genotypic responses observed in vitro. *Biomaterials* **2007,** *28*, 4535-4550.

[10] Shekaran, A.; Garcia, A. J., Extracellular matrix-mimetic adhesive biomaterials for bone repair. *J. Biomed. Mater. Res. Part A* **2011,** *96A*, 261-272.

[11] Hynes, R. O., Integrins: versatility, modulation, and signaling in cell adhesion. *Cell* **1992,** *69*, 11-25.

[12] Goffin, J. M.; Pittet, P.; Csucs, G.; Lussi, J. W.; Meister, J. J.; Hinz, B., Focal adhesion size controls tension-dependent recruitment of alpha-smooth muscle actin to stress fibers. *The Journal of cell biology* **2006,** *172*, 259-68.

[13] Geiger, B.; Bershadsky, A.; Pankov, R.; Yamada, K. M., Transmembrane crosstalk between the extracellular matrix--cytoskeleton crosstalk. *Nature reviews. Molecular cell biology* **2001,** *2*, 793-805.

[14] Harbers, G.; Grainger, D., In *An introduction to biomaterials*, Guelcher, S.; Hollinger, J., Eds. CRC press: New York, **2006**; 15-45.

[15] Massia, S. P.; Hubbell, J. A., An RGD spacing of 440 nm is sufficient for integrin alpha V beta 3-mediated fibroblast spreading and 140 nm for focal contact and stress fiber formation. *The Journal of cell biology* **1991,** *114*, 1089-100.

[16] Lim, J. Y.; Donahue, H. J., Cell sensing and response to micro- and nanostructured surfaces produced by chemical and topographic patterning. *Tissue Eng.* **2007,** *13*, 1879-91.

[17] Maheshwari, G.; Wells, A.; Griffith, L. G.; Lauffenburger, D. A., Biophysical integration of effects of epidermal growth factor and fibronectin on fibroblast migration. *Biophys J* **1999,** *76*, 2814-23.

[18] DiMilla, P. A.; Barbee, K.; Lauffenburger, D. A., Mathematical model for the effects of adhesion and mechanics on cell migration speed. *Biophys J* **1991,** *60*, 15-37.

[19] DiMilla, P. A.; Stone, J. A.; Quinn, J. A.; Albelda, S. M.; Lauffenburger, D. A., Maximal migration of human smooth muscle cells on fibronectin and type IV collagen occurs at an intermediate attachment strength. *The Journal of cell biology* **1993,** *122*, 729-37.

[20] Lauffenburger, D. A.; Horwitz, A. F., Cell migration: a physically integrated molecular process. *Cell* **1996,** *84*, 359-69.

[21] Schuh, E.; Hofmann, S.; Stok, K.; Notbohm, H.; Muller, R.; Rotter, N., Chondrocyte redifferentiation in 3D: the effect of adhesion site density and substrate elasticity. *Journal of biomedical materials research. Part A* **2012,** *100*, 38-47.

[22] Rowley, J. A.; Mooney, D. J., Alginate type and RGD density control myoblast phenotype. *J Biomed Mater Res* **2002,** *60*, 217-23.

[23] Chen, C. S.; Mrksich, M.; Huang, S.; Whitesides, G. M.; Ingber, D. E., Micropatterned surfaces for control of cell shape, position, and function. *Biotechnol. Progr.* **1998,** *14*, 356-63.

[24] Chen, C. S.; Alonso, J. L.; Ostuni, E.; Whitesides, G. M.; Ingber, D. E., Cell shape provides global control of focal adhesion assembly. *Biochem Biophys Res Commun* **2003,** *307*, 355-61.

[25] Yang, S. P.; Lee, T. M., The effect of substrate topography on hFOB cell behavior and initial cell adhesion evaluated by a cytodetacher. *Journal of materials science. Materials in medicine* **2011,** *22*, 1027-36.

[26] Loesberg, W. A.; te Riet, J.; van Delft, F. C.; Schon, P.; Figdor, C. G.; Speller, S.; van Loon, J. J.; Walboomers, X. F.; Jansen, J. A., The threshold at which substrate nanogroove dimensions may influence fibroblast alignment and adhesion. *Biomaterials* **2007,** *28*, 3944-51.

[27] Boot-Handford, R. P.; Tuckwell, D. S., Fibrillar collagen: the key to vertebrate evolution? A tale of molecular incest. *Bioessays* **2003,** *25*, 142-51.

[28] Gurdak, E., *Supramolecular organization of collagen layers adsorbed on polymers (Thesis)*. University catholique de Louvain, 2006.

[29] Alberts, B.; Johnson, A.; Lewis, j., *biology of the cell*. 4th edition ed.; Garland: New York, 2002.

[30] Heino, J.; Huhtala, M.; Kapyla, J.; Johnson, M. S., Evolution of collagen-based adhesion systems. *The international journal of biochemistry & cell biology* **2009,** *41*, 341-8.

[31] Hulmes, D. J., Building collagen molecules, fibrils, and suprafibrillar structures. *J Struct Biol* **2002,** *137*, 2-10.

[32] Brodsky, B.; Ramshaw, J. A. M., The collagen triple-helix structure. *Matrix Biol.* **1997,** *15*, 545-554.

[33] Schnell, J., Evidence for the existence of hydrophobic interactions as a stabilizing factor in collagen structure. *Arch Biochem Biophys* **1968,** *127*, 496-502.

[34] Li, Y.; Asadi, A.; Monroe, M. R.; Douglas, E. P., pH effects on collagen fibrillogenesis in vitro: Electrostatic interactions and phosphate binding. *Materials Science and Engineering: C* **2009,** *29*, 1643-1649.

[35] Prockop, D. J.; Fertala, A., Inhibition of the self-assembly of collagen I into fibrils with synthetic peptides. Demonstration that assembly is driven by specific binding sites on the monomers. *The Journal of biological chemistry* **1998,** *273*, 15598-604.

[36] Kadler, K. E.; Holmes, D. F.; Trotter, J. A.; Chapman, J. A., Collagen fibril formation. *Biochem. J.* **1996,** *316*, 1-11.

[37] Kadler, K. E.; Hill, A.; Canty-Laird, E. G., Collagen fibrillogenesis: fibronectin, integrins, and minor collagens as organizers and nucleators. *Curr Opin Cell Biol* **2008,** *20*, 495-501.

[38] Gelman, R. A.; Poppke, D. C.; Piez, K. A., Collagen fibril formation in vitro. The role of the nonhelical terminal regions. *The Journal of biological chemistry* **1979,** *254*, 11741-5.

[39] Piez, K. A., In *Encyclopedia of polymer sciences and engineering*, Kroschwitz, J., Ed. Willey, NY: New York, 1985; Vol. 3, pp 699-727.

[40] Rößler, S.; Scharnweber, D.; Wolf, C.; Worch, H., Investigation of the adsorption of tropocollagen type I on titanium and Ti6Al4V. *Journal of Adhesion Science & Technology* **2000,** *14*, 453-465.

[41] Hattori, S.; Adachi, E.; Ebihara, T.; Shirai, T.; Someki, I.; Irie, S., Alkali-treated collagen retained the triple helical conformation and the ligand activity for the cell adhesion via alpha2beta1 integrin. *J Biochem* **1999,** *125*, 676-84.

[42] Miles, C. A.; Bailey, A. J., Thermally labile domains in the collagen molecule. *Micron* **2001,** *32*, 325-32.

[43] Shouhong, X.; Junpei, Y.; Isamu, M.; Masakatsu, Y., Effects of denaturation and association of collagen on adsorption behavior: two-dimensional nanostructure and its property. *Colloid & Polymer Science* **2007,** *285*, 899-906.

[44] Trelstad, R. L.; Hayashi, K.; Gross, J., Collagen fibrillogenesis: intermediate aggregates and suprafibrillar order. *Proc Natl Acad Sci U S A* **1976,** *73*, 4027-31.

[45] Penners, G.; Priel, Z.; Silberberg, A., Irreversible adsorption of triple-helical soluble collagen monomers from solution to glass and other surfaces. *J. Colloid Interface Sci.* **1981,** *80*, 437-444.

[46] Dupont-Gillain, C. C.; Jacquemart, I.; Rouxhet, P. G., Influence of the aggregation state in solution on the supramolecular organization of adsorbed type I collagen layers. *Colloids Surf., B* **2005,** *43*, 179-86.

[47] Wood, G. C.; Keech, M. K., The formation of fibrils from collagen solutions. 1. The effect of experimental conditions: kinetic and electron-microscope studies. *The Biochemical journal* **1960,** *75*, 588-98.

[48] Gross, J.; Kirk, D., The heat precipitation of collagen from neutral salt solutions: some rate-regulating factors. *The Journal of biological chemistry* **1958,** *233*, 355-60.

[49] Jacquemart, I.; Pamula, E.; De Cupere, V. M.; Rouxhet, P. G.; Dupont-Gillain Ch, C., Nanostructured collagen layers obtained by adsorption and drying. *J Colloid Interface Sci* **2004,** *278*, 63-70.

[50] Pamula, E.; De Cupere, V.; Dufrene, Y. F.; Rouxhet, P. G., Nanoscale organization of adsorbed collagen: influence of substrate hydrophobicity and adsorption time. *J. Colloid Interface Sci.* **2004,** *271*, 80-91.

[51] Dupont-Gillain, C. C.; Nysten, B.; Rouxhet, P. G., Collagen adsorption on poly(methyl methacrylate): net-like structure formation upon drying. *Polym. Int.* **1999,** *48*, 271-276.

[52] Dupont-Gillain Ch, C.; Pamula, E.; Denis, F. A.; De Cupere, V. M.; Dufrene, Y. F.; Rouxhet, P. G., Controlling the supramolecular organisation of adsorbed collagen layers. *Journal of materials science. Materials in medicine* **2004,** *15*, 347-53.

[53] Dupont-Gillain, C. C.; Rouxhet, P. G., AFM study of the interaction of collagen with polystyrene and plasma-oxidized polystyrene. *Langmuir* **2001,** *17*, 7261-7266.

[54] Elliott, J. T.; Woodward, J. T.; Umarji, A.; Mei, Y.; Tona, A., The effect of surface chemistry on the formation of thin films of native fibrillar collagen. *Biomaterials* **2007,** *28*, 576-85.

[55] Dupont-Gillain, C. C.; Pamula, E.; Denis, F. A.; Rouxhet, P. G., Nanostructured layers of adsorbed collagen: Conditions, mechanisms and applications. *Prog. Colloid Polym. Sci.* **2004,** *128*, 98-104.

[56] Dupont-Gillain Ch, C.; Gurdak, E.; Rouxhet, P., In *Encyclopedia of surface and colloid science*, Somasundaran, P., Ed. Taylor & Francis: London, 2007.

[57] Denis, F. A.; Hanarp, P.; Sutherland, D. S.; Gold, J.; Mustin, C.; Rouxhet, P. G.; Dufrene, Y. F., Protein adsorption on model surfaces with controlled nanotopography and chemistry. *Langmuir* **2002,** *18*, 819-828.

[58] Leow, W. W.; Hwang, W., Epitaxially Guided Assembly of Collagen Layers on Mica Surfaces. *Langmuir* **2011,** *27*, 10907-10913.

[59] Zhang, L.; Webster, T. J., Nanotechnology and nanomaterials: Promises for improved tissue regeneration. *Nano Today* **2009,** *4*, 66-80.

[60] Webster, T. J.; Ergun, C.; Doremus, R. H.; Siegel, R. W.; Bizios, R., Specific proteins mediate enhanced osteoblast adhesion on nanophase ceramics. *J Biomed Mater Res* **2000,** *51*, 475-83.

[61] Webster, T. J.; Ergun, C.; Doremus, R. H.; Siegel, R. W.; Bizios, R., Enhanced osteoclast-like cell functions on nanophase ceramics. *Biomaterials* **2001,** *22*, 1327-33.

[62] Webster, T. J.; Ejiofor, J. U., Increased osteoblast adhesion on nanophase metals: Ti, Ti6Al4V, and CoCrMo. *Biomaterials* **2004,** *25*, 4731-9.

[63] Kim, T. G.; Shin, H.; Lim, D. W., Biomimetic Scaffolds for Tissue Engineering. *Adv. Funct. Mater.* **2012,** *22*, 2446-2468.

[64] Venugopal, J. R.; Low, S.; Choon, A. T.; Kumar, A. B.; Ramakrishna, S., Nanobioengineered electrospun composite nanofibers and osteoblasts for bone regeneration. *Artif Organs* **2008,** *32*, 388-97.

[65] Chen, J.; Xu, J.; Wang, A.; Zheng, M., Scaffolds for tendon and ligament repair: review of the efficacy of commercial products. *Expert review of medical devices* **2009,** *6*, 61-73.

[66] Ekblad, T.; Liedberg, B., Protein adsorption and surface patterning. *Curr. Opin. Colloid Interface Sci.* **2010,** *15*, 499-509.

[67] Denis, F. A.; Pallandre, A.; Nysten, B.; Jonas, A. M.; Dupont-Gillain, C. C., Alignment and assembly of adsorbed collagen molecules induced by anisotropic chemical nanopatterns. *Small* **2005,** *1*, 984-91.

[68] Li, L.; Hitchcock, A. P.; Robar, N.; Cornelius, R.; Brash, J. L.; Scholl, A.; Doran, A., X-ray microscopy studies of protein adsorption on a phase-segregated polystyrene/polymethyl methacrylate surface. 1. Concentration and exposure-time dependence for albumin adsorption. *J. Phys. Chem. B* **2006,** *110*, 16763-16773.

[69] Amiji, M.; Park, K., Prevention of protein adsorption and platelet adhesion on surfaces by PEO/PPO/PEO triblock copolymers. *Biomaterials* **1992,** *13*, 682-92.

[70] Lee, J. H.; Kopecek, J.; Andrade, J. D., Protein-resistant surfaces prepared by PEO-containing block copolymer surfactants. *J Biomed Mater Res* **1989,** *23*, 351-68.

[71] Dewez, J. L.; Berger, V. V.; Schneider, Y. J.; Rouxhet, P. G., Influence of Substrate Hydrophobicity on the Adsorption of Collagen in the Presence of Pluronic F68, Albumin, or Calf Serum. *J Colloid Interface Sci* **1997,** *191*, 1-10.

[72] Sudo, H.; Kodama, H. A.; Amagai, Y.; Yamamoto, S.; Kasai, S., In vitro differentiation and calcification in a new clonal osteogenic cell line derived from newborn mouse calvaria. *The Journal of cell biology* **1983,** *96*, 191-8.

[73] Gronthos, S.; Stewart, K.; Graves, S. E.; Hay, S.; Simmons, P. J., Integrin Expression and Function on Human Osteoblast-like Cells. *J. Bone Miner. Res.* **1997,** *12*, 1189-1197.

[74] Reyes, C. D.; García, A. J., α2β1 integrin-specific collagen-mimetic surfaces supporting osteoblastic differentiation. *J. Biomed. Mater. Res. Part A* **2004,** *69A*, 591-600.

[75] En-Nosse, M.; Hartmann, S.; Trinkaus, K.; Alt, V.; Stigler, B.; Heiss, C.; Kilian, O.; Schnettler, R.; Lips, K. S., Expression of non-neuronal cholinergic system in osteoblast-like cells and its involvement in osteogenesis. *Cell and tissue research* **2009,** *338*, 203-15.

[76] Zhang, Z.; Gu, B.; Zhang, W.; Kan, G.; Sun, J., The enhanced characteristics of osteoblast adhesion to porous Zinc–TiO2 coating prepared by plasma electrolytic oxidation. *Appl. Surf. Sci.* **2012,** *258*, 6504-6511.

[77] Taylor, J. F., Spin coating: An overview. *Met. Finish.* **2001,** *99*, 16-21.

[78] Walheim, S.; Boltau, M.; Mlynek, J.; Krausch, G.; Steiner, U., Structure formation via polymer demixing in spin-cast films. *Macromolecules* **1997,** *30*, 4995-5003.

[79] Pape, p.; Plueddemann, E., In *Silanes and other coupling agents*, Koninklijke Wöhrman BV ed.; Mittal, K., Ed. the Netherlands, 1992; pp 105-116.

[80] Sundrani, D.; Sibener, S. J., Spontaneous Spatial Alignment of Polymer Cylindrical Nanodomains on Silicon Nitride Gratings. *Macromolecules* **2002,** *35*, 8531-8539.

[81] Darling, S. B., Directing the self-assembly of block copolymers. *Prog. Polym. Sci.* **2007,** *32*, 1152-1204.

[82] Delcroix, M. F.; Zuyderhoff, E. M.; Genet, M. J.; Dupont-Gillain, C. C., Optimization of cryo-XPS analyses for the study of thin films of a block copolymer (PS-PEO). *Surf. Interface Anal.* **2012,** *44*, 175-184.

[83] Bodiguel, H.; Montes, H.; Fretigny, C., Depth sensing and dissipation in tapping mode atomic force microscopy. *Rev. Sci. Instrum.* **2004,** *75*, 2529-2535.

[84] Cimmino, S.; Martuscelli, E.; Silvestre, C., Miscibility prediction based on the corresponding states theory: poly(ethylene oxide)/atactic poly(methyl methacrylate) system. *Polymer* **1989,** *30*, 393-398.

[85] Martuscelli, E.; Silvestre, C.; Addonizio, M. L.; Amelino, L., Phase structure and compatibility studies in poly(ethylene oxide)/poly(methyl methacrylate) blends. *Die Makromolekulare Chemie* **1986,** *187*, 1557-1571.

[86] Callewaert, M.; Gohy, J.-F.; Dupont-Gillain, C. C.; Boulangé-Petermann, L.; Rouxhet, P. G., Surface morphology and wetting properties of surfaces coated with an amphiphilic diblock copolymer. *Surf. Sci.* **2005,** *575*, 125-135.

[87] Wu, J.; Zhao, M.; Nguyen, T.; Gu, X., Effects of Relative Humidity and Nanoparticle Incorporation on Nanostructures of PS-b-PEO Diblock Copolymer. *MRS Online Proceedings Library* **2007,** *1056*, null-null.

[88] Brandrup, J.; Immergut, E. H.; Grulke, E. A., *Polymer handbook*. 4th ed.; Wiley: New York, **1999**.

[89] Johnson, R. E., Jr.; Dettre, R. H., In *Surface Colloid Sci.*, Matijevic, E., Ed. Willey-Interscience: New York, **1969**; Vol. 2, 85-153.

[90] Neumann, A. W.; Good, R. J., Thermodynamics of contact angles. I. Heterogeneous solid surfaces. *J. Colloid Interface Sci.* **1972,** *38*, 341-358.

[91] Marmur, A., From hygrophilic to superhygrophobic: theoretical conditions for making high-contact-angle surfaces from low-contact-angle materials. *Langmuir* **2008,** *24*, 7573-9.

[92] Gurdak, E.; Rouxhet, P. G.; Dupont-Gillain, C. C., Factors and mechanisms determining the formation of fibrillar collagen structures in adsorbed phases. *Colloids Surf., B* **2006,** *52*, 76-88.

[93] Pankov, R.; Yamada, K. M., Fibronectin at a glance. *J Cell Sci* **2002,** *115*, 3861-3.

[94] Renner, L.; Pompe, T.; Salchert, K.; Werner, C., Dynamic alterations of fibronectin layers on copolymer substrates with graded physicochemical characteristics. *Langmuir* **2004,** *20*, 2928-33.

[95] Arima, Y.; Iwata, H., Effect of wettability and surface functional groups on protein adsorption and cell adhesion using well-defined mixed self-assembled monolayers. *Biomaterials* **2007,** *28*, 3074-82.

[96] Dupont-Gillain, C. C.; Alaerts, J. A.; Dewez, J. L.; Rouxhet, P. G., Patterned layers of adsorbed extracellular matrix proteins: influence on mammalian cell adhesion. *Biomed Mater Eng* **2004,** *14*, 281-91.

[97] Keselowsky, B. G.; Collard, D. M.; Garcia, A. J., Surface chemistry modulates fibronectin conformation and directs integrin binding and specificity to control cell adhesion. *J. Biomed. Mater. Res. Part A* **2003,** *66A*, 247-259.

[98] Elliott, J. T.; Woodward, J. T.; Langenbach, K. J.; Tona, A.; Jones, P. L.; Plant, A. L., Vascular smooth muscle cell response on thin films of collagen. *Matrix biology : journal of the International Society for Matrix Biology* **2005,** *24*, 489-502.

[99] Shrivastava, A.; Radziejewski, C.; Campbell, E.; Kovac, L.; McGlynn, M.; Ryan, T. E.; Davis, S.; Goldfarb, M. P.; Glass, D. J.; Lemke, G.; Yancopoulos, G. D., An orphan receptor tyrosine kinase family whose members serve as nonintegrin collagen receptors. *Molecular cell* **1997,** *1*, 25-34.

[100] Dalby, M. J.; Childs, S.; Riehle, M. O.; Johnstone, H. J.; Affrossman, S.; Curtis, A. S., Fibroblast reaction to island topography: changes in cytoskeleton and morphology with time. *Biomaterials* **2003,** *24*, 927-35.

[101] Dalby, M. J.; Giannaras, D.; Riehle, M. O.; Gadegaard, N.; Affrossman, S.; Curtis, A. S., Rapid fibroblast adhesion to 27nm high polymer demixed nano-topography. *Biomaterials* **2004,** *25*, 77-83.

# PART II

# Detailed presentation

# Chapter I

# An AFM, XPS and wettability study of the surface heterogeneity of PS/PMMA-r-PMAA demixed thin films


### *Summary*

A series of homopolymer / random copolymer blends was used to produce heterogeneous surfaces by demixing in thin films. The chosen homopolymer is polystyrene (PS) and the random copolymer is poly(methyl methacrylate)-r-poly(methacrylic acid) (PMMA-r-PMAA). Combining unconventionally the information from atomic force microscopy (AFM) images, X-ray photoelectron spectroscopy (XPS) data, water contact angle measurements and PS selective dissolution, it appears that the surfaces obtained from blends with a high PS content (90/10 to 70/30) display pits with a bottom made of PMMA-r-PMAA, randomly distributed in a PS matrix. On the other hand, the surfaces obtained from blends with a low PS content (30/70 to 10/90) display randomly distributed PS islands surrounded by a PMMA-r-PMAA matrix. The morphology of the heterogeneous films is thought to be governed by the higher affinity of PMMA-r-PMAA for the solvent (dioxane), which leads to the elevation of the PS phase compared to the PMMA-r-PMAA phase, and to surface enrichment by PMMA-r-PMAA.

# 1. Introduction

A number of important properties of polymer materials, including their interaction with biological systems, are controlled by their surface chemistry and morphology [1-5]. Therefore, to study protein or cell interactions with polymer materials, the surface composition and morphology of these materials need to be very well characterized. Polymer blends, which are widely studied, show surface properties which are often a combination of those of the pure polymers, and their surface composition is often different from that of the bulk [6]. Furthermore, because of the immiscibility of most polymers, the surface of polymer blends usually presents segregated structures with domains predominantly constituted of each individual polymer [7-10].

The polystyrene / poly(methyl methacrylate) (PS/PMMA) blend is a well-known combination of immiscible polymers for which bulk and surface phase separation have been observed. Islands/matrix and pits/matrix morphologies were both reported [7-10]. Changing the relative polymer proportions in such blends influences the geometry of the observed domains [11]. The component with the lower surface free energy, i.e. PS, tends to be enriched at the surface in order to minimise the polymer-air surface tension [12]. However, PS/PMMA thin films obtained by spin-coating may be far from equilibrium due to the rapid solvent evaporation during the spin-coating process. Their thickness and surface morphology are mainly due to factors such as the concentration of the polymers in the blend [9,13,14], the speed of spin-coating [11,13,15], the choice of the solvent [7,10,11], and the chemical nature of the substrate [7,13]. In some studies, annealing was performed to get closer to equilibrium [8,12,16].

Random copolymers, consisting of a random sequence of two different monomers, do not lead to surface segregation because of the absence of sequences of the same monomer with a sufficient length. Methacrylate random copolymers, like poly(methyl methacrylate)-r-poly(methacrylic acid) (PMMA-r-PMAA) and poly(methyl methacrylate)-r-poly(trimethylaminoethyl methacrylate) (PMMA-r-TMAEMA), were used to bring a negative or positive charge to PMMA in order to study the

influence of surface charge on bacterial adhesion [17,18]. Besides, segregated structures were produced by spin-coating a solution of PMMA-r-PMAA on top of a PS substratum which dissolved during the process [10]. In this case, the heterogeneous morphology is composed of a homopolymer phase (PS) and of another phase (PMMA-r-PMAA) with a larger chemical diversity compared to pure PMMA. The interest of this kind of blends lies in the possibility to control the proportion of a given chemical function in the copolymer phase by varying the proportion of the two monomers in the random copolymer. Furthermore, the acidic functions of PMAA could be used for further surface functionalisation or grafting.

In this study, we use a series of homopolymer/random copolymer blends to produce heterogeneous substrates by demixing in thin films. The chosen homopolymer is polystyrene (PS) while the random copolymer is poly(methyl methacrylate)-r-poly(methacrylic acid) (PMMA-r-PMAA) with 20 % of methacrylic acid units. The aim of this work is to characterize in detail the surface morphologies obtained for different proportions of PS and PMMA-r-PMAA in the blends. The obtained surfaces are analyzed by X-ray photoelectron spectroscopy (XPS) using thorough and original data treatments, atomic force microscopy (AFM) and wetting measurements. Selective dissolutions are also performed to identify the presence of a given polymer in the observed domains, thereby getting more insight into the obtained morphologies and their formation mechanism.

## 2. Materials and methods

### 2.1. Preparation Preparation of thin films of PS/PMMA-r-PMAA

Demixed thin polymer films were produced by spin-coating (speed = 5000 rpm, acceleration = 20,000 rpm/s, time = 40 s) a 40 µl drop of blends of PMMA-r-PMAA (random copolymer with 80% of PMMA and 20% of PMAA, $M_w \sim 10^6$ ; from Polysciences, Warrington, USA) and PS ($M_w \sim$ 230,000, $M_n \sim$ 140,000; from Merck, Germany) dissolved in dioxane (Fluka, Switzerland) onto a PMMA plate. In order to obtain a range of substrates having different morphologies, a series of seven polymer solutions

containing different PS/PMMA-r-PMAA ratios (90/10, 85/15, 80/20, 70/30, 30/70, 20/80 and 10/90 w/w) was prepared; the total polymer concentration was always 10 g/l. Homogeneous films of PS and PMMA-r-PMAA were also used as controls (100/0 and 0/100, respectively). Note that the thickness of the spin-coated films was measured by ellipsometry for homogeneous PS and PMMA-r-PMAA spin-coated onto silicon wafers using the same spin-coating conditions. It was about 40 nm in both cases. The PMMA plates, used as substrates, were obtained by compression molding of a PMMA powder ($M_w$ ~ 996,000, $T_g$ 125° C ; from Aldrich, USA) between two glass plates at 240°C. These plates were cut in order to obtain disks of PMMA (12 mm diameter) which were cleaned by ultrasound treatment in water for one minute and dried under a nitrogen flow before the spin-coating process. A high molecular mass PMMA was selected to avoid PMMA dissolution during spin-coating.

## 2.2. Selective dissolution

In order to identify the PS domains at the sample surface, selective dissolution of the PS phase was achieved. The samples were immersed in 20 ml of cyclohexane (Fluka, Switzerland) at 45°C for 2 hours. They were then washed 5 times with hot cyclohexane under agitation and were finally abundantly rinsed with ethanol (Fluka, Switzerland) and dried under a nitrogen flow.

## 2.3. Atomic Force Microscopy (AFM)

The AFM analyses were performed with a Nanoscope III apparatus (Digital instruments, Santa Barbara, USA) in contact mode. The analyses were performed under milli-Q water and at room temperature. The $Si_3N_4$ tips had a spring constant of about 0.01 N/m and a radius of curvature of about 20 nm (Park Scientific Instruments, Mountain View, USA). The scan rate was about 5 Hz and the applied force was the minimum value allowing to keep the contact between tip and sample. For each sample, at least four areas were imaged in height mode. Images were plane-fitted using the image analysis software provided with the microscope. The Nanoscope Bearing analysis was used to determine the proportion of the surface occupied by the

inclusions. The bearing analysis calculates and displays the bearing-ratio curve and surface-height histograms for selected lines or areas on images. The bearing-ratio curve is the integral of the surface-height histogram. It represents the percentage of points above a reference plane as a function of the depth of that plane below the highest point.

## 2.4. X-ray Photoelectron Spectroscopy (XPS)

The XPS analyses were performed with a Kratos Axis Ultra spectrometer (Kratos Analytical – Manchester – UK) equipped with a monochromatised aluminium X-ray source (powered at 10 mA and 15 kV). The pressure in the analysis chamber was around $10^{-6}$ Pa. The angle φ between the normal to the sample surface and the lens axis was 0° unless specified otherwise. Analyses at φ = 70° were also performed in order to collect information on a thinner surface layer. The hybrid lens magnification mode was used with the slot aperture resulting in an analysed area of 700 µm x 300 µm. Charge stabilisation was achieved by using the Kratos Axis device. The pass energy was set at 40 eV for the detailed scans. In these conditions, the energy resolution gives a full width at half maximum (FWHM) of the Ag $3d_{5/2}$ peak of about 0.9 eV and a maximal signal counts of 1 038 000 counts/second. The following sequence of spectra was recorded: survey spectrum, C 1s, O 1s and C 1s again to check the stability of charging potential and the absence of degradation of the samples during the analysis. The binding energies were calculated with respect to the C-(C,H) component of the C 1s peak fixed at 284.8 eV. Molar concentration ratios were calculated using peak areas normalised according to acquisition parameters and sensitivity factors provided by the manufacturer. Peak decomposition was achieved with the Casa XPS software (Casa Software Ltd, UK), after subtraction of a linear baseline.

## 2.5. Water contact angle measurements

Static water contact angles ($\Theta_w$) were measured at ambient temperature using the sessile drop method and image analysis of the drop profile. The instrument, using a CCD camera and an image analysis processor, was purchased from Electronisch Ontwerpbureau De Boer (The

Netherlands). The water (milli-Q, Millipore, Molsheim, France) droplet volume was 0.3 µl, and the contact angle was measured 5 seconds after the drop was deposited on the sample. For each sample, the reported value is the average of the results obtained on at least 10 droplets.

## 3. Results

Topographic AFM images are presented for four of the seven PS/PMMA-r-PMAA polymer blends and for the corresponding homogeneous films are shown in Figure 1.

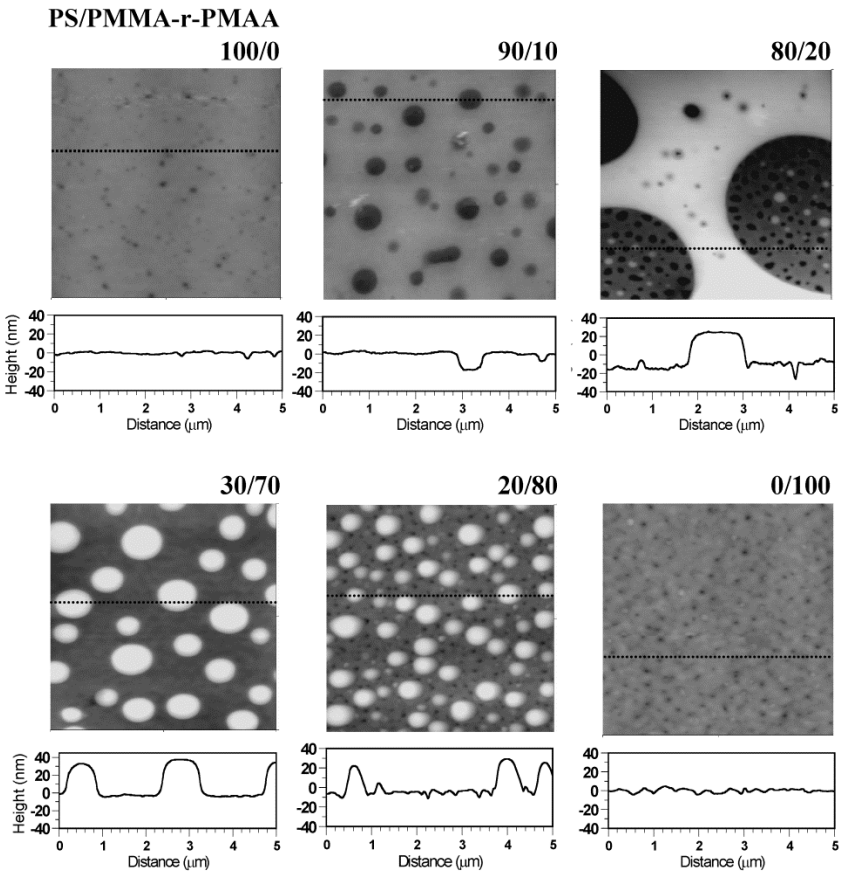


**Figure 1:** Representative AFM images (high mode, 5 x 5 µm²; vertical grey scale = 50 nm) of thin films of blends of PS and PMMA-r-PMAA (composition of the blend indicated on top of each image). The cross-sections were taken at the position indicated by the dotted lines.

While the control PS and PMMA-r-PMAA films are rather flat, the demixed films present a typical surface relief. For the blends with a high PS content (90/10 and 80/20), the obtained surfaces display randomly distributed inclusions which are below the matrix level (pits). The pit diameter increases with the PMMA-r-PMAA content. For the blends with a high PMMA-r-PMAA content (30/70, 20/80), the obtained surfaces also display randomly distributed inclusions, which are in this case higher than the matrix level (islands). The island diameter increases with the PS content. Table 1 summarizes information extracted from the AFM images presented in Figure 1 as well as from AFM images acquired on the other investigated blend compositions (images not shown). The depth of the pits or the height of the islands, measured on cross-sections, are in the range of 20-50 or 30-40 nm respectively. The proportion of the surface occupied by the inclusions was determined thanks to the Nanoscope bearing analysis. For blends with a high PS/PMMA-r-PMAA ratio presenting pits, it increased from 14 to ~ 50% with the PMMA-r-PMAA content. It was close to 30% for the islands made of blends with a low PS/PMMA-r-PMAA ratio.

**Table 1:** Data extracted from AFM images of thin films of blends of PS and PMMA-r-PMAA.

| | PS / PMMA -r-PMAA | | | | | | | | |
|---|---|---|---|---|---|---|---|---|---|
| | **100 / 0** | **90 / 10** | **85 / 15** | **80 / 20** | **70/30** | **30 / 70** | **20 / 80** | **10 / 90** | **0 / 100** |
| **Surface features** | Flat | Pits | Pits | Pits | Pits | Islands | Islands | Islands | Flat |
| **Depth of pits or height of islands[a] (nm)** | / | 19 (4) | 48 (10) | 38 (8) | 35 (4) | 37 (3) | 32 (4) | 36 (8) | / |
| **Diameter of inclusions[a] (µm)** | / | 0.6 (0.2) | 1.6 (0.7) | 3.0 (0.5) | 3.3 (0.4) | 0.7 (0.2) | 0.5 (0.1) | 0.4 (0.1) | / |
| **Area fraction of inclusions[a] (%)** | / | 14 (2) | 38 (5) | 50 (2) | 48 (2) | 28 (2) | 26 (1) | 28 (3) | / |

[a] Standard deviation is given between brackets (data extracted from 4 images and at least 5 pits or islands per image)

Static water contact angles and raw XPS data are presented in Table 2. The water contact angles of the random copolymer PMMA-r-PMAA (66°) and of PS (85°) are close to those reported in the literature for these polymers [10]. The water contact angle measured on demixed thin films shows intermediate values, which increase with the PS content. The XPS

Survey spectra show only the presence of oxygen and carbon (note that hydrogen atoms are not detected by XPS). The elemental composition of the surface is expressed in mole fraction O/(O+C). On pure PS, there is a low concentration of oxygen which is attributed to contamination from air, to additives or to catalyst residues present in the polymer. For PMMA-r-PMAA, the mole percentage of oxygen is expected to be 29.5%. The slightly lower experimental value may be mainly attributed to an underestimation of the proportion of oxygen (10% to 15%), owing to the sensitivity factors provided by the manufacturer, as also indicated by the analysis of other materials. The surface elemental composition of blend films is intermediate between those of the two pure polymers. Analyses performed at φ = 70°, which allow a thinner (about 3 times) surface layer to be probed, do not show significant difference with the analyses performed at φ = 0° for the pure polymers. For the PS/PMMA-r-PMAA blends 90/10 and 30/70, analysis at φ = 70° revealed a slight increase and decrease of the oxygen content, respectively, compared to the values recorded at φ = 0°.

**Table 2:** Water contact angle ($\Theta_w$) and XPS data for thin films of blends of PS and PMMA-r-PMAA

| | PS / PMMA -r- PMAA | | | | | | | | |
|---|---|---|---|---|---|---|---|---|---|
| | **100 / 0** | **90 / 10** | **85 / 15** | **80 / 20** | **70/30** | **30 / 70** | **20 / 80** | **10 / 90** | **0 / 100** |
| $\Theta_w$[a] | 85.0 (2.9) | 84.5 (1.7) | 82.0 (1.0) | 80.0 (0.8) | 81.5 (1.4) | 73.5 (0.6) | 71.5 (0.9) | 67.0 (1.8) | 65.5 (1.5) |
| **O / (O + C) (%)** **0°**[b] | 1.2 | 4.2 | 10.4 | 15.0 | 14.2 | 20.4 | 21.1 | 22.5 | 25.6 |
| *70°*[b] | *1.0* | *6.2* | | | | *18.8* | | | *25.0* |
| **f (%)** | 0 | 11 | 41 | 61 | 57 | 82 | 88 | 94 | 100 |
| **f′ (%)** | 0 | 8 | 31 | 49 | 48 | 77 | 81 | 100 | 100 |

[a] Standard deviation is given between brackets (10 measurements at least)

[b] Angle φ between the normal to the sample surface and the lens axis. Note that a thicker surface layer is probed a φ = 0° compared to φ = 70°.

f : PMMA-r-PMAA area fraction determined from XPS data at φ = 0°with a method based on the oxygen and carbon mole fractions (see text for details).

f ′: PMMA-r-PMAA area fraction determined from XPS data at φ = 0° with a method based on peak decomposition (see text for details).

The C 1s peaks recorded on the pure polymers and on the PS/PMMA-r-PMAA blends are presented in Figure 2, together with the chemical formulas of the polymers.

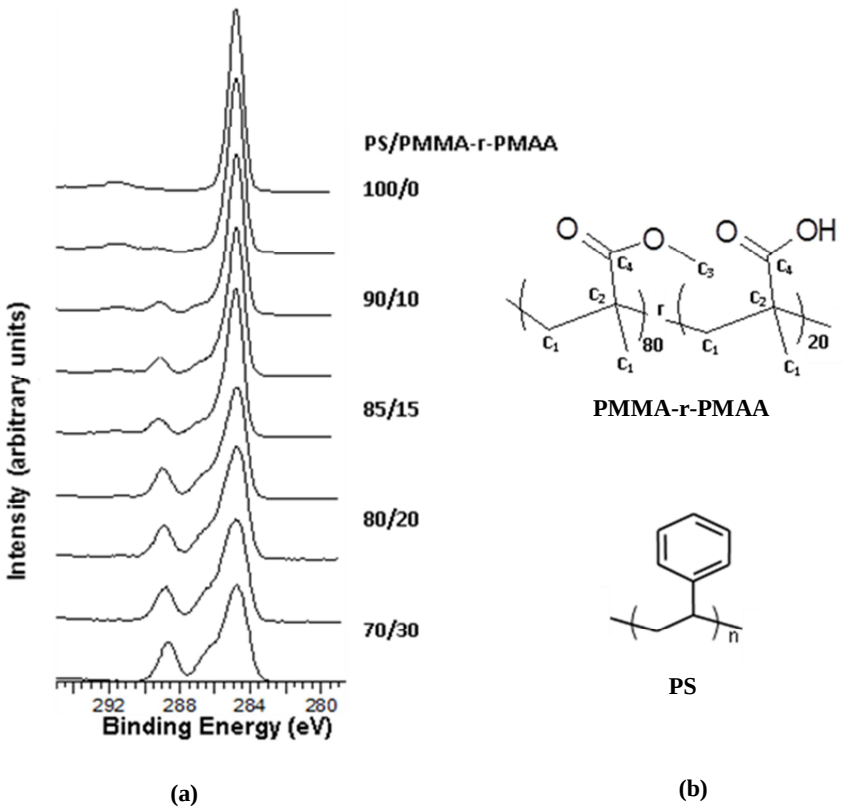


**Figure 2**: (a) C 1s peaks obtained by XPS on thin films of blends of PS and PMMA-r-PMAA; (b) PMMA-PMAA and PS chemical formulas. (note that PMMA-r-PMAA is a random copolymer).

The C 1s peak of PS contains a main component, at 284.8 eV, which corresponds to carbon bound to carbon and/or hydrogen ( C- (C,H)), and a shake-up peak at 292 eV due to $\Pi$-$\Pi^*$ transitions in the aromatic ring. The C 1s peak of PMMA-r-PMAA is expected to present four components [19] which correspond to the different types of carbon atoms (see Figure 2b): at 284.8 eV for carbon bound only to carbon or hydrogen (C- (C,H), "$C_1$"); at 285.5 eV for carbon bound to a carbon itself bound to two oxygens ( C- (COO), "$C_2$"); at 286.6 eV for carbon singly bound to oxygen (C-O, "$C_3$") and at 288.8 eV for carbon involved in an ester or acid function (O-C=O,"$C_4$"). The proportions obtained experimentally for these four components are respectively, 41.1 %, 20.5 %, 17.9 %, 20.5 %. These experimental values correspond very well with the theoretical values which

are respectively, 42 %, 21 %, 16 %, 21 %. The C 1s peaks obtained for the PS/PMMA-r-PMAA demixed thin films clearly show a contribution of both polymers, which follows the expected trends.

In order to evaluate the proportion of the two polymers at the surface, the XPS data have been treated using two different methods, which combine differently experimental data and modelling approximations. The first method consists in computing roughly the surface fraction made of PMMA-r-PMAA starting from the C and O mole fractions determined by XPS. If the surface is considered as made of patches of PS and PMMA-r-PMAA which are thicker than the analysed depth, and if the differences of density and (C+O) concentration between the two pure polymers are neglected, the O/C ratio measured on the blends, $(O/C)_{exp}$, can be expressed as: [10,11]

$$\left(\frac{O}{C}\right)_{exp} \approx \frac{f\, O_{PA}^{exp} + (1-f)\, O_{PS}^{exp}}{f\, C_{PA}^{exp} + (1-f)\, C_{PS}^{exp}} \qquad \text{[eq. 1]}$$

where f is the PMMA-r-PMAA surface fraction, $O_{PS}^{exp}$ and $O_{PA}^{exp}$ are the oxygen mole fraction, and $C_{PS}^{exp}$ and $C_{PA}^{exp}$ are the carbon mole fraction given by the XPS analysis of pure PS and pure PMMA-r-PMAA, respectively. The computed f values are presented in Table 2.

The second method consists in decomposing the C 1s peak of each heterogeneous surface with two components corresponding to the C 1s peak of pure PS and the C 1s peak of pure PMMA-r-PMAA. An example of such decomposition is shown in Figure 3. This decomposition gives the respective contributions X and Y of PS and PMMA-r-PMAA in the C 1s peak of heterogeneous surfaces. These contributions X and Y can be converted into the surface fraction of PMMA-r-PMAA (f′) as follows:

$$\frac{Y}{X} = \frac{C_{PA}^{*}\, f'}{C_{PS}^{*}(1-f')} \qquad \text{[eq. 2]}$$

where $C_{PS}^{*}$ and $C_{PA}^{*}$ are the carbon molar concentrations in PS and PMMA-r-PMAA, respectively. These carbon molar concentrations were computed from the stoechiometry of each polymer and from the polymer

density (1.04 g/cm$^3$ for PS and 1.19 g/cm$^3$ for PMMA-r-PMAA) [20]. $C^*_{PS}$ is equal to 79.7 and $C^*_{PA}$ is equal to 58.3 mmole/cm$^3$. The computed f ′ values are presented in Table 2. In most cases, they are slightly lower than f. Owing to the similarity of the C 1s and O 1s peaks between ester and carboxylic acid functions, no further information can be obtained on the respective concentration of methyl methacrylate and methacrylic acid monomers at the surface.

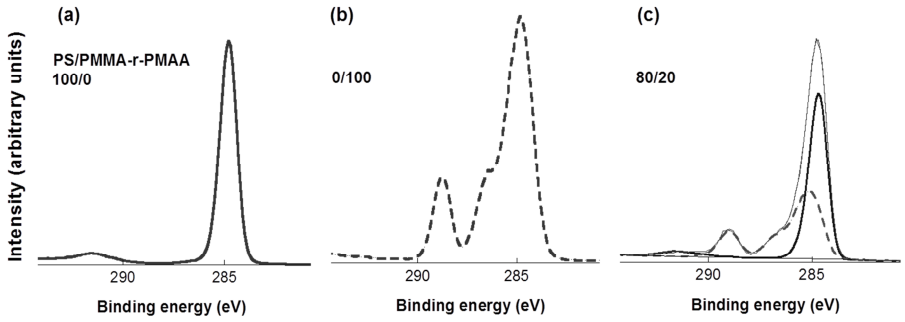


**Figure 3:** Illustration of the method used to evaluate the surface fraction of PS and PMMA-r-PMAA in mixed thin films from the shape of the C 1s peak. (a) C 1s peak of pure PS, (b) C 1s peak of pure PMMA-r-PMAA, (c) C 1s peak of PS/PMMA-r-PMAA 80/20, decomposed using a linear combination of the C 1s peaks shown in (a) and (b).

In order to identify the PS domains without ambiguity, the selective dissolution of PS was achieved on one heterogeneous surface displaying randomly distributed pits (90/10) and on another one displaying randomly distributed islands (30/70). AFM images recorded after PS dissolution are presented in Figure 4. The PS/PMMA-r-PMAA 90/10 surface, which showed pits before selective dissolution (see Figure 1), shows randomly distributed islands (height ~ 15 nm, diameter ~ 800 nm and area fraction ~ 26 %) after selective dissolution. Two kinds of islands are observed: some are surrounded by a crest (height ~ 15 nm, with respect to the center of inclusion), while other ones are not. The PS/PMMA-r-PMAA 30/70 surface, which showed islands before selective dissolution (see Figure 1), shows randomly distributed pits (depth ~ 30 nm, diameter ~ 1200 nm and area

fraction ~ 15 %), also surrounded by a crest, after selective dissolution. The information extracted from AFM images after PS dissolution is summarized in Table 3.

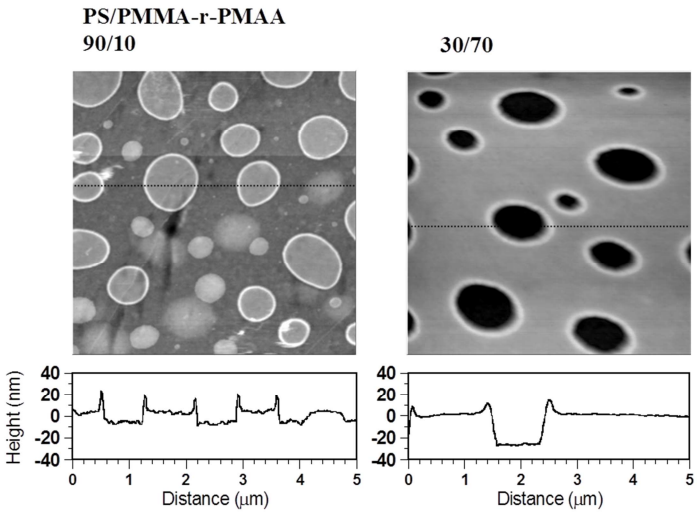


**Figure 4:** AFM images (high mode, 5 x 5 μm²; vertical grey scale = 50 nm) obtained after selective dissolution of PS on the PS/PMMA-r-PMAA 90/10 (left) and 30/70 (right) heterogeneous surfaces. The cross-sections were taken at the position indicated by the dotted lines.

The surfaces of PS/PMMA-r-PMAA 90/10 and 30/70 blends after PS dissolution were also analysed by XPS (see Table 3, lower part), together with control samples. If PS was entirely removed by the dissolution process, the composition of pure PMMA-r-PMAA should be obtained in the four cases. Actually, a significant amount of PS remains present on the samples which initially contained a large proportion of PS. The PMMA-r-PMAA surface fraction after PS dissolution was quantified using the calculation methods explained above (f and f′ determination) and is presented in Table 3 (lower part). In order to probe a thinner surface layer, XPS analysis were performed at φ = 70°. For pure PS, the O/(O+C) ratio decreases relatively by ~ 40% compared to analysis performed at φ = 0°, and for the surface of the 90/10 blend, it decreases by ~ 20 %. This indicates that a thin layer of PS remains at the surface of these samples after selective dissolution. The 100 % of copolymer area obtained in the 30/70 blend can be explained by the

fact that the methods used are not enough sensitive to detect small amount of PS. When the PS amount is too small, the PS shake up is confused with the baseline, therefore the methods don't detect the PS.

**Table 3:** AFM and XPS data obtained on thin films of blends of PS and PMMA-r-PMAA after selective dissolution of the PS phase.

| | PS / PMMA -r-PMAA | | | |
|---|---|---|---|---|
| | **100 / 0** | **90 / 10** | **30 / 70** | **0 / 100** |
| ***AFM*** | | | | |
| **Surface features** | / | Islands + crests | Pits + crests | / |
| **Depth of pits or height of islands and crest[a] (nm)** | / | 16 (5)<br>+15 (3) | 31 (6)<br>+11 (3) | / |
| **Diameter of inclusions[a] (µm)** | / | 0.8 (0.2) | 1.3 (0.3) | / |
| **Area fraction of inclusions[a] (%)** | / | 26 (3) | 16 (2) | / |
| ***XPS*** | | | | |
| **O / (O + C) (%) 0°[b]** | 15.4 | 19.2 | 23.9 | 25.6 |
| ***70°[b]*** | *8.5* | *15.9* | *22.9* | *26.0* |
| **f (%)** | 64 | 80 | 100 | 100 |
| **f '(%)** | 72 | 88 | 100 | 100 |

[a] Standard deviation is given between brackets (10 measurements at least)

[b] Angle φ between the normal to the sample surface and the lens axis. Note that a thicker surface layer is probed a φ = 0° compared to φ = 70°.

f : PMMA-r-PMAA area fraction determined from XPS data at φ = 0°with a method based on the oxygen and carbon mole fractions (see text for details).

f ′: PMMA-r-PMAA area fraction determined from XPS data at φ = 0° with a method based on peak decomposition (see text for details).

## 4. Discussion

AFM images obtained on thin films of a series of blends of PS and PMMA-r-PMAA showed that the surface of blends with a high PS content (from 90/10 to 70/30) presents pits with a diameter increasing with the increase in PMMA-r-PMAA content, while the surface of blends with a high PMMA-r-PMAA content (from 30/70 to 10/90) presents islands with a diameter decreasing with the decrease in PS content.

XPS data confirm that both polymers are present at the surface. The PS-rich phase was removed by immersing the samples in cyclohexane, thereby revealing the remaining PMMA-r-PMAA phase. XPS analyses after treatment by cyclohexane showed that the removal of PS was not complete. Furthermore, analyses at $\varphi = 70°$ showed a decrease of oxygen concentration compared to analyses at $\varphi = 0°$ while before PS dissolution (Table 2), no significant difference was observed between analyses probing different depths. This shows that some PS remains at the extreme surface after dissolution. Since AFM analyses clearly show different surface topographies before and after dissolution and given the enrichment of the remaining PS at the extreme surface, it can be assumed that a thin layer of PS is deposited on the whole surface during the dissolution step.

After PS dissolution, the surface made by the PS/PMMA-r-PMAA 90/10 blend displays islands, some of which are surrounded by crests while others are not. The islands with crest would correspond to pits which could be seen on the surface before dissolution, while the islands showing no crest would be buried inside the bulk before dissolution. In the same way, the surface made by the PS/PMMA-r-PMAA blend 30/70 displays, after the PS phase dissolution, randomly distributed pits also surrounded by a crest.

The comparison of AFM images before and after dissolution shows that the surface of the PMMA-r-PMAA phases, in the as-cast, is always at a lower level than the surface of the PS phases. The solvent affinity for each phase was reported to influence the structure of demixed thin films [7]. As dioxane is a better solvent for PMMA than for PS [20], PS will turn into a solid phase earlier than PMMA-r-PMAA during film formation by spin-coating. Subsequent evaporation of the remaining solvent leads to a collapse of the more soluble polymer (PMMA-r-PMAA), and to the elevation of the other phase (PS)[7]. The presence of the crests, which are in all cases made of PMMA-r-PMAA, was tentatively explained in the literature by the difference of surface tension between the phases [7]. We would rather attribute their formation to adhesion of PMMA-r-PMAA on the more elevated edges of the PS phase which precipitate first.

These observations and considerations lead to the conclusion that the bottom of the pits would be made of PMMA-r-PMAA, surrounded by an elevated PS matrix, while islands would be made of PS surrounded by a lowered PMMA-r-PMAA matrix, as schematically depicted in Figure 5. The surface coverage by the inclusions, as directly measured on AFM images, would then represent the PMMA-r-PMAA pits surface fraction in the case of blends from 90/10 to 70/30, and the PS islands surface fraction for blends from 30/70 to 10/90 (Table 1). The relationship between the surface coverage by the inclusions observed by AFM (Table 1) and the surface coverage by PMMA-r-PMAA deduced from XPS (Table 2) is thus straightforward: they should be similar for the blends with a low PMMA-r-PMAA content, and complementary for the blends with a low PS content, which is indeed the case.

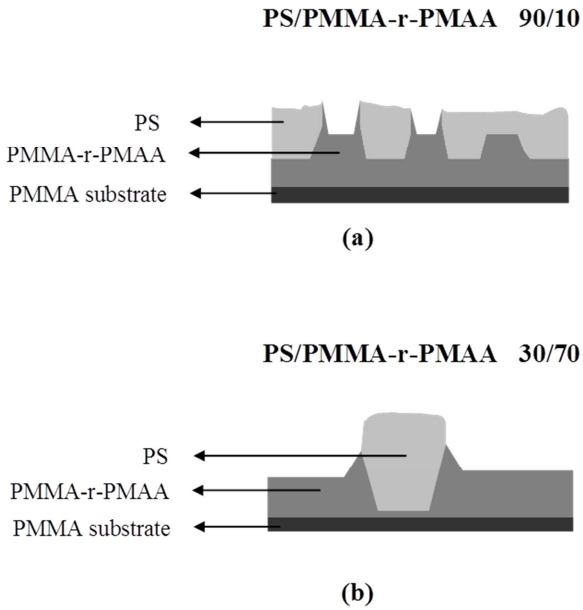


**Figure 5:** Schematic representation of a cross-section through the thin films made from a (a) PS/PMMA-r-PMAA 90/10 blend, (b) and a PS/PMMA-r-PMAA 30/70 blend.

To study the link existing between the blend and surface composition, a comparison of the PMMA-r-PMAA surface fraction (deduced from XPS: f

and f′ - Table 2 - and AFM data – Table 1) with the polymer weight fraction of PMMA-r-PMAA in solution is shown in Figure 6a. The PMMA-r-PMAA fraction is higher at the surface compared to the solution, i.e. the thin films display a surface excess of PMMA-r-PMAA. This trend is especially pronounced for low PMMA-r-PMAA content. If surface composition was driven by surface energy, which is lower for PS than for PMMA-r-PMAA, a surface enrichment of PS would be expected. The reason for the enrichment in PMMA-r-PMAA may be related to the spin-coating process, which leads to rapid evaporation of the solvent, preventing the film to reach the equilibrium state. The different solubilities of PMMA-r-PMAA and PS in dioxane cause demixing of the polymers as the solvent evaporates, leading to surface enrichment of the component with the highest solubility [9].

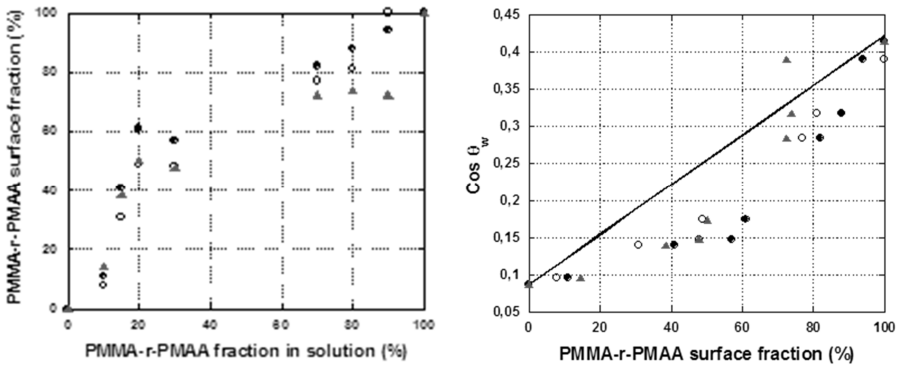


**Figure 6:** Evolution of (a) the PMMA-r-PMAA surface fraction in function of the PMMA-r-PMAA fraction in solution; (b) the water contact angle of thin films in function of the PMMA-r-PMAA surface fraction (solid line: Cassie's law). The PMMA-PMAA surface fraction was evaluated by XPS: f (●) and f'(○) (see Table 2 and text for details) as well as on AFM images (▲).

Both PS and PMMA-r-PMAA are rather hydrophobic polymers, as shown by high water contact angles, but PMMA-r-PMAA is the less hydrophobic, in agreement with the presence of polar functions. The demixed thin films present intermediate hydrophobicity. Figure 6b shows the evolution of cosine of the water contact angle with the surface PMMA-r-PMAA fraction evaluated by XPS and AFM. Clearly, the evolution is not

linear. For heterogeneous surfaces, the Cassie's law predicts that the cosine of the water contact angle is the average of the cosine of the contact angles of the pure phases weighted by their respective surface fraction (line indicated in the graph) [21]. However, this law may no longer apply to systems presenting phases with a significant size (> 100 nm). In that case, the evolution of the static water contact angle, which may be assimilated to an advancing contact angle, is mainly governed by the more hydrophobic phase, on which the three-phases contact line remains anchored [21]. This explains the shape of the curve presented in Figure 6b, with cos $\theta_w$ values lower in all cases than those expected from Cassie's law, due to the predominant effect of PS domains.

## 5. Conclusion

A series of PS/PMMA-r-PMAA heterogeneous substrates was produced by demixing in thin films. Blends with a high PS content (90/10 to 70/30) display randomly distributed pits with a bottom made of PMMA-r-PMAA, surrounded by a PS matrix. Blends with a low PS content (30/70 to 10/90) display randomly distributed PS islands surrounded by a PMMA-r-PMAA matrix. Original and thorough quantitative treatment of the XPS data, on the one hand, and of the AFM images, on the other hand, allowed the fraction of the surface occupied by each polymer to be estimated. A good agreement was found between these methods. Compared to the initial blend composition, the obtained heterogeneous surfaces are, at low PMMA-r-PMAA content, enriched in PMMA-r-PMAA. Selective dissolution of the PS phase gave more insight into the morphology of the observed structures, and showed PMMA-r-PMAA crests at the interface with PS. The surface relief created by the inclusions, the PMMA-r-PMAA crest formation and the surface enrichment in PMMA-r-PMAA may be explained by the higher solubility of PMMA-r-PMAA compared to PS in the solvent used for spin-coating. The correlation existing between the surface PMMA-r-PMAA fraction and the cosine of the water contact angle deviates from linearity (i.e. does not follow Cassie's law) which may be attributed to the predominant effect of the more hydrophobic PS domains. The obtained heterogeneous

surfaces are currently used to investigate their influence on protein adsorption and on cell behaviour [22].

## 6. References

[1] M.J.Dalby, D.Giannaras, M.O.Riehle, N.Gadegaard, S.Affrossman, A.S.G.Curtis, Biomaterials 25 (2003) 77.

[2] M.J.Dalby, L.Di Silvio, E.J.Harper, W.Bonfield, Biomaterials 23 (2001) 569.

[3] E.Pamula, V.De Cupere, Y.F.Dufrene, P.G.Rouxhet, J. Colloid Interface Sci. 271 (2004) 80.

[4] S.E.Woodcock, W.C.Johnson, Z.Chen, J. Colloid Interface Sci. 292 (2005) 99.

[5] J.Y.Lim, J.C.Hansen, C.A.Siedlecki, R.W.Hengstebeck, J.Cheng, N.Winograd, H.J.Donahue, Biomacromolecules 6 (2005) 3319.

[6] G.Krausch, M.Hipp, M.Boeltau, O.Marti, J.Mlynek, Macromolecules 28 (1995) 260.

[7] S.Walheim, M.Boeltau, J.Mlynek, G.Krausch, U.Steiner, Macromolecules 30 (1997) 4995.

[8] Z.Qi, Z.Li, X.Xie, Macromol. Chem. Phys. 205 (2004) 1116.

[9] C.Ton-That, A.G.Shard, R.H.Bradley, Polymer 43 (2002) 4973.

[10] C.M.Dekeyser, S.Biltresse, J.Marchand-Brynaert, P.G.Rouxhet, C.Dupont-Gillain, Polymer 45 (2004) 2211.

[11] C.Ton-That, A.G.Shard, D.O.H.Teare, R.H.Bradley, Polymer 42 (2000) 1121.

[12] C.Ton-That, A.G.Shard, R.Daley, R.H.Bradley, Macromolecules 33 (2000) 8453.

[13] K.Tanaka, A.Takahara, T.Kajiyama, Macromolecules 29 (1996) 3232.

[14] L.Cui, Y.Ding, X.Li, Z.Wang, Y.Han, Thin Solid Films 515 (2006) 2038.

[15] C.Ton-That, A.G.Shard, R.H.Bradley, Langmuir 16 (2000) 2281.

[16] L.Kailas, B.Nysten, P.Bertrand, Surf. Interface Anal. 36 (2004) 1227.

[17] B.Gottenbos, H.C.van der Mei, F.Klatter, D.W.Grijpma, J.Feijen, P.Nieuwenhuis, H.J.Busscher, Biomaterials 24 (2003) 2707.

[18] B.Gottenbos, D.W.Grijpma, H.C.van der Mei, J.Feijen, H.J.Busscher, J. Antimicrob. Chemother. 48 (2001) 7.

[19] G.Beamson, D.Briggs, High resolution XPS of organic polymers: the scienta ESCA300 Database, John Wiley, Chichester, 1992.

[20] J. Brandrup, E.H. Immergut, E.A. Grulke, Polymer Handbook, 4$^{th}$ edition, John Wiley, Hoboken, 1999.

[21] R.E. Johnson, R.H. Dettre, in: Surface and Colloid Science, Volume 2, Matijevic E. (Ed.), Wiley-Interscience, New York and London, 1969, 85.

[22] C.M.Dekeyser, E.Zuyderhoff, R.E.Giuliano, H.J.Federoff, Ch.C.Dupont-Gillain, P.G.Rouxhet, J. Biomed. Mater. Res. submitted (2007).

# Chapter II

# Nano-organized collagen layers obtained by adsorption on phase-separated polymer thin films


### *Summary*

The organization of adsorbed type I collagen layers was examined on a series of polystyrene (PS)/ poly(methyl methacrylate) (PMMA) heterogeneous surfaces obtained by phase separation in thin films. These thin films were prepared by spin coating from solutions in either dioxane or toluene of PS and PMMA in different proportions. Their morphology was unraveled combining the information coming from X-ray photoelectron spectroscopy (XPS), atomic force microscopy (AFM) and water contact angle measurements. Substrates with PMMA inclusions in a PS matrix and conversely, substrates with PS inclusions in a PMMA matrix were prepared, the inclusions being either under the form of pits or islands, with diameters in the submicrometer range. The organization of collagen layers obtained by adsorption on these surfaces was then investigated. On pure PMMA, the layer was quite smooth with assemblies of a few collagen molecules, while bigger assemblies were found on pure PS. On the heterogeneous surfaces, it appeared clearly that the diameter and length of collagen assemblies was modulated by the size and surface coverage of the PS domains. If the PS domains, either surrounding or surrounded by the PMMA phase, were above 600 nm wide, a heterogeneous distribution of collagen was found, in agreement with observations made on pure polymers. Otherwise, fibrils

could be formed, that were longer compared to those observed on pure polymers. Besides, the surface nitrogen content determined by XPS, which is linked to the protein adsorbed amount, increased roughly linearly with the PS surface fraction, whatever the size of PS domains, suggesting that adsorbed collagen amount on heterogeneous PS/PMMA surfaces is a combination of that observed on the pure polymers. This work thus shows that PS/PMMA surface heterogeneities can govern collagen organization. This opens the way to a better control of collagen supramolecular organization at interfaces, which could in turn allow cell – material interactions to be tailored.

# 1. Introduction

The understanding and control of cell behavior on artificial materials is a key issue for the elaboration of innovative approaches in the field of biomaterials. The critical step for colonization of a material by cells is cell adhesion on the surface of the material. This adhesion step is mediated by adhesion proteins (such as collagen, fibronectin, laminin, etc) containing specific adhesion sequences which serves as ligand for cell receptors.[1] The nature of the proteins as well as their conformation and organization within the adsorbed layer may strongly influence the receptor-ligand recognition, and thereby modify cell adhesion and further cell behavior.[2, 3] Accordingly, understanding and controlling the supramolecular organization of adhesion protein layers on artificial surfaces is a challenge of importance.[4-6]

Type I collagen is a frequently used adhesion protein for *in vitro* cell applications. Furthermore, this extracellular matrix protein plays an important role in the formation of tissues and organs, and influences cell expression in many cases. Collagen organization was shown to strongly influence cell behavior at interfaces.[3, 7] The collagen type I molecules are semiflexible rods of approximately 300 nm in length and 1.5 nm in diameter and have the ability to self-assemble. The association of five molecules serves as a basis for the formation of microfibrils which can further grow into larger fibers. Fibrils have been shown to form *in vitro* as well as *in vivo*.[8, 9]

While adsorption is driven for most proteins by a gain of conformational entropy, collagen adsorption is mainly due to a gain of solvent entropy when hydrophobic patches of the molecule contact either hydrophobic substrates areas or hydrophobic patches from other collagen molecules.[9] Besides, it has been shown that adsorbed collagen structure strongly depends on the adsorption conditions, the following factors being crucial: characteristics of the collagen solution used for the adsorption (concentration,[10] state of aggregation,[10, 11] collagen conformation (native vs. denatured),[12, 13] pH,[11, 14] ionic strength[14, 15]), duration of adsorption,[12, 16] as well as drying step after adsorption.[17, 18] It was also demonstrated that the substrate surface properties were critical for adsorbed collagen

organization.[7, 19] Regarding the influence of surface hydrophobicity, Gurdak et al observed that the tendency of collagen to form fibrils in the adsorbed phase was correlated with the contact angle of the surface: the more the surface was hydrophobic, the more collagen formed fibrils.[10] In addition to that, Pamula et al observed a higher affinity of collagen for polystyrene compared to surface- oxidized polystyrene.[16] Regarding surface topography, Denis et al compared the formation of collagen fibrillar structures on $CH_3$-terminated self-assembled monolayers on smooth or rough substrates and demonstrated that roughness may prevent fibril formation, which was attributed to a reduced lateral mobility of adsorbed molecules.[20]

Since the micro- or nanopatterning of proteins has been shown to strongly influence cell behavior, it has become an active area of investigation.[4-6] Many advanced techniques, such as micro-contact printing and microfluidic patterning, have been developed to pattern proteins on surfaces. However, these techniques are expensive, cumbersome and cannot be easily scaled up for widespread use and large production.[6] Therefore, more direct and easier approaches are now envisioned. Since protein organization after adsorption is strongly influenced by surface chemical composition, proteins can be directly adsorbed onto heterogeneous polymer thin films to obtain protein patterns. Recent reports have demonstrated that block copolymers could be used as protein pattern templates. Liu et al used diblock copolymers containing two hydrophobic blocs, namely polystyrene-b-polyisoprene (PS-b-PI) and showed that albumin and fibronectin tend to adsorb selectively on PS domains. Soft PI domains would be protein repellent compared to hard PS domains because of the high molecular mobility of PI at room temperature.[21, 22] PS domains also seem to be more favorable to protein adsorption than more hydrophilic blocks such as poly(methyl methacrylate) (PMMA). Kumar et al used an amphiphilic diblock copolymer of PS-b-PMMA to control the spatial distribution of fibronectin, albumin and immunoglobulin G (IgG), by using short adsorption times and low protein concentrations. Their results indicated that protein adsorption was highly favored on the PS blocks as well as on the PS/PMMA interfaces.[23] Using a similar copolymer, Lau et al also observed that IgG accumulated at PS/PMMA interfaces, and mentioned that the adsorbed

amount on the PS/PMMA copolymer surface was not an average of the adsorption behavior on PS and PMMA but was enhanced with respect to both types of polymer surfaces.[24] Matsusaki et al showed that a PS-b-PMMA copolymer with a 48 nm lamellar spacing could be used to align proteins after short adsorption times. Fibronectin, fibrinogen and γ-globulin were found to be forced to align on the PS domains while collagen did not show any preferred orientation after adsorption.[25] However, it was also shown that collagen could be aligned on amphiphilic patterns of similar size obtained by a combination of electron-beam lithography and silane grafting, using longer adsorption times.[26]

Besides the use of copolymers to obtain heterogeneous thin films, an even more simple method is the preparation of phase-separated polymer blend surfaces. While amphiphilic diblock copolymers separate into domains on the nanometer scale, thin films of immiscible polymer mixtures separate with domain sizes typically on the submicro- to micrometer scale.[27] It was demonstrated that this type of heterogeneous surfaces could also be used to obtain protein patterns. Dekeyser et al investigated the organization of fibronectin on blends of PS and poly(methyl methacrylate) – poly(methacrylic acid) random copolymer (PMMA-r-PMAA). Different states of aggregation of adsorbed fibronectin were observed on PS and PMMA-r-PMAA and these behaviors were maintained on phase-separated samples, leading to substrates with heterogeneous protein organizations.[2] Besides, PS/PMMA blends were also studied as templates for protein patterning. As observed on PS-b-PMMA copolymers after short adsorption time, albumin was found to adsorb preferentially on PS and at PS/PMMA interfaces. Furthermore, by investigating longer adsorption times on those blends, a net loss of protein from the interfaces was observed together with a gain on the PMMA domains.[28]

In this study, we investigate the influence of heterogeneous substrates on the organization of adsorbed type I collagen. The heterogeneous substrates were produced by phase separation in thin films of blends of PS, a hydrophobic polymer, and PMMA, a more hydrophilic polymer. A series of substrates with different morphologies, chemistries and wettabilities was obtained by varying the polymer concentration ratio and the solvent used for

thin film elaboration. The surfaces obtained before and after collagen adsorption were analyzed by X-ray photoelectron spectroscopy (XPS), atomic force microscopy (AFM) and wetting measurements.

# 2. Materials and methods

## 2.1. Preparation of thin films of PS/PMMA

Phase-separated polymer thin films were produced by spin-coating (speed = 5000 rpm, acceleration = 20,000 rpm/s, time = 40 s) a 40 µl drop of blends of PMMA ($M_w$ ~ 996,000 g/mol, $T_g$ 125° C ; from Aldrich, USA) and PS ($M_w$ ~ 230,000 g/mol, $M_n$ ~ 140,000 g/mol; from Merck, Germany) dissolved in a common solvent (dioxane (Fluka, Switzerland) or toluene (Merck, Germany)) onto a silanized glass coverslip (12 mm in diameter; Menzel-Glaser, Germany). The silane used for grafting the glass coverslips, methacryloxypropyltrimethoxysilane (MOPTMS; Gelest, Germany), was chosen in order to improve polymer adhesion to glass. The glass coverslips were cleaned by immersion for 30 min in a freshly prepared piranha solution (30 % $H_2O_2$:98 % $H_2SO_4$, 1:3). After that, the silanization reaction was performed for 4 h, using a silane concentration of 0.01M in dioxane. Finally, the grafted coverslips were rinsed a couple of times with ethanol and dried under a nitrogen flow. The obtained silanized glass was rather hydrophilic (water contact angle of about 30°) meaning that the amount of grafted MOPTMS is low but still sufficient to improve adhesion. After spin coating on these substrates, the thickness of the PS and PMMA films was about 40 nm, as consistently measured by ellipsometry and by AFM (on a scratch produced on the film in the latter case). In order to obtain substrates having different morphologies, several polymer solutions containing different PS/PMMA ratios were prepared in either dioxane or toluene: 90/10 w/w in dioxane (90/10d), 30/70 w/w in dioxane (30/70d), 05/95 w/w in toluene (05/95t) and 30/70 w/w in toluene (30/70t). The total polymer concentration was always 10 g/l. Homogeneous films of PS and PMMA, prepared in the same conditions as stated above from solution in toluene, were also used as controls (pure PS (100/0t) and pure PMMA (0/100t), respectively).

## 2.2. Collagen adsorption

Collagen from calf skin (90 % type I and 10 % type III) was purchased as a 4 mg/ml solution from Biochrom AG, UK. Collagen solution at 25 µg/ml was prepared by dilution at 4°C in phosphate buffer saline (PBS) (pH 7.4; PBS tablets, Invitrogen, USA) and then warmed at 37°C for 15 min just before proceeding to adsorption. The samples were placed in a multiwell tissue culture plate (12-well plate, one sample per well), 2ml of the collagen solution were poured into each well and the plate was incubated at 37°C for 3 h. The samples were then rinsed with ultra-pure water (milli-Q, Millipore, Molsheim, France) without being withdrawn from the solution, and dried under nitrogen flow.

## 2.3. Atomic Force Microscopy (AFM)

The AFM analyses were performed in air and at room temperature with a Nanoscope IIIa multimode apparatus (Digital Instruments, Santa Barbara, USA) in tapping mode. The tips used were made of silicon, and had a spring constant comprised between 20 and 80 N/m and a resonance frequency in air between 212 and 319 kHz (Bruker, Palaiseau, France). The scan rate was about 0.6 Hz and all images were recorded in moderate tapping (set-point amplitude ratio, $r_{sp}$= 0.6-0.8). Randomly chosen zones were imaged for each sample and for each zone, height and phase images were recorded upon scanning. All obtained images were processed with the Nanoscope analysis software, using either flattening or plane fit according to the relief characteristics, with the minimal polynomial order needed. The proportion of the surface occupied by the inclusions was determined using the "bearing analysis" function of the Nanoscope analysis software. The bearing analysis calculates and displays height histograms and bearing-ratio curves for selected areas on images. The bearing-ratio curve is the integral of the height histogram; it represents the fraction of data points above a reference plane as a function of the depth of that plane below the highest point.

## 2.4. X-ray Photoelectron Spectroscopy (XPS)

The XPS analyses were performed with a Kratos Axis Ultra spectrometer (Kratos Analytical – Manchester – UK) equipped with a monochromatised aluminium X-ray source (powered at 10 mA and 15 kV). The pressure in the analysis chamber was about $10^{-6}$ Pa. The direction of the photoelectron collection was normal to the sample surface. Analysis was performed in the hybrid lens mode with the slot aperture, resulting in an analysed area of 700 µm x 300 µm. The pass energy was set at 160 eV for the wide scan and at 40 eV for narrow scans. In the latter conditions, the energy resolution gives a full width at half maximum (FWHM) of the Ag $3d_{5/2}$ peak of a standard silver sample of about 0.9 eV. Charge stabilization was achieved by using the Kratos Axis device. The following sequence of spectra was recorded: survey spectrum, C 1s, O 1s, N 1s, Si 2p and C 1s again to check the stability of charging potential and the absence of degradation of the samples during the analysis. The binding energies were calculated with respect to the C-(C,H) component of the C 1s peak fixed at 284.8 eV. Molar concentration ratios were calculated using peak areas normalized according to acquisition parameters and sensitivity factors provided by the manufacturer. Peak decomposition was achieved with the Casa XPS software (Casa Software Ltd, UK), after subtraction of a linear baseline. The results were expressed in element mole fractions, excluding hydrogen which is not detected by XPS.

## 2.5. Water contact angle measurements

Static water contact angles ($\Theta_w$) were measured at ambient temperature using the sessile drop method and image analysis of the drop profile. The instrument, using a CCD camera and an image analysis processor, was purchased from Electronisch Ontwerpbureau De Boer (The Netherlands). The water (milli-Q, Millipore, Molsheim, France) droplet volume was 0.3 µl, and the contact angle was measured 5 s after the drop was deposited on the sample. For each sample, the reported value is the average of the results obtained on at least 9 droplets.

# 3. Results and discussion

## 3.1. Characterization of the substrates before collagen adsorption

Typical AFM images of the prepared PS/PMMA polymer films are presented in Figure 1. Different topographies were observed (see height images): the 30/70t and 30/70d samples present islands (with domains up to 1 µm in length and ~8 nm in height, and domains from 150 to 450 nm in diameter and ~2 nm in height, respectively), the 05/95t film presents holes (from 50 to 150 nm in diameter and ~8 nm deep) and the 90/10d film has little topography. Note that pure PS and pure PMMA films show quite smooth topography (data not shown). Contrast was also observed on the phase images. For the blends 30/70t, 30/70d and 05/95t, the observed inclusions correspond to the one found on height images, while for the 90/10d, a phase contrast is also recorded, showing inclusions (from 50 to 300 nm in diameter) which were not apparent on the height image. The phase contrast indicates the location of PS and PMMA surface or subsurface areas. PS areas are indeed revealed as dark regions, with a phase shift smaller than for the light PMMA regions.[24, 29] This may be attributed to a difference in adhesion between the silicon cantilever and PS or PMMA. From then on, PS fraction in surface or subsurface is determined for each blend by measuring the proportion of the surface occupied by the inclusions on the phase images (see Table 1). The results show that the more the PS content in solution increases, the more PS covers the surface. The surface coverage by PS is however not identical to its proportion in solution (see discussion below). Furthermore, the solvent used influences this surface coverage: for 30/70 PS /PMMA blends, the measured PS surface fraction is 61 % in the case of toluene while it is only 36 % with dioxane.

Static water contact angle values measured on these films are presented in Table 1. The values measured on pure PMMA (71°) and pure PS (90°) are close to those reported in the literature for these polymers[27, 30] and the contact angles measured on phase-separated thin films show intermediate values, which increase with the PS content of the polymer solution.

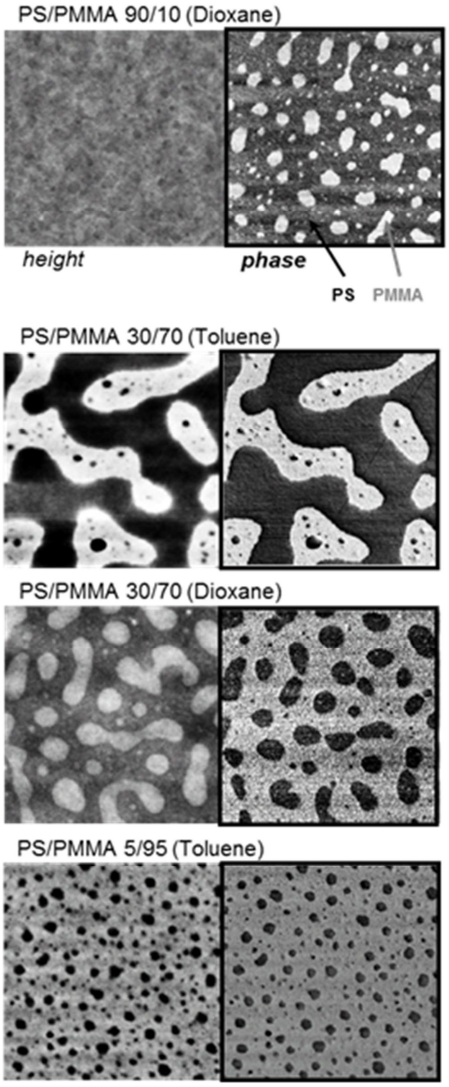


**Figure 1:** AFM images (2.5 x 2.5 µm²) obtained on four PS/PMMA blends. For each blend, height (Z=10 nm) and phase (z=10°, framed image) images are presented. Solvent and PS/PMMA ratio used are indicated above the corresponding images. On the phase images, PS areas appear in dark and PMMA areas appear in light (see text for details). Scale bars = 500 nm.

The surface elemental composition of the films was determined by XPS. The XPS survey spectra showed, as expected, only the presence of oxygen and carbon (data not shown). Table 1 presents the elemental composition of the films determined from individual spectra, expressed in O/C mole fraction ratio (note that less than 1 % of Si was sometimes

recorded on the individual spectra). On pure PS, the oxygen signal was below the detection limit as expected for this polymer, while for PMMA, the ratio was slightly lower (33 %) than the value expected based on PMMA stoichiometry (40 %). This difference may be mainly attributed to an underestimation of the proportion of oxygen, in reason of the inaccuracy of the sensitivity factors provided by the manufacturer, as also indicated by the analysis of other materials. The surface elemental composition of blend films is intermediate between those of the two pure polymers, and the O/C ratio is increasing with the PMMA content of the polymer solution. The 30/70 PS/PMMA blends behave again differently, a higher O/C ratio being recorded on the one prepared from dioxane compared to the one prepared from toluene, in agreement with the lower PS fraction measured by AFM on the former compared to the latter.

**Table 1:** Water contact angle ($\Theta_w$), XPS and AFM data for thin films of PS and PMMA

| | PS / PMMA solvent | | | | | |
|---|---|---|---|---|---|---|
| | **100 / 0 toluene** | **90 / 10 dioxane** | **30/70 toluene** | **30/70 dioxane** | **05/95 toluene** | **0/100 toluene** |
| ***Contact angle*** | | | | | | |
| $\Theta_w$ (°)[a] | 90.2 ± 0.6 | 85.2 ± 1.1 | 84.7 ± 0.3 | 75.5± 0.8 | 74.8 ± 0.4 | 70.8 ± 0.5 |
| ***XPS*** | | | | | | |
| n[b] | 6 | 3 | 6 | 2 | 2 | 5 |
| (O / C) * 100 [c] | 0 (0) | 4 (1) | 8 (2) | 20 (1) | 28 (2) | 33 (1) |
| PS fraction in surface, f (%)[c] | 100 (1) | 82 (2) | 70 (8) | 32 (2) | 10 (2) | 0 (2) |
| ***AFM*** | | | | | | |
| n[d] | | 3 | 6 | 3 | 5 | |
| PS fraction in surface (%)[c] | / | 79 (1) | 61 (10) | 36 (1) | 16 (1) | / |

[a] Contact angle is given with confidence interval at 95% (at least 9 measurements)
[b] Number of measurements on independent samples
[c] Standard deviation is given between brackets
[d] Number of measurements on independent images

The C 1s spectra recorded on the pure polymers and on the four PS/PMMA blends are presented in Figure 2. The C 1s peak of PS contains a main component which corresponds to carbon bound to carbon and/or hydrogen ( C- (C,H)), situated slightly below 284.8 eV due to the aromatic character of carbon atoms, and a shake-up peak around 292 eV due to Π-Π*

transitions in the aromatic ring. The C 1s peak of PMMA presents, as expected, four components[31] which correspond to the different types of carbon atoms: carbon bound only to carbon or hydrogen at 284.8 eV (C-(C,H)); carbon bound to a carbon itself bound to two oxygen atoms at 285.5 eV ( C-(COO)); carbon singly bound to oxygen at 286.6 eV (C-O) and carbon involved in an ester function at 288.8 eV (O-C=O).

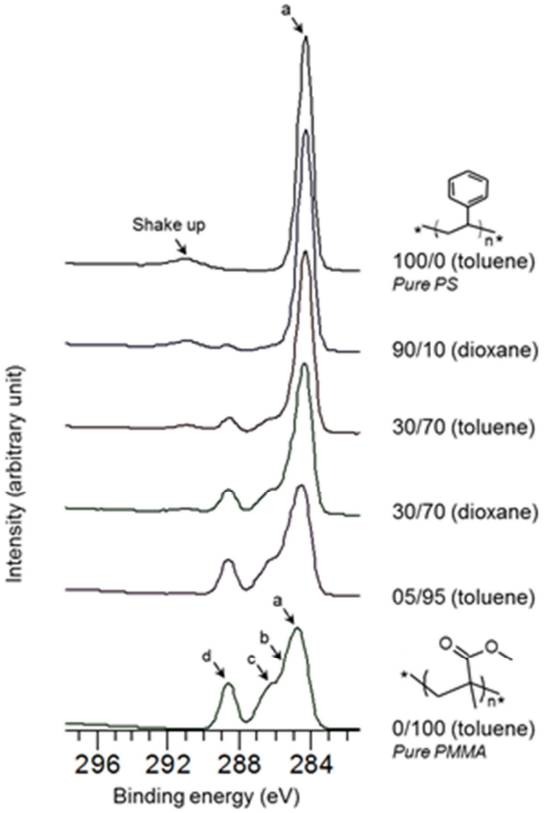


**Figure 2:** C1s spectra for polymer films according to the PS/PMMA ratio in solution. (a)-(d) indicate different components of the pure polymers C1s spectra: C-(C,H) (a), C-COO (b), C-O (c), O-C=O (d). The chemical structure of PS and PMMA are given in insets.

The C 1s peaks obtained for the PS/PMMA phase-separated thin films clearly show a contribution of both polymers which allow classifying them according to the importance of the components attributed to PS: 100/0 > 90/10d > 30/70t > 30/70d > 05/95t > 0/100 (in descending order). XPS data have been further treated to evaluate the proportion of both polymers in

the surface layer probed by XPS (depth of about 10 nm). The method used consists in computing the PS surface fraction starting from the C and O mole fractions determined by XPS. If the surface is considered as made of patches of PS and PMMA which are thicker than the analyzed depth, and if the differences of density and (C+O) concentration between the two pure polymers are neglected, the O/C ratio measured on the blends, $(O/C)_{exp}$, can be expressed as:

$$\left(\frac{O}{C}\right)_{exp} \approx \frac{f\, O_{PS}^{exp} + (1-f)\, O_{PMMA}^{exp}}{f\, C_{PS}^{exp} + (1-f)\, C_{PMMA}^{exp}} \qquad \text{[eq. 1]}$$

where f is the PS surface fraction, $O_{PS}^{exp}$ and $O_{PMMA}^{exp}$ are the oxygen mole fraction and $C_{PS}^{exp}$ and $C_{PMMA}^{exp}$ are the carbon mole fraction given by the XPS analysis of pure PS and pure PMMA, respectively. The computed f values, reported in Table 1, are in good agreement with the PS surface fractions calculated from AFM images.

Contact angle values measured on phase-separated thin films (see Table 1) confirm that both polymers are present at the extreme surface, indicating that the PS fraction calculated with AFM and with XPS should not only be related to the subsurface. Combining these results, it appears that the 5/95t and 30/70d blends show a PMMA matrix with PS inclusions (pits and islands, respectively), while the 30/70t and 90/10d blends show a PS matrix with PMMA inclusions (islands and no apparent topography, respectively). The morphology of these films appears to fall into two categories: surfaces prepared from toluene with elevated PMMA phases, and surfaces prepared from dioxane with PS elevated phases or no topography. This difference can be explained by the respective solubility of the polymers in each of the solvents (see Supporting Information for more details regarding the factors affecting the morphology of these films, p134).

The surface fraction of PS, determined by XPS and AFM, differs significantly from the PS fraction introduced in solution (see Table 1 for details and Table S-1 in Supporting Information for summary, p135). Note that these values can only be compared assuming similar densities for PS and PMMA, which is reasonable ($\rho_{PMMA}$~1.15 and $\rho_{PS}$~1.05).[32] For

PS/PMMA blends at equilibrium in air, surface enrichment by PS would be expected since this would lower the surface energy. Thin films produced by spin coating are however not at equilibrium. The component with the highest solubility is then supposed to be enriched in the surface layer.[33] PS is indeed significantly more present at the interface compared to the solution for films prepared with toluene. This is less clear for PMMA in the case of dioxane. This could again be explained by the high molecular mass of the PMMA used. As a longer polymer chain at the surface suffers a more severe conformational entropy penalty, the surface is more favorably covered by the component with a lower molecular mass.[34]

The phase-separated thin films present intermediate hydrophobicity compared to pure PS and pure PMMA, as shown by their intermediate water contact angle values (see Table 1). These values are not linearly correlated with the PS fraction in surface (see Supporting Information, Figure S-1, p135) but seem to be linked to the hydrophobicity of the polymer forming the matrix. Indeed, the 90/10d and the 30/70t blends, which present a PS matrix, have water contact angle values (85.2° and 84.7°) closer to the one of pure PS, while these of 30/70d and 5/95t blends (75.5° and 74.8°, respectively), which present a PMMA matrix, are closer to the one of pure PMMA. For a chemically heterogeneous surface, the Cassie's law predicts that the cosine of the water contact angle is the average of the cosines of the contact angles of the pure phases weighted by their respective surface fraction.[35] In the present work, such a correlation is not observed, neither for toluene nor for dioxane, and whatever the size of the inclusions. This law however applies to regularly distributed heterogeneities of a limited size, and smooth and default-free surfaces, which is not the case here.

## 3.2. Characterization of the substrates after collagen adsorption

The collagen layer organization on the pure polymers and on the phase-separated thin films was assessed by AFM. Height tapping mode images of collagen adsorbed on the pure polymers are shown on Figure 3. The layer appears to be quite smooth on pure PMMA, with collagen assemblies of a few molecules, about 4 nm in height and from 300 to 600 nm in length. This height could be attributed to the formation of pentamers. In

the case of pure PS, the size and the shape of collagen assemblies appear to be different. Assemblies seem to be composed of several arms of ~300 nm in length and 10 nm in height associated together in an anchoring knot of ~20 nm in height. These results are in good agreement with previous observations respectively made on PMMA[18] and on PS[10-12, 16, 17]. It was shown that the key parameter of the supramolecular organization of adsorbed collagen layers was substrate hydrophobicity. Collagen molecules adsorbed on hydrophobic surfaces would interact through some segments with the substratum and would leave other segments protruding into the solution, which would be free for self-assembly with other collagen molecules. On hydrophilic surfaces, the rate of adsorption would be slowed down, leaving time for the molecules to interact with their full length with the substrate. Adsorbed collagen would then form a mechanically resistant layer of entangled molecules, which are unavailable for self-assembly with other collagen molecules.[17]

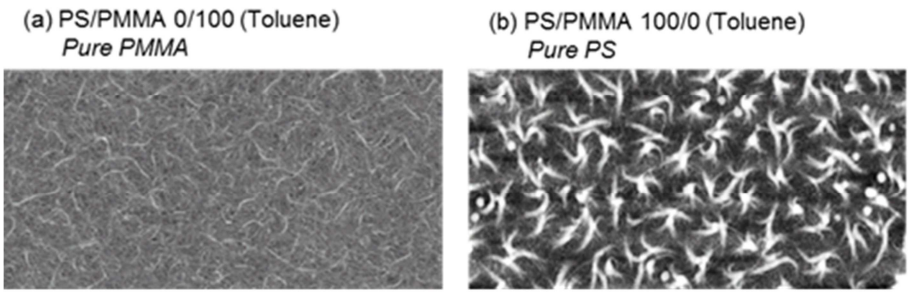


**Figure 3 :** AFM images (5 x 2.5 µm²; z = 30 nm, height mode) obtained on (a) pure PMMA and (b) pure PS films after collagen adsorption. Scale bars = 500 nm.

On heterogeneous PS/PMMA thin films, adsorbed collagen organization is different depending on the PS/PMMA ratio and the solvent used, as illustrated in Figure 4. On the films presenting a PMMA matrix with PS inclusions (05/95t and 30/70d), the height of assemblies appears to be smaller than the one of those observed on the films presenting a PS matrix with PMMA inclusions (30/70t and 90/10d).

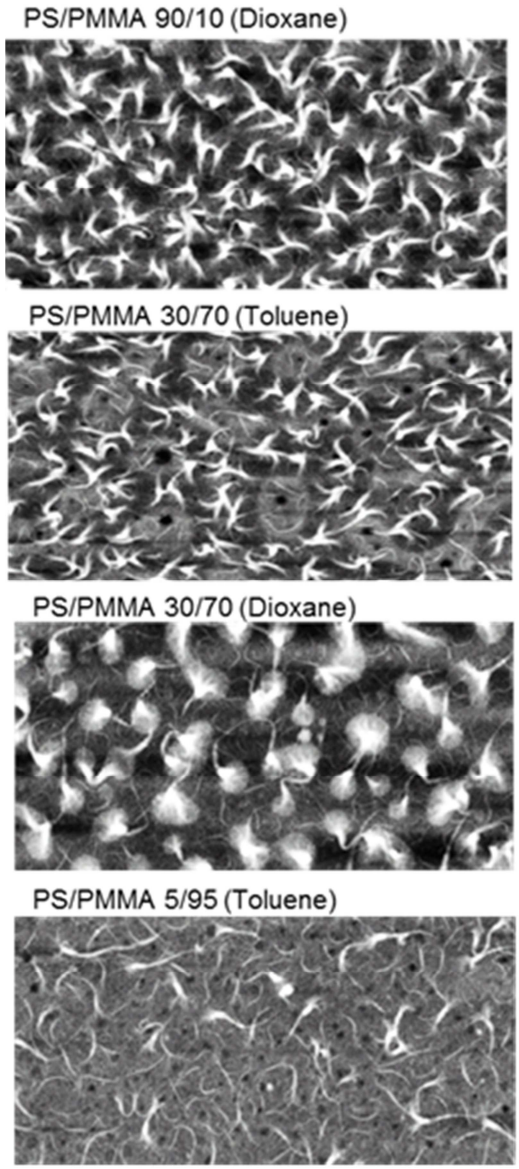


**Figure 4:** AFM images (5 x 2.5 µm²; z = 30 nm, height mode) obtained on heterogeneous PS/PMMA thin films after collagen adsorption. Solvent and PS/PMMA ratio used for thin film preparation are indicated above each image. Scale bars = 500 nm.

On the 05/95t film, which has PS inclusions with a surface coverage of about 10 %, the size of most of the assemblies is similar to that observed on pure PMMA, and a few bigger assemblies (up to 1 µm in length and 15 nm in

height), covering ~4 % of the surface, appear to be anchored in the PS inclusions. It seems that these PS inclusions of 50 to 150 nm wide are too small to allow the formation of big assemblies such as those found on pure PS. In the case of the 30/70d film (30 % of PS in the surface layer), the PS inclusions are larger (up to 450 nm). After collagen adsorption, the PMMA matrix is also covered by assemblies similar than on pure PMMA, and PS inclusions are clearly identified as the anchoring points for the formation of bigger assemblies, which extend further into the PMMA matrix. Because these assemblies tend to bridge two inclusions, their length can be very high (more than 1 µm) and their height varies from ~20 nm on inclusions to 4 – 8 nm when they reach the matrix. By comparison, the collagen layers observed on the heterogeneous films with a PS matrix (30/70t and 90/10d) are closer to those observed on pure PS, and most of the assemblies show a shape and size that are similar to those found on pure PS. On the 30/70t blend, these big assemblies clearly avoid areas corresponding to the PMMA inclusions, which appear to be covered by smaller assemblies, having similar sizes than those observed on pure PMMA. Finally, the collagen layer observed on the 90/10d blend, which corresponds to a surface covered at 80 % by PS, is very similar to that observed on pure PS, but some smaller assemblies similar to those observed on PMMA are observed as well.

As already demonstrated by the contact angle measurements combined with AFM phase images and XPS analyses on the phase-separated thin films, the morphology of the obtained collagen layers confirms the surface chemical heterogeneity of substrates, which leads to different modes of collagen assembly. The results also confirm that assemblies observed in adsorbed collagen layers are not formed in solution, prior to adsorption, but are built at the interface, through the assembly of free segments of adsorbed molecules, as previously demonstrated.[11] Moreover, the longer assemblies obtained on the 05/95t and 30/70d films compared to the ones observed on the pure polymers show that the size of PS inclusions in a PMMA matrix could interfere with the length of the obtained assemblies. If the size of inclusions is below 600 nm in diameter, the assemblies usually found on PS (several arms of 300 nm) cannot be formed. Similarly, on the films presenting a PS matrix (30/70t and 90/10d), assemblies closer to those

observed on pure PS were found because the distance between PMMA inclusions is longer than 600 nm. Whatever the surface, collagen assemblies found on PS areas seem to have anchoring knots with a higher height than the rest of the assembly. Under liquid, these knots would be the anchoring point of collagen molecules on the PS areas, leaving free segments in the solution. These free segments would then be pushed along the surface plane by the drying step, as evidenced before.[17] To enhance the observation of the position of these knots on the heterogeneous surfaces, a topographic Z scale with different colors was used, allowing specific topographic features to be highlighted. Figure 5 shows the adsorbed collagen organization on pure PS and on the 30/70d blend with the multiple colors scale. The anchoring knots clearly appear in blue. It seems that these knots are preferentially located at the interface between PS and PMMA areas rather than in the middle of the PS inclusions (see Figure 5b).

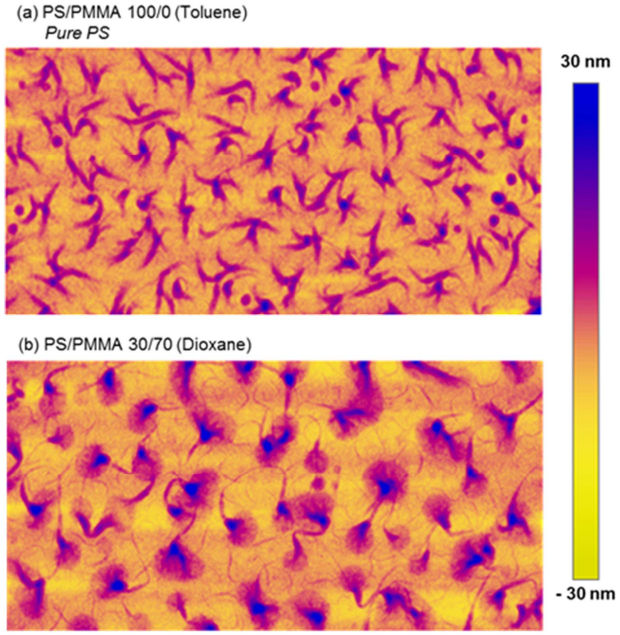


**Figure 5:** AFM images (5 x 2.5 µm²; z = 30 nm, height mode) recorded after collagen adsorption on (a) pure polystyrene and (b) PS/PMMA 30/70d. A multiple color scale was used to highlight the presence and location of anchoring knots in collagen assemblies. Scale bars = 500 nm.

The nitrogen surface concentration, which is related to the detected amount of collagen, was determined by XPS on a series of PS/PMMA films after collagen adsorption. Figure 6 illustrates the influence of the PS fraction in the surface layer on the detected nitrogen mole fraction after collagen adsorption. It shows that the nitrogen surface concentration increases roughly linearly with the PS surface fraction, suggesting that collagen adsorbed amount on heterogeneous PS/PMMA surfaces can be described as a combination of that observed on the pure polymers. Accordingly, even if the phase-separated thin film presents inclusions smaller than 600 nm in diameter, interfering with the length of the formed collagen assemblies as shown above, the detected collagen amount remains a combination of the amounts detected after adsorption on the pure polymers, weighted by their respective surface coverage levels. Such a result contrasts with previous studies performed with other proteins on PS/PMMA heterogeneous surfaces.[23, 24, 28]

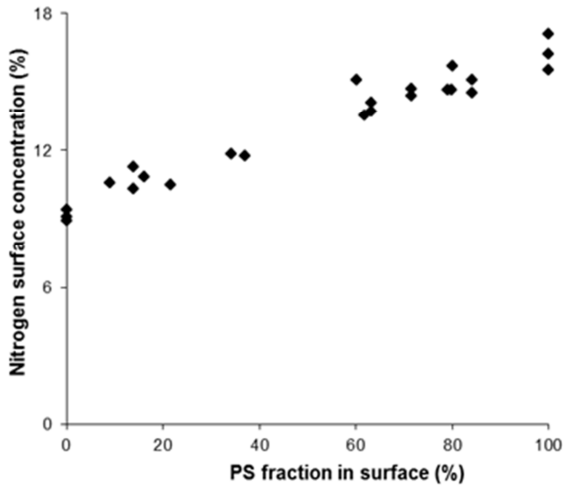


**Figure 6.** Evolution of the nitrogen surface concentration determined by XPS after collagen adsorption in function of the PS surface fraction determined by XPS on PS/PMMA thin films before adsorption.

These studies indicated that adsorbed albumin amounts found on heterogeneous surfaces were not an average of those found on the pure

polymers because of an accumulation of adsorbed proteins in the interfacial areas between the PS and PMMA domains. Even if preferential anchoring points are observed here in these interfacial areas, there is no evidence for the accumulation of collagen molecules at the contact lines between the matrix and the inclusions. This difference can be attributed to the driving force for adsorption, which strongly depends on the protein deformability.[36] While albumin is known to change its conformation upon adsorption to maximize interactions with the substrate, this is not the case for collagen in reason of its more rigid structure.

Our results also differ from a previous study related to collagen adsorption on PS/PMMA heterogeneous surfaces.[37] While we show that the diameter and length of collagen assemblies is modulated by the size and surface coverage of surface heterogeneities, these authors obtained branched structures on PMMA and network structures on PS. These different behaviors can be explained by the use of different adsorption conditions. Woodcock and coworkers used high concentrations, short adsorption times and slow drying steps, while we used low concentrations, longer adsorption times and fast drying steps. However, both works demonstrate that collagen adsorption on phase-separated thin films leads to a behavior which is intermediate compared to the one observed on the pure polymers.

## 4. Conclusion

A series of PS/PMMA heterogeneous thin films was produced by phase separation upon spin coating, and four interesting substrates were identified: substrates with PMMA inclusions in a PS matrix and conversely, substrates with PS inclusions in a PMMA matrix, the inclusions being either under the form of pits or islands, with diameters in the submicrometer range. These surface morphologies can be linked to the respective solubility of the polymers in each of the solvents and to the very high molecular mass of the used PMMA compared to PS. The organization of collagen layers obtained by adsorption on the pure polymers was different depending on the nature of the polymer: the layer was quite smooth with assemblies of a few molecules on pure PMMA, while bigger assemblies were found on pure PS. The

organization of collagen layers obtained by adsorption on heterogeneous thin films was dependent on the size of PS areas. If the PS domains, either surrounding or surrounded by the PMMA phase, are above 600 nm wide, the surface presents a heterogeneous distribution of collagen in agreement with observations made on pure polymers. Otherwise, longer fibrils than those observed on pure polymers can be formed. Besides, XPS results showed that the detected collagen adsorbed amount was correlated with the PS surface fraction. As collagen contains recognition sequences for osteoblasts, current experiments include the culture of such cells on the created heterogeneous collagen layers.

# 5. References

[1] Giliberti, D. C.; White, K. K.; Dee, K. C., In *Polym. Biomater. (2nd Ed.)*, Marcel Dekker, Inc.: New York, N. Y, 2002; pp 361-375.

[2] Dekeyser, C. M.; Zuyderhoff, E.; Giuliano, R. E.; Federoff, H. J.; Dupont-Gillain Ch, C.; Rouxhet, P. G., A rough morphology of the adsorbed fibronectin layer favors adhesion of neuronal cells. *J. Biomed. Mater. Res. Part A* **2008,** *87*, 116-28.

[3] Keresztes, Z.; Rouxhet, P. G.; Remacle, C.; Dupont-Gillain, C., Supramolecular assemblies of adsorbed collagen affect the adhesion of endothelial cells. *J. Biomed. Mater. Res. Part A* **2006,** *76*, 223-33.

[4] Ekblad, T.; Liedberg, B., Protein adsorption and surface patterning. *Curr. Opin. Colloid Interface Sci.* **2010,** *15*, 499-509.

[5] Shekaran, A.; Garcia, A. J., Extracellular matrix-mimetic adhesive biomaterials for bone repair. *J. Biomed. Mater. Res. Part A* **2011,** *96A*, 261-272.

[6] Geissler, M.; Xia, Y. N., Patterning: Principles and some new developments. *Adv. Mater.* **2004,** *16*, 1249-1269.

[7] Elliott, J. T.; Woodward, J. T.; Umarji, A.; Mei, Y.; Tona, A., The effect of surface chemistry on the formation of thin films of native fibrillar collagen. *Biomaterials* **2007,** *28*, 576-85.

[8] Boot-Handford, R. P.; Tuckwell, D. S., Fibrillar collagen: the key to vertebrate evolution? A tale of molecular incest. *Bioessays* **2003,** *25*, 142-51.

[9] Kadler, K. E.; Holmes, D. F.; Trotter, J. A.; Chapman, J. A., Collagen fibril formation. *Biochem. J.* **1996,** *316*, 1-11.

[10] Gurdak, E.; Rouxhet, P. G.; Dupont-Gillain, C. C., Factors and mechanisms determining the formation of fibrillar collagen structures in adsorbed phases. *Colloids Surf., B* **2006,** *52*, 76-88.

[11] Dupont-Gillain, C. C.; Jacquemart, I.; Rouxhet, P. G., Influence of the aggregation state in solution on the supramolecular organization of adsorbed type I collagen layers. *Colloids Surf., B* **2005,** *43*, 179-86.

[12] Gurdak, E.; Booth, J.; Roberts, C. J.; Rouxhet, P. G.; Dupont-Gillain, C. C., Influence of collagen denaturation on the nanoscale organization of adsorbed layers. *J. Colloid Interface Sci.* **2006,** *302*, 475-84.

[13] Elliott, J. T.; Tona, A.; Woodward, J. T.; Jones, P. L.; Plant, A. L., Thin films of collagen affect smooth muscle cell morphology. *Langmuir* **2003,** *19*, 1506-1514.

[14] Jiang, F. Z.; Horber, H.; Howard, J.; Muller, D. J., Assembly of collagen into microribbons: effects of pH and electrolytes. *J. Struct. Biol.* **2004,** *148*, 268-278.

[15] Liang, Z.; Zhou, C.; Zeng, R.; Cai, H.; Guo, Z., Visualization of the nanoscale assembly of type I collagen on PLA by AFM. *Scanning* **2010,** *32*, 104-11.

[16] Pamula, E.; De Cupere, V.; Dufrene, Y. F.; Rouxhet, P. G., Nanoscale organization of adsorbed collagen: influence of substrate hydrophobicity and adsorption time. *J. Colloid Interface Sci.* **2004,** *271*, 80-91.

[17] Dupont-Gillain, C. C.; Pamula, E.; Denis, F. A.; Rouxhet, P. G., Nanostructured layers of adsorbed collagen: Conditions, mechanisms and applications. *Prog. Colloid Polym. Sci.* **2004,** *128*, 98-104.

[18] Dupont-Gillain, C. C.; Nysten, B.; Rouxhet, P. G., Collagen adsorption on poly(methyl methacrylate): net-like structure formation upon drying. *Polym. Int.* **1999,** *48*, 271-276.

[19] Elliott, J. T.; Halter, M.; Plant, A. L.; Woodward, J. T.; Langenbach, K. J.; Tona, A., Evaluating the performance of fibrillar collagen films formed at polystyrene surfaces as cell culture substrates. *Biointerphases* **2008,** *3*, 19.

[20] Denis, F. A.; Hanarp, P.; Sutherland, D. S.; Gold, J.; Mustin, C.; Rouxhet, P. G.; Dufrene, Y. F., Protein adsorption on model surfaces with controlled nanotopography and chemistry. *Langmuir* **2002,** *18*, 819-828.

[21] Liu, D.; Wang, T.; Keddie, J. L., Protein Nanopatterning on Self-Organized Poly(styrene-b-isoprene) Thin Film Templates. *Langmuir* **2009,** *25*, 4526-4534.

[22] Liu, D.; Abdullah, C. A. C.; Sear, R. P.; Keddie, J. L., Cell adhesion on nanopatterned fibronectin substrates. *Soft Matter* **2010,** *6*, 5408-5416.

[23] Kumar, N.; Parajuli, O.; Gupta, A.; Hahm, J. I., Elucidation of protein adsorption behavior on polymeric surfaces: Toward high-density, high-payload protein templates. *Langmuir* **2008,** *24*, 2688-2694.

[24] Lau, K. H.; Bang, J.; Hawker, C. J.; Kim, D. H.; Knoll, W., Modulation of protein-surface interactions on nanopatterned polymer films. *Biomacromolecules* **2009,** *10*, 1061-6.

[25] Matsusaki, M.; Omichi, M.; Kadowaki, K.; Kim, B. H.; Kim, S. O.; Maruyama, I.; Akashi, M., Protein nanoarrays on a highly-oriented lamellar surface. *Chem. Commun.* **2010,** *46*, 1911-1913.

[26] Denis, F. A.; Pallandre, A.; Nysten, B.; Jonas, A. M.; Dupont-Gillain, C. C., Alignment and assembly of adsorbed collagen molecules induced by anisotropic chemical nanopatterns. *Small* **2005,** *1*, 984-91.

[27] Zuyderhoff, E. M.; Dekeyser, C. M.; Rouxhet, P. G.; Dupont-Gillain, C. C., An AFM, XPS and wettability study of the surface heterogeneity of PS/PMMA-r-PMAA demixed thin films. *J. Colloid Interface Sci.* **2008,** *319*, 63-71.

[28] Li, L.; Hitchcock, A. P.; Robar, N.; Cornelius, R.; Brash, J. L.; Scholl, A.; Doran, A., X-ray microscopy studies of protein adsorption on a phase-segregated polystyrene/polymethyl methacrylate surface. 1. Concentration and exposure-time dependence for albumin adsorption. *J. Phys. Chem. B* **2006,** *110*, 16763-16773.

[29] Buck, E.; Fuhrmann, J., Surface-induced microphase separation in spin-cast ultrathin diblock copolymer films on silicon substrate before and after annealing. *Macromolecules* **2001,** *34*, 2172-2178.

[30] Alaerts, J. A.; De Cupere, V. M.; Moser, S.; Van den Bosh de Aguilar, P.; Rouxhet, P. G., Surface characterization of poly(methyl methacrylate) microgrooved for contact guidance of mammalian cells. *Biomaterials* **2001,** *22*, 1635-42.

[31] Beamson, G.; Briggs, D. *High resolution XPS of organic Polymers. The Scienta ESCA300 Database*, John Wiley: Chichester, 1992.

[32] Brandrup, J.; Immergut, E. H.; Grulke, E. A., *Polymer handbook*. 4th ed.; Wiley: New York, 1999.

[33] Ton-That, C.; Shard, A. G.; Teare, D. O. H.; Bradley, R. H., XPS and AFM surface studies of solvent-cast PS/PMMA blends. *Polymer* **2001,** *42*, 1121-1129.

[34] Tanaka, K.; Takahara, A.; Kajiyama, T., Surface molecular aggregation structure and surface molecular motions of high-molecular-weight polystyrene low-molecular-weight poly(methyl methacrylate) blend films. *Macromolecules* **1998,** *31*, 863-869.

[35] Johnson, R. E., Jr.; Dettre, R. H., In *Surface Colloid Sci.*, Matijevic, E., Ed. Willey-Interscience: New York, 1969; Vol. 2, pp 85-153.

[36] Norde, W., In *Biopolymers at Interfaces (2nd Edition)*, Malmsten, M., Ed. Marcel Dekker, Inc: New York, 2003; Vol. 110, pp 21-43.

[37] Woodcock, S. E.; Johnson, W. C.; Chen, Z., Collagen adsorption and structure on polymer surfaces observed by atomic force microscopy. *J. Colloid Interface Sci.* **2005,** *292*, 99-107.

[38] Walheim, S.; Boltau, M.; Mlynek, J.; Krausch, G.; Steiner, U., Structure formation via polymer demixing in spin-cast films. *Macromolecules* **1997,** *30*, 4995-5003.

# Supporting information material :

## NANO-ORGANIZED COLLAGEN LAYERS OBTAINED BY ADSORPTION ON PHASE- SEPARATED POLYMER THIN FILMS

### Factors affecting the phase structures of the obtained PS/PMMA films:

The morphology of the obtained PS/PMMA films appears to fall into two categories: surfaces prepared from toluene with elevated PMMA phases, and surfaces prepared from dioxane with PS elevated phases or no topography. This difference can be explained by the respective solubility of the polymers in each of the solvents. Since PS and PMMA have similar glass transition temperatures, the less soluble phase is indeed more quickly depleted of the solvent and turns solid earlier than the other phase. Subsequent evaporation of remaining solvent leads to a further collapse of the more soluble phase, which is thus finally less elevated than the other one.[38] In order to evaluate the affinity of each polymer for each solvent, the solubility parameter $\delta$ of the polymers and solvents can be used, a lower value of $|\delta_{polymer} - \delta_{solvent}|$ indicating a better solubility. By using mean values for PS ($\delta_{PS}$ = 18.3 $(MPa)^{1/2}$)[32] and PMMA ($\delta_{PMMA}$ = 19.6 $(MPa)^{1/2}$)[32] , it appears that toluene ($\delta_{toluene}$ = 18.2 $(MPa)^{1/2}$)[32] has a higher affinity for PS while dioxane ($\delta_{dioxane}$ = 20.5 $(MPa)^{1/2}$)[32] is a better solvent for PMMA (see Table S-1, p135), leading to PMMA and PS elevated phases in the case of toluene and dioxane, respectively, as was already reported in other works[27, 38]. In the present study, the height of the elevated structures is different for films elaborated from toluene or dioxane (~8 nm for toluene compared to ~2 nm or less in the case of dioxane). The height of elevated phases depends in principle on the difference between PS and PMMA solubility in the chosen solvent. A higher difference of solubility between both polymers for the solvent should indeed lead to a larger height difference between phases. The difference between PS and PMMA solubilities is similar in dioxane or in toluene (see $\Delta$solubility in Table 2). The values of $\delta_{PS}$ and $\delta_{PMMA}$ should however be used with caution, since they can vary depending on the characteristics of the polymer used. For instance, the PMMA used in the present study has a very high molecular mass ($M_w$ ~996,000), which may lower its solubility in both solvents. In that case, a higher height difference is expected between the PS and PMMA domains formed in toluene compared to dioxane, in agreement with the observed topographies.

(1) Walheim, S.; Boltau, M.; Mlynek, J.; Krausch, G.; Steiner, U., *Macromolecules* **1997,** *30*, 4995-5003.

(2) Brandrup, J.; Immergut, E. H.; Grulke, E. A., *Polymer handbook*. 4th ed.; Wiley: New York, 1999.

(3) Zuyderhoff, E. M.; Dekeyser, C. M.; Rouxhet, P. G.; Dupont-Gillain, C. C., *J. Colloid Interface Sci.* **2008,** *319*, 63-71.

**Table S-1.** Solubility of PS and PMMA in toluene[32] and dioxane[32] and summary of surface fractions of both polymers in the prepared thin films. See text for details.

| Solvent | $\lvert\delta_{polymer} - \delta_{solvent}\rvert$ | | Δ solubility | Surface fraction PS/PMMA | | |
|---|---|---|---|---|---|---|
| | PS | PMMA | | 90/10 | 30/70 | 5/95 |
| toluene | 0.1 | 1.4 | 1.3 | / | ~75/25 | ~13/87 |
| dioxane | 2.2 | 0.9 | 1.3 | ~80/20 | ~35/65 | / |

(2) Brandrup, J.; Immergut, E. H.; Grulke, E. A., *Polymer handbook*. 4th ed.; Wiley: New York, 1999.

**Figure S-1.** Evolution of the cosine of the water angle ($\theta_w$) of thin films in function of the PS surface fraction evaluated by XPS (solid line: Cassie's law). Error bars show the confidence interval at 95 %.

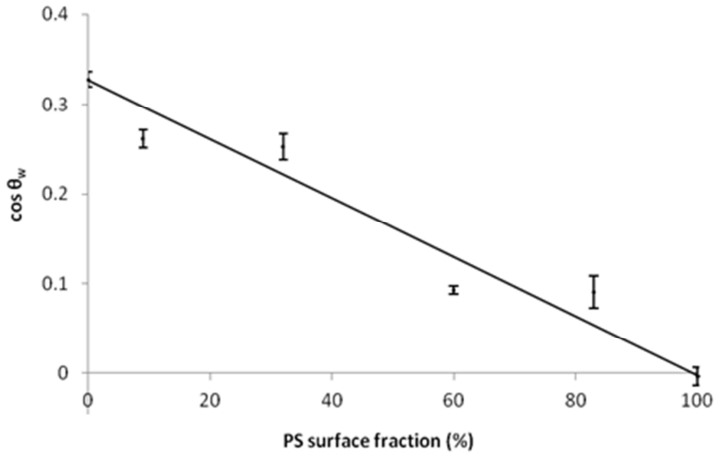

# Chapter III

# Improvement of preosteoblast adhesion through heterogeneous collagen layers prepared on PS/PMMA thin *(In preparation)*


## *Summary*

The aim of this work was to investigate the responses of preosteoblast cells (MC3T3-E1) on surfaces with chemical patterns and to study the impact of an adsorbed collagen layer. These chemical patterned surfaces were produced by phase separation in thin films of blends of polystyrene (PS), and poly(methyl methacrylate) (PMMA). Heterogeneous collagen organized layers were then obtained by collagen adsorption on these heterogeneous PS/PMMA films. The responses of MC3T3-E1cells to the bare PS, PMMA and PS/PMMA films as well as to these with collagen organized layers were examined after short culture times (4h and 6 days). Positive effects of heterogeneities (in terms of film surface chemical composition and collagen organization) on cell morphology, developed cell area and cell density were obserevd. Two main effects were revealed: (i) a higher cell density is always observed on heterogeneous films compared to the corresponding pure polymers (PS or PMMA), (ii) the developed cell area on heterogeneous films is intermediate between the ones observed on the pure polymers. This work shows that biointerfaces with chemical heterogeneities or with particular collagen organizations trigger particular cell behaviors. It opens new perspectives for biomaterials science and tissue engineering.

# 1. Introduction

The interactions between cells and solid surfaces are crucial to several biological phenomena and to a wide variety of biomaterials. Since cells are sensitive to their surroundings, the performance of biomaterials strongly depends on their surface properties which can have a huge influence on different cell behaviors such as adhesion, proliferation, migration, differentiation and apoptosis.[1] Surface properties related to chemistry (composition[2], crystallinity[3], charge[4]) as well as to topography (roughness, pit or morphologies of surface features[5-7]) have long been recognized as critical for regulating cell functions. Since cells rest *in vivo* on patterned interfaces (the extracellular matrix is a highly structured environment), biomimetic studies on man-made patterned surfaces have likewise drawn attention. Investigations have been ma inly focused on the scale (micro- or nanopatterning) and on the iso- or anisotropic character of the patterned surfaces, with a view to induce specific cell functions.

Polymer demixing is a simple method to create topographic and/or chemical surface heterogeneities. Using this technique, the morphology of the obtained chemical and topographic features (pits, ribbons, islands or even no relief) as well as their size (submicro- to micrometer scale) can be controlled by adjusting the proportion of the polymer and their concentration, and the chosen solvent. Annealed phase-separated films of polystyrene / polybromostyrene (PS/PBrS) showed a surface composition typical of pure PS with a topography composed of islands with a height on the nanoscale. It was demonstrated that the behavior of fibroblasts[8], endothelial cells[9] and osteoblasts differed depending on the islands height and cell type. Generally, a better cell spreading and cytoskeleton organization were observed on surfaces with the lowest islands height (13 nm). Likewise, blends of PS and poly(n-butyl methacrylate) were used to produce nano-islands with a closer packing and narrower width. Fibroblasts were shown to produce more filopodia on small nano-islands (height of 10 nm) and on flat control.[10] Poly(l-lactic acid)/PS blends with different concentration ratio were used to produce chemically heterogeneous surfaces showing either pits or islands on the nanoscale. Osteoblast adhesion was shown to be stimulated by heterogeneous surfaces compared to

homogeneous ones, and this was more pronounced in the presence of nano-islands compared to nanopits.[5]

However, the above-cited works did not include an investigation of protein adsorption on the created surfaces. Cell adhesion to synthetic materials is mediated by extracellular matrix proteins called adhesion proteins (such as fibronectin, collagen, vitronectin, etc), which adsorb on the materials. The initial cell-material interaction is thus a complex interplay between surface properties, protein adsorption and protein type. Consequently, the effects of a particular patterned surface on cell behaviors are partly due to the state of organization of the underlying protein layer. Most of the works trying to link the state of protein organization on patterned surfaces and the subsequent cell behavior are dedicated to fibronectin[11-16] while only a few studies focused on collagen.

Type I collagen, an adhesion protein from the extracellular matrix, is frequently used to coat supports for *in vitro* cell culture. This protein has a semiflexible rod-like shape of approximately 300 nm in length and 1.5 nm in diameter and has the ability to self-assemble. The association of five collagen molecules serves as a basis for the formation of microfibrils which can further grow into larger fibers (with a periodicity of 67 nm, ranging from 50 nm to 500 nm wide and up to several micron long). The spatial distribution and aggregation states of collagen were shown to strongly affect cell behavior. The fibril structure of collagen has led to distinct change in gene expression and morphological profile. For example, different densities of collagen fibril can be obtained by using different substrate chemistries[17] or by varying collagen concentration in the solution from which the films were prepared[18, 19]. In both cases, it was shown that cells were more spread on collagen films with a lower fibril density. Collagen denaturation (by heat or by use of acidic condition) was also used to create collagen films without fibrillar structure. In the case of vascular smooth muscle cells[18] and pulmonary stem cells[20], the area of cells on denatured collagen films was significantly larger than that of cells on thin films of native fibrillar collagen. On the contrary, in the case of myoblast cells,[21] a more stellate morphology was developed and the spreading and proliferation were faster on native collagen compared to cells on denatured collagen films. Furthermore, the use

of discontinuous collagen films prepared by adsorption followed by dewetting improved cell spreading and cytoskeleton organization compared to native continuous layers.[19, 22] Until now, to our knowledge, only one work investigated the organization of collagen layer on chemical patterns in order to link its subsequent effect to cell behavior. Elliott *et al.*[17] studied the effect of substrates of varying surface energy by using mixtures of OH- and $CH_3$-terminated thiols on vascular smooth muscle cells morphology. Their results showed that the formation of large fibrils did not occur on the hydrophilic surfaces and mentioned a water contact angle limit of 63° below which large fibril assembly would not form. Cellular morphology experiment on these substrates showed that substrates covered with a high density of large collagen fibrils induce a minimally spread non-proliferative phenotype[17]

In a previous study, we showed that the supramolecular organization of type I collagen could be modulated by its adsorption on heterogeneous polystyrene/poly(methyl methacrylate) (PS/PMMA) polymer thin films. A correlation between hydrophobicity and the formation of large fibrils was also highlighted. Larger fibrils were observed on PS compared to PMMA, PS being more hydrophobic than PMMA. On PS/PMMA films, which present intermediate hydrophobicity, we found that the higher the PS fraction in surface on the bare film, the larger the fibrils developed on the film. Additionally, the morphologies of the formed collagen assemblies was also found to be directed by the size of PS and PMMA domains of the heterogeneous films.[23]

This study focuses on the responses of preosteoblast cells (MC3T3-E1) to this range of collagen organized layers. General morphologies as well as cell areas developed by the cells were examined by immunofluorescence microscopy thanks to three fluorescent dyes (staining for cytoskeletons, nucleus and vinculin). Besides cell morphology, cell activity and cell density were also investigated. The aim is to evaluate the impact of collagen organized layers on cell responses.

## 2. Materials and methods2.1. Preparation of collagen organized layers on thin films of PS/PMMA

Collagen organized layers were obtained by adsorption on heterogeneous substrates produced by phase separation in thin films of blends of polystyrene (PS), and poly(methyl methacrylate) (PMMA). The preparation and characterization of these films was the subject of a previous study.[23] The preparation method and characterization technics used will be briefly presented in this section (For details of the procedures see reference[23]).

### *2.1.1. Preparation of PS/PMMA thin films*

Phase-separated polymer thin films were produced by spin-coating (speed = 5000 rpm, acceleration = 20,000 rpm/s, time = 40 s) of blends of PMMA ($M_w$ ~ 996,000 g/mol, $T_g$ 125° C ; from Aldrich, USA) and PS ($M_w$ ~ 230,000 g/mol, $M_n$ ~ 140,000 g/mol; from Merck, Germany) dissolved in a common solvent (dioxane or toluene) onto a glass coverslip treated with methacryloxypropyltrimethoxysilane (MOPTMS). To obtain substrates having different morphologies, several polymer solutions containing different PS/PMMA ratios were prepared either in dioxane (90/10 w/w and 30/70 w/w) or in toluene (30/70 w/w and 05/95 w/w). The total polymer concentration was always 10 g/l. Homogeneous films of PS and PMMA, prepared in the same conditions from solution in toluene, were also used as controls.

### *2.1.2. Collagen adsorption*

Type I Collagen from calf skin was purchased as a 4 mg/ml solution from Biochrom AG, UK. Collagen solution at 25 µg/ml was prepared by dilution in phosphate buffer saline (PBS) (pH 7.4; PBS tablets, Invitrogen, USA). The samples were placed in a multiwell tissue culture plate (12-well plate, one sample per well), 2ml of the collagen solution were poured into each well and the plate was incubated at 37°C for 3 h. The samples were then rinsed with PBS without being withdrawn from the solution.

### *2.1.3. Techniques of surface characterization*

The surfaces obtained before and after collagen adsorption were analyzed by X-ray photoelectron spectroscopy (XPS), atomic force microscopy (AFM) and wetting measurements.

*Atomic force microscopy*

The AFM analyses were performed in air and at room temperature with a Nanoscope IIIa multimode apparatus in tapping mode. The tips used were made of silicon, and had a spring constant comprised between 20 and 80 N/m and a resonance frequency in air between 212 and 319 kHz (Bruker, Palaiseau, France). Height and phase images were recorded in moderate tapping and were processed with the Nanoscope analysis software.

*X-ray photoelectron spectroscopy*

The XPS analyses were performed with a Kratos Axis Ultra spectrometer (Kratos Analytical – Manchester – UK) equipped with a monochromatised aluminium X-ray source. Analysis was performed in the hybrid lens mode with the slot aperture, resulting in an analysed area of 700 µm x 300 µm. The following sequence of spectra was recorded: survey spectrum, C 1s, O 1s, N 1s, Si 2p and C 1s again to check the stability of charging potential and the absence of degradation of the samples during the analysis.

To determine the PS surface fraction, f, of the blend polymer films, molar concentrations of oxygen and carbon were calculated using O 1s and C1s peak areas. If the blend surface was considered as made of patches of PS and PMMA which are thicker than the analyzed depth, the O/C ratio measured on the blends, $(O/C)_{exp}$, can be expressed as:

$$\left(\frac{O}{C}\right)_{exp} \approx \frac{f\, O_{PS}^{exp} + (1-f)\, O_{PMMA}^{exp}}{f\, C_{PS}^{exp} + (1-f)\, C_{PMMA}^{exp}} \qquad \text{[eq. 1]}$$

where f is the PS surface fraction, $O_{PS}^{exp}$ and $O_{PMMA}^{exp}$ are the oxygen mole fraction and $C_{PS}^{exp}$ and $C_{PMMA}^{exp}$ are the carbon mole fraction given by the XPS analysis of pure PS and pure PMMA, respectively.

*Water contact angle measurements*

Static water contact angles ($\Theta_w$) were measured at ambient temperature using the sessile drop method and image analysis of the drop profile. For each sample, the reported value is the average of the results obtained on at least 9 droplets.

## 2.2. Cell experiments on the collagen organized layers

### *2.2.1. Cell culture*

Osteoblast-like cells isolated from mice calvaria (cell line MC3T3-E1 subclone 14, ATTC-CEL-2594), were cultured in α-MEM (Modified Eagle Medium, Invitrogen, Belgium) supplemented with 10% (v/v) fetal bovine serum (Harlan, Loughborough, UK), 1% sodium pyruvate (100 mM (Sigma)), and containing 100 U/ml penicillin and 100 µg/ml streptomycin (Invitrogen), at 37°C in a fully humidified atmosphere with 5% $CO_2$. Cells were removed from the culture plates by rinsing in PBS and incubating in a trypsin-ethylene diamine tetraacetic acid (EDTA) solution (Invitrogen). After trypsin inactivation with complete medium, the cells were collected and centrifuged for 6 min at 1000 rpm. The resulting pellet was resuspended in complete medium. Cells were seeded on test substrates, sterilized in ethanol for 30 min prior to cell inoculation, at 25 000 cells/well in 24 multi-wells plates.

### *2.2.2. Cell response analysis*

*Cell morphology*

After 4h, 1 day or 6 days of culture, substrates were washed in PBS. Adherent cells were fixed with paraformaldehyde solution in PBS (4% w/v) for 20 min and permeabilized with 0.05% (v/v) Triton X-100 solution. After blocking with a 1% BSA solution in PBS, cells were incubated with anti-vinculin antibody solution (1:175) (MAB3574, Millipore). Cells were washed and reacted with (FITC)-conjugated secondary antibody (1:200) (AP124F, Millipore). To detect actin simultaneously, (TRITC)-conjugated phalloidin (1:400) (FAK100, Millipore) was added in the secondary antibody solution. Finally, the substrates were washed before being mounted

in Vectashield containing DAPI (Vector Laboratories, Peterborough, UK) to also stain the nucleus. Triple-stained cells were observed using a fluorescent microscope (Leica DM RA/RXA).

*Cell density and cell area*

DAPI images were used to evaluate cell density. Therefore, nucleus were detected and counted using the "ImageJ" software. Cell areas were determined based on merged images of the three stainings. Merged images were first treated using "ImageJ" to evaluate the total surface coverage by cells, which was then divided by the cell density to obtain the average cell area. Reported cell densities were normalized by the cell density evaluated on clean glass after 4 h of culture (use as a positive control), which was included in the experiment. Mean values and confidence intervals (95 % level of confidence) are reported from at least five images per test substrate. These statistics were calculated based on one experiment where each type of films was repeated 3 times.

*Cell activity evaluation*

The alamarBlue assay was used as a measurement of cell metabolic activity. This assay incorporates a fluorometric growth indicator based on detection of metabolic activity. Specifically, the system incorporates an oxidation-reduction indicator that fluoresces in response to chemical reduction of growth medium resulting from cell growth. Cells were cultured for six days. Each day, the culture medium was removed and the test substrates were washed with PBS. 1 ml of fresh culture medium with 50 µl of resazurin-based solution (Sigma, TOX8-1KT) was added onto each well. After 4 h of reaction time, 150 µl of supernatant was transferred in a 96-well plate. Fluoresence was read using an excitation wavelength of 544 nm and an emission wavelength of 590 nm in a microplate reader (SPECTRAmax GEMINI XS microplate fluorometer (Molecular Devices LLC.)). The fluorescence value corresponding to a blank sample on which no cell adhered was subtracted, and the obtained value was then normalized by the fluorescence intensity obtained with a positive control substrate, clean glass which was included in each experiment. The results correspond to the mean

and standard deviation calculated on the basis of one experiment where each type of films was repeated three times.

## 3. Results

### 3.1. Characterization of the films before and after collagen adsorption

Four PS/PMMA heterogeneous surfaces were obtained by phase separation in thin films by varying either the solvent or the polymer ratio of the polymer solutions. An overview of their surface properties is given in Figure 1. On the films characterized before collagen adsorption, four distinct PS surface fractions determined by XPS ($PS_{XPS}$) were obtained, ranging from 16% to 79%. AFM height images show that these films present a weak topography: 8 nm in height, 2 nm in height and almost flat, for $PS_{XPS}$ of 61% or 16%, 36% and 79%, respectively. The contrast recorded on the AFM images in phase mode indicates the location of PS and PMMA surface or subsurface areas. PS areas are indeed revealed as dark regions, with a smaller phase shift compared to PMMA regions, which appear in lighter color. The films presenting 16% and 36% of PS are made of a PMMA matrix with PS inclusions in the form of pits or islands, respectively. The films presenting 61% and 79% of PS display a PS matrix with PMMA inclusions in the form of islands or presenting no apparent topography, respectively. Static water contact angle of these phase-separated films show intermediate values compared to the pure PMMA and PS films, and these values increase with the PS fraction in surface. A more detailed examination and discussion of the surface morphology of similar films was published previously.[23]

These four phase-separated films along with the pure PS and PMMA films were then characterized after collagen adsorption by AFM in height mode (Figure 1). The collagen layer appears to be quite smooth on PMMA, with isolated collagen molecules and assemblies of a few molecules, while the collagen assemblies found on PS seem to be composed of several arms associated together in an anchoring knot. On heterogeneous PS/PMMA

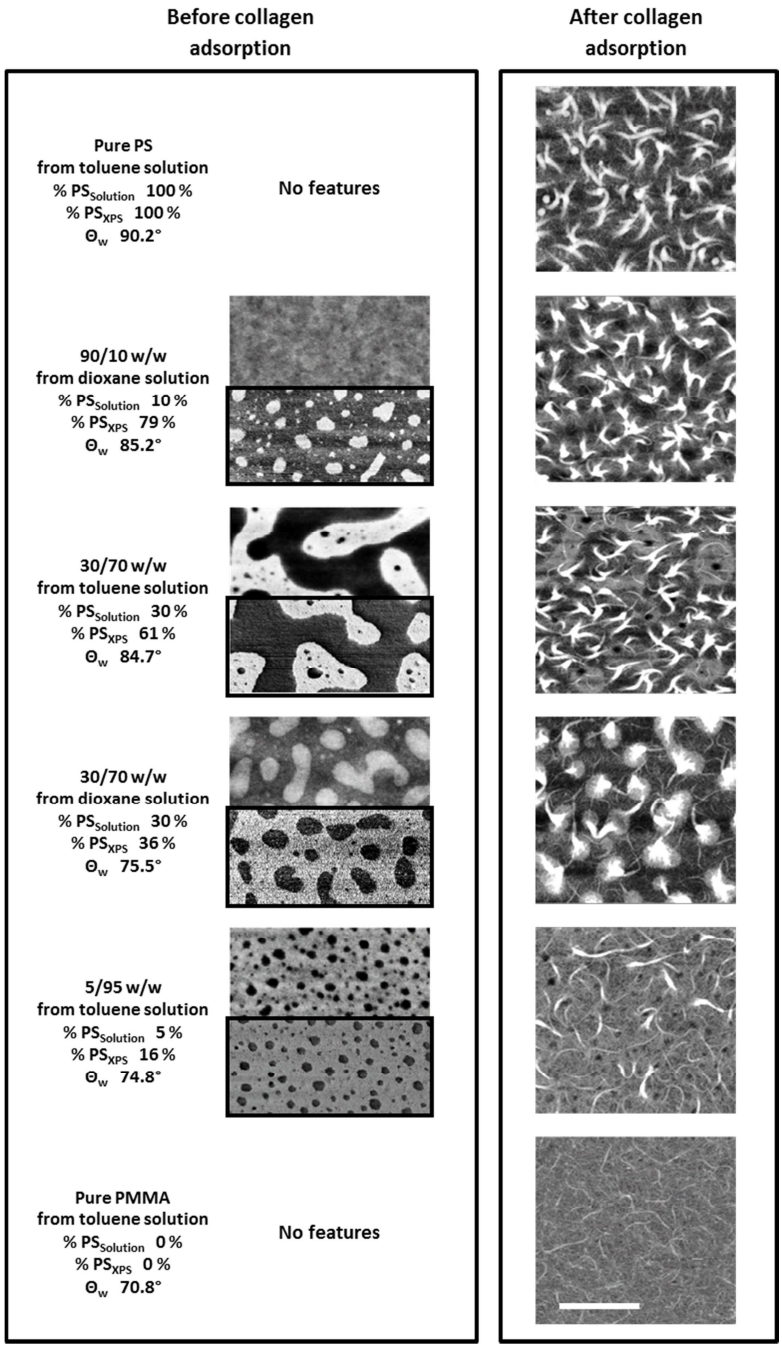


**Figure 1:** Characterization of the demixed polymer films before collagen adsorption (polymer ratios, solvents, PS fractions in solution ($PS_{solution}$), PS fraction in surface determined by XPS ($PS_{XPS}$), water contact angle ($\theta_w$), AFM height images (1.25 x 2.5 µm², z =10 nm) and phase images (1.25 x 2.5 µm², z = 10°; surrounded by solid line)), and after collagen adsorption (AFM height images (2.5 x 2.5 µm², z =30 nm)). White scale bar represents 1µm.

films, adsorbed collagen organization seem to depend on the polymer forming the matrix (PS or PMMA) and on the size of the PS domains. On the films presenting a PMMA matrix with PS inclusions (films with $PS_{XPS}$ of 16% and of 36%), the assemblies height appears to be smaller and their length longer compared to those observed on pure PS. This is probably because the PS inclusions of these films are too small to allow the formation of similar fibrils to those obtained on pure PS. On the films presenting a PS matrix with PMMA inclusions (films with $PS_{XPS}$ of 61% and of 79%), assemblies closer to those observed on pure PS were found. In these films, the PS domains are large enough to allow the formation of pure PS fibrils.

### 3.2. Cell behavior on the tested films

MC3T3-E1 osteoblast-like cells were cultured on pure PS and PMMA films, and on four other heterogeneous films presenting similar morphologies than those above-characterized. In this case, a $PS_{XPS}$ of 15%, 21%, 64% and 78% was calculated for these films which will be named as 15%PS, 21%PS, 64%PS and 78%PS, hereafter. MC3T3-E1 cells were cultured for 4 h, 1 day and 6 days.

Figure 2 shows the morphologies adopted by the cells on some of these films and on glass (used as a positive control), without collagen coating, after 4 h and 6 days of culture. After 4 h of culture, many cells have already spread on glass while only a few cells with small spreading are found on the polymer films. More cells were found on pure PMMA and on the 15%PS film. On PS, only a few extremely rounded cells, with almost no indication of cell attachment to the surface, were present. After 6 days of culture, cells nearly reach confluence on glass and develop a higher area. On the polymer films, a lot of cells are now observed on pure PMMA and on 15%PS, with more cells with larger spreading on PMMA and rather elongated cells on 15%PS. Again, only a few apoptotic cells were observed on pure PS. Finally, a small number of cells is observed on the 78%PS film, with an elongated and poorly spread shape.

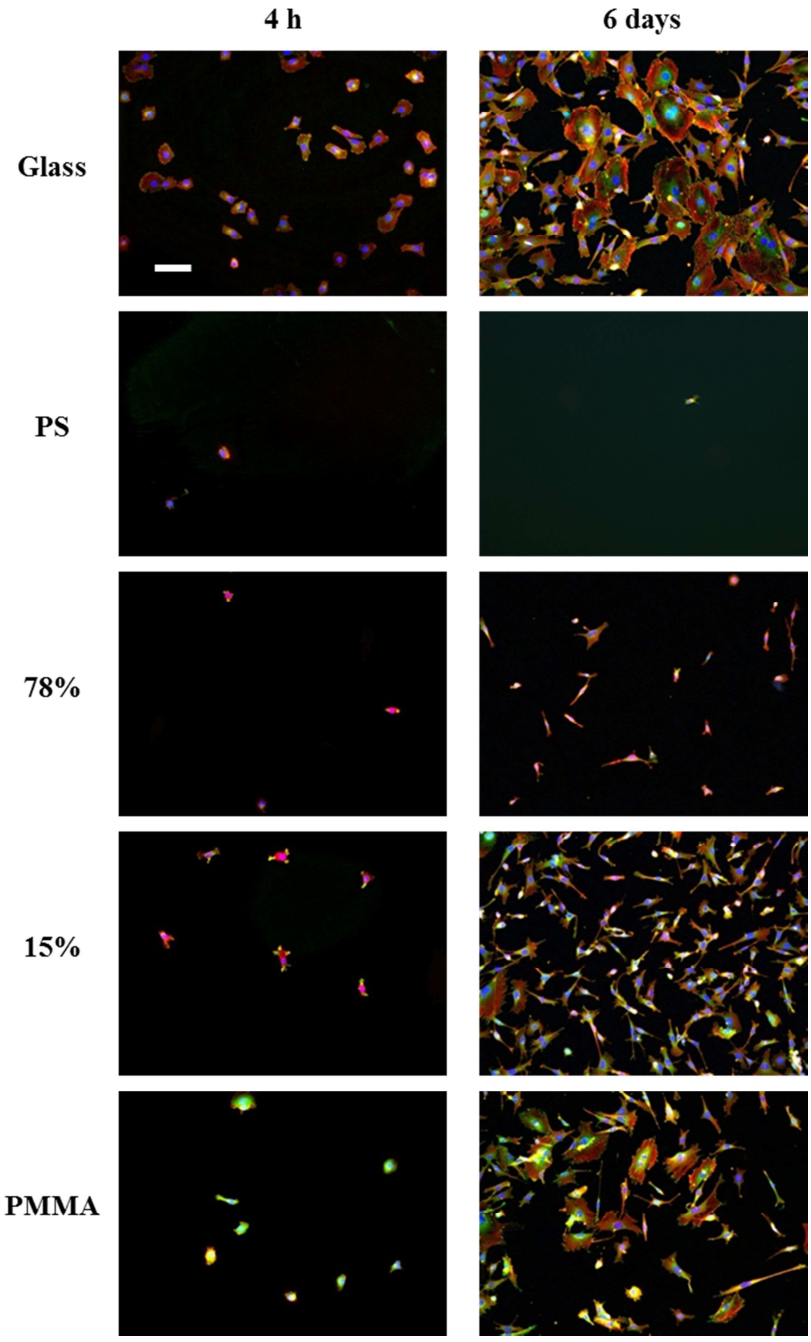


**Figure 2:** Actin (red), vinculin (green) and nucleus (blue) staining for MC3T3-E1 cells cultured for 4 h and 6 days, on glass, pure PMMA, pure PS and on two heterogeneous polymer films. The substrates were not coated with collagen prior to cell seeding (scale bar = 100 µm).

Figure 3 presents representative photographs of the morphologies displayed by the cells on the different polymer films and on glass which were conditioned by collagen adsorption before cells inoculation. After 4 h of culture, the morphologies observed on glass are similar to the ones observed without collagen conditioning, and cell spreading seems more important. On PMMA and on 15%PS, the morphologies are also similar but densities seem higher compared to Figure 2. In contrast to these films, the morphologies observed on pure PS and on 78%PS are completely different from the ones observed on polymer films in absence of collagen. The cells are here more spread compared to films without collagen. Cell shape of 78%PS is closer to the one observed on pure PS, with however a stronger elongation. After 6 days of culture, cells mainly adopt well-spread rounded-shape on glass. On pure PMMA and on 15%PS films, large spread cells with round shapes are observed along with more cells with more elongated shapes. On pure PS and on 78%PS, cells developed elongated shapes with a less spread cell area.

Cell densities and cell areas were quantified after 4 h, 1 day and 6 days of culture as shown in Figure 4. After 4 h of culture, cell densities are much higher on polymer films with collagen coatings than on those without, and are generally significantly higher on heterogeneous PS/PMMA substrates compared to pure polymer films (Figure 4A). The corresponding average cell areas are presented in Figure 4B. In the case of a pure PMMA, cell areas are similar with and without collagen coatings, while in the case of pure PS, a strong increase is observed in presence of collagen. Cell areas developed on heterogeneous films are intermediate between those exhibited on the pure PS and PMMA films. We then observe a trend which seems to be linked to the PS content in the films: in the case of collagen coating, the more the film contains PS, the more the cell is spread. When there is no collagen coating, the reverse tendency is found. After 6 days of culture, the densities obtained on films with or without collagen coating are generally similar. The corresponding cell areas are generally higher on films with collagen coatings, and for both cases, the more PMMA the film contains,

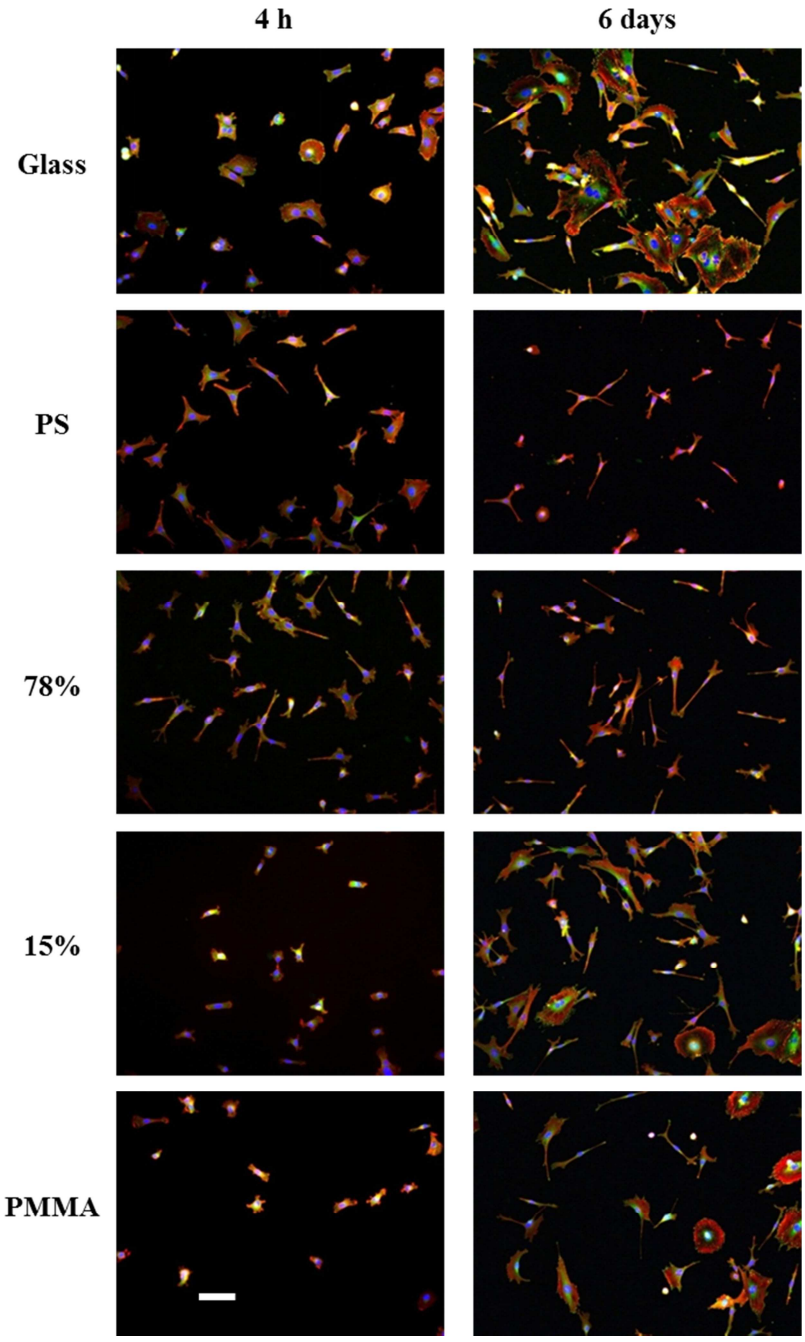


**Figure 3:** Actin (red), vinculin (green) and nucleus (blue) staining for MC3T3-E1 cells cultured for 4 h and 6 days on glass, pure PMMA, pure PS and on two heterogeneous polymer films. The substrates were coated with collagen prior to cell seeding (scale bar = 100 µm).

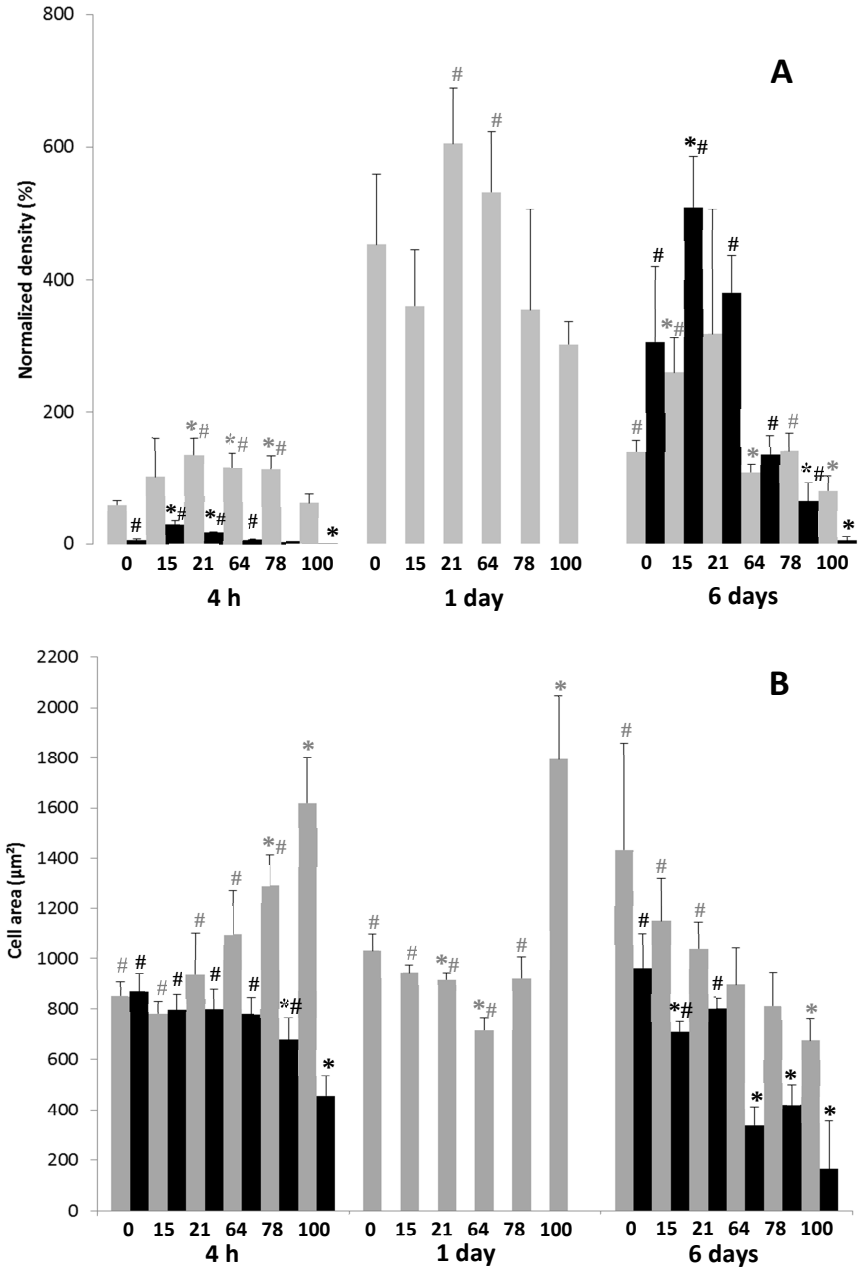


**Figure 4:** MC3T3-E1 cell density (A) and cell area (B) after 4 h, 1 day and 6 days of cell culture on pure PMMA (0%) and PS (100%), and on 4 heterogeneous polymer films (15%, 21%, 64% and 78%). The grey and black bars refer to substrate that were previously treated with collagen or not, respectively. Error bars report confidence intervals (95 % level of confidence). Statistical significance assessed by Student-t test is shown as * ($p < 0.01$) when compared with PMMA control and # ($p < 0.01$) when compared with PS control.

the more cells are spread. After 1 day of culture, the observed quantified cell densities and cell areas seem to be intermediate compare to 4 h and 6 days of incubation (note that no data are available for substrate without collagen).

Cell metabolic activity on films without collagen coating after 1, 3 and 6 days of culture is presented in Figure 5A. After the first day of culture, the cell activity is very high on pure PMMA (close to that observed on glass control, as indicated by the value close to 100%). As deduced from microscope observations (no cell adhesion), the fluorescence recorded on pure PS can be considered as a background signal coming from cells developing outside of the sample in the multiwell plate. That fluorescence value was then considered as a blank which was subtracted from all other samples. On heterogeneous films, cell activity is high on films with a PMMA matrix (15%PS and 21%PS) and very low on films with a PS matrix (64%PS and 78%PS). After 3 and 6 days of cell incubation, cell activity decreases on all films. Figure 5B presents cell activity on polymer films which are coated with collagen prior to cell seeding. After 1 day of incubation, cell activity is very high on pure polymer films and on 15%PS and 78%PS films, and lower on the 21%PS and 64%PS films. After 3 and 6 days of culture, cell activity was generally similar in all cases. A lower value is still reached after 6 days of culture on PS78%.

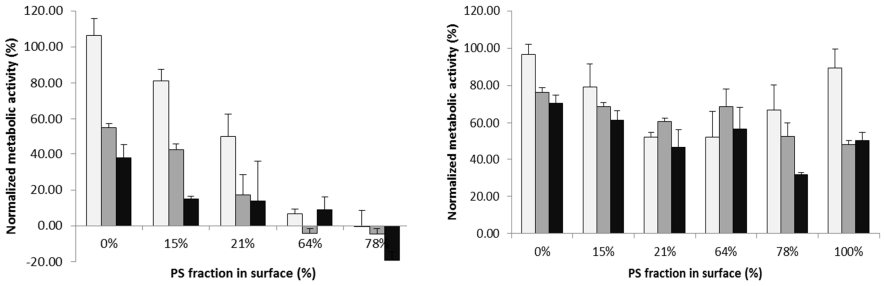


**Figure 5:** MC3T3-E1 cell metabolic activity as determined by alamar blue assay on pure PMMA, pure PS and on heterogeneous PS/PMMA films after 1 day (white bars), 3 days (grey bars) and 6 days (black bars) of culture. (A) Films without collagen coating prior to cell inoculation, (B) films conditioned with a collagen coating prior to cell inoculation. The errors bars show the standard deviation (n=3).

# 4. Discussion

## 4.1. MC3T3-E1 osteoblast-like cell line on bare polymer films (without collagen layer)

Without precoating of collagen, MC3T3-E1 cells were shown to attach very poorly on polymer films (either on homogeneous or heterogeneous films) compared to glass ones. Even if the attachment is weak, we saw it is still possible for cells to further adhere on the surface in absence of an adhesion protein coating before cell incubation. This is not surprising since cells are able to produce their own adhesion proteins. Furthermore, culture was realized in a serum conditioning medium which contains proteins, including adhesive ones. The presence of serum can also explain the poor cell adhesion observed on PS films. Albumin, which is abundant in serum, is a small protein which adsorbs quickly. Later, a competition for adsorption will occur between albumin and other proteins, which will rather turn in favor of adhesive proteins on hydrophilic surfaces, but in favor of albumin on hydrophobic surfaces.[24] For this reason, cells usually do not adhere very well on hydrophobic surface in presence of serum, since the surface remains mainly covered by albumin, which does not provide adhesion signals to the cells.[19, 22, 25, 26]

Surface wettability is one of the most important factors determining cell adhesion. It was reported in the literature that cells adhere well on moderately wettable surfaces, with a water contact angles of 40° to 60°, depending on the conditions, cell types, etc.[26-28] In the present work, the elaborated thin polymer films have water contact angle values above 70°, which can explain why cell attachment is so poor compared to glass. However surface wettability is not the sole factor influencing cell behavior, and both roughness and surface chemistry were shown to play an important role, quite independent of wettability.[29, 30] For example, air-plasma-treated glass (PTG) and air-plasma treated quartz (PTQ) presented the same surface wettability but adhesion of osteoblast cells was clearly higher on PTQ compared to PTG.[29] The cause of the attachment preference for the quartz surface chemistry remains unsolved.

In this work, the elaborated PS/PMMA film surfaces present chemical heterogeneities along with a slight topographic contrast (depth of pits or height of islands are ~0-8 nm). This topographic contrast should not be considered as insignificant since it was clearly demonstrated that cell adhesion can be influenced by surface features as small as 10 nm.[31] The influence of topography generated by polymer demixing on cell behavior was also highlighted. Using PS/PBrS blends and annealing, a series of films of homogeneous chemical composition presenting islands of different height, was produced. It was demonstrated that fibroblast adhesion and focal adhesion formation were greater on 13 nm high islands but lower on 95 nm high islands, than on planar PS control.[8] Another study showed that 9 to 29 nm scale (in depth or height) nanopits or nanoislands produced using PS and poly(L-lactic acid) (PLLA) phase separation induced greater human foetal osteoblastic (hFOB) cell adhesion than did flat PLLA control.[5] Furthermore, the cell line was shown to respond differently to these topographies. Rat calvarial osteoblast cells[32] were seen to adhere to all surface in the same way, while hFOB[6] adhesion and bone cell differentiation were stimulated significantly on 11 nm high islands compared to 85 nm islands or flat PS. It was suggested that primary cultured rat calvarial bone cells could have intrinsically less ability of adhesion and proliferation and thus minimal variation with respect to substratum surface characteristics relative to a readily proliferating hFOB cell line.[6]

In our case, after 4 h, we observe a significantly higher cell density on the heterogeneous films (except for the 78%PS) compared to pure polymer, and a maximum seems to be reached for films presenting a PMMA matrix (15%PS and 21%PS). This effect seems then to be only correlated with the chemical heterogeneities of the surfaces as different cell densities were observed for the same topographic contrast (e.g. pits depth of 8 nm for the 15%PS film and islands height of 8 nm for the 64%PS film). Additionally, cell response in terms of density seems to be linked to the PMMA content of the heterogeneous films and is thus not a simple linear combination of responses observed on pure polymer films. The higher density is then reached on heterogeneous films presenting a high PMMA content (15%PS). In contrast to cell density, cell spreading appears to be similar for most of

films and is lower on PS and 78%PS films. The cell response, here, would be linked to the PS content of the films, the higher the PS content, the lower cells spread.

After 6 days, we observed that cell proliferation was still possible on these polymer films, even if the initial attachment was poor. The cell densities on pure PMMA, and on polymer films with a PMMA matrix (15%PS and 21%PS films) are significantly higher than those observed on pure PS and on films with a PS matrix (64%PS and 78%PS films), and are actually higher than on the positive control (glass). The highest density is again observed on heterogeneous film with a high PMMA content (15%PS).

## 4.2. MC3T3-E1 osteoblast-like cell line on polymer films conditioned with a collagen layer

After 4 h of culture on the substrates treated with a collagen layer prior to cell seeding, the MC3T3-E1 adhesion is clearly higher than on substrates without collagen layer, and the densities observed on heterogeneous films are significantly higher than on the pure polymer films and on the positive control (glass). As it was observed on films without collagen coating, cell density is positively affected by heterogeneous films, but, here a clear optimum was not observed. Regarding cell spreading, as observed on films without collagen coating, cell responses is also linked to the PS content of the films, but cell areas are higher and the shape and trend are inverted compared to films without collagen coating. Cell spreading is similar on pure PMMA in absence or presence of a collagen coating, but larger on pure PS after collagen conditioning. An intermediate behavior is observed on heterogeneous films. After 6 days, cell density becomes lower than that observed on films without collagen coating. The developed cell areas remain higher on collagen coated films but the shape and trend are now similar to those without coating. This inversion in the trend between 4 h and 6 days to finally be similar to films without coating would suggest that collagen layers would not be stable after 6 days in culture medium and would reorganize in a layer close to that observed on films without collagen.

Cells are continuously synthesizing and excreting proteins and other ECM constituents which can, associated with proteins and serum conditioning medium constituents, clearly modify the protein layer present on the surface at the very beginning of the cell culture.

While the average cell area, after 4 h, is similar on PS and glass (data not shown), the developed shapes are very different. The cells are flattened with a nearly rounded shape to semi-rounded on glass and they are more stellate on PS films. The cell morphology is indicative of the function developed by the cell. Stellate shapes indicate motility while rounded flattened cell with clear developed focal contact implies proliferation. Consequently, cells developing a stellate shape do not easily reach confluence.[8, 33] Here on PS, cells have indeed not reached confluence yet after 6 days of culture while in the case of glass without collagen coating, the confluence is nearly reached. This could be explained by an inhibition of proliferation induced by the underlying collagen pattern. After 6 days, we can also observe that several cells are widely spread with a rounded shape, developing clear focal contacts (as seen on the vinculin staining) on pure PMMA and 15%PS films. This means that cells would be ready to proliferate on those substrates.

Collagen organization certainly influences cell morphology, density and spreading either by modifying the exposure of ligands available for cells or by offering different mechanical environment for cells. In a previous study, it was shown that large fibrils as well as collagen monomers or smaller assemblies induced cell attachment to the substrate by means of the same integrins ($\alpha1\beta1$ and $\alpha2\beta1$).[34] However, the activity of other cell receptors for collagen, including the discoidin receptor, was only detected on fibrillar collagen.[35] Moreover, it has been shown that different types of collagen organization (fibrils *vs* monomers) generated layers with different mechanical properties: on PMMA, the collagen layer would be more compact, less compressible, and more mechanically resistant than on PS, where collagen appeared to form a stable but still flexible matrix.[36] Both explanations, or their combination, could potentially explain why cell behaviors strongly vary with collagen organization.

## 5. Conclusion

The impact of bare and collagen-coated PS/PMMA films on cell behavior, after short culture times (4 h and 6 days), was investigated. Collagen adsorption prior to cell inoculation was shown to affect cell behavior mainly after 4 h. A longer culture time (6 days) would induce a reorganization of the protein layer, which would lead to protein layers giving similar cues to the cells in absence or presence of collagen precoating. Moreover, two other effects were revealed, both in absence or presence of collagen precoating and whatever the culture duration. First, the developed cell area on heterogeneous films is a linear contribution of the behaviors observed on the pure polymers. Cell areas were always higher on collagen-coated homogeneous films (on PS after 4 h and on PMMA after 6 days). Secondly, cell density is positively affected by the heterogeneity of the surface, a higher cell density being observed on heterogeneous films compared to the corresponding pure polymers. The highest cell density was always obtained on heterogeneous films (any PS/PMMA films with collagen after 4 h and on 15%PS and 21%PS without collagen after 6 days). This work emphasizes the importance of the study of adsorbed proteins on chemically heterogeneous surfaces. Their organization is here identified as a crucial factor, which could be controlled by the underlying surface chemical composition. These results also suggest that MC3T3-E1 cells are sensitive to heterogeneities (in term of surface chemical composition and collagen organization). It is then tempting to speculate that these cells may also rely on this kind of stimuli for differentiation. The challenge now is to investigate longer term responses such as cell differentiation, as well as responses of other osteoblast cell lines on these types of cues.

# 6. Bibliography

[1] Stevens, M. M.; George, J. H., Exploring and engineering the cell surface interface. *Science* **2005,** *310*, 1135-8.

[2] Lim, J. Y.; Liu, X.; Vogler, E. A.; Donahue, H. J., Systematic variation in osteoblast adhesion and phenotype with substratum surface characteristics. *Journal of biomedical materials research. Part A* **2004,** *68*, 504-12.

[3] Lim, J. Y.; Donahue, H. J., Cell sensing and response to micro- and nanostructured surfaces produced by chemical and topographic patterning. *Tissue Eng.* **2007,** *13*, 1879-91.

[4] Qiu, Q.; Sayer, M.; Kawaja, M.; Shen, X.; Davies, J. E., Attachment, morphology, and protein expression of rat marrow stromal cells cultured on charged substrate surfaces. *J Biomed Mater Res* **1998,** *42*, 117-27.

[5] Lim, J. Y.; Hansen, J. C.; Siedlecki, C. A.; Hengstebeck, R. W.; Cheng, J.; Winograd, N.; Donahue, H. J., Osteoblast adhesion on poly(L-lactic acid)/polystyrene demixed thin film blends: effect of nanotopography, surface chemistry, and wettability. *Biomacromolecules* **2005,** *6*, 3319-27.

[6] Lim, J. Y.; Hansen, J. C.; Siedlecki, C. A.; Runt, J.; Donahue, H. J., Human foetal osteoblastic cell response to polymer-demixed nanotopographic interfaces. *Journal of the Royal Society, Interface / the Royal Society* **2005,** *2*, 97-108.

[7] Lim, J. Y.; Dreiss, A. D.; Zhou, Z.; Hansen, J. C.; Siedlecki, C. A.; Hengstebeck, R. W.; Cheng, J.; Winograd, N.; Donahue, H. J., The regulation of integrin-mediated osteoblast focal adhesion and focal adhesion kinase expression by nanoscale topography. *Biomaterials* **2007,** *28*, 1787-97.

[8] Dalby, M. J.; Childs, S.; Riehle, M. O.; Johnstone, H. J.; Affrossman, S.; Curtis, A. S., Fibroblast reaction to island topography: changes in cytoskeleton and morphology with time. *Biomaterials* **2003,** *24*, 927-35.

[9] Dalby, M. J.; Riehle, M. O.; Johnstone, H.; Affrossman, S.; Curtis, A. S., In vitro reaction of endothelial cells to polymer demixed nanotopography. *Biomaterials* **2002,** *23*, 2945-54.

[10] Dalby, M. J.; Riehle, M. O.; Johnstone, H. J.; Affrossman, S.; Curtis, A. S., Nonadhesive nanotopography: fibroblast response to poly(n-butyl methacrylate)-poly(styrene) demixed surface features. *Journal of biomedical materials research. Part A* **2003,** *67*, 1025-32.

[11] Gonzalez-Garcia, C.; Sousa, S. R.; Moratal, D.; Rico, P.; Salmeron-Sanchez, M., Effect of nanoscale topography on fibronectin adsorption, focal adhesion size and matrix organisation. *Colloids Surf., B* **2010,** *77*, 181-190.

[12] Gugutkov, D.; Altankov, G.; Rodriguez Hernandez, J. C.; Monleon Pradas, M.; Salmeron Sanchez, M., Fibronectin activity on substrates with controlled --OH density. *Journal of biomedical materials research. Part A* **2010,** *92*, 322-31.

[13] Perez-Garnes, M.; Gonzalez-Garcia, C.; Moratal, D.; Rico, P.; Salmeron-Sanchez, M., Fibronectin distribution on demixed nanoscale topographies. *The International journal of artificial organs* **2011,** *34*, 54-63.

[14] Dolatshahi-Pirouz, A.; Jensen, T.; Kraft, D. C.; Foss, M.; Kingshott, P.; Hansen, J. L.; Larsen, A. N.; Chevallier, J.; Besenbacher, F., Fibronectin adsorption, cell adhesion, and proliferation on nanostructured tantalum surfaces. *Acs Nano* **2010,** *4*, 2874-82.

[15] Dekeyser, C. M.; Zuyderhoff, E.; Giuliano, R. E.; Federoff, H. J.; Dupont-Gillain Ch, C.; Rouxhet, P. G., A rough morphology of the adsorbed fibronectin layer favors adhesion of neuronal cells. *J. Biomed. Mater. Res. Part A* **2008,** *87*, 116-28.

[16] Ballester-Beltran, J.; Cantini, M.; Lebourg, M.; Rico, P.; Moratal, D.; Garcia, A. J.; Salmeron-Sanchez, M., Effect of topological cues on material-driven fibronectin fibrillogenesis and cell differentiation. *Journal of materials science. Materials in medicine* **2012,** *23*, 195-204.

[17] Elliott, J. T.; Woodward, J. T.; Umarji, A.; Mei, Y.; Tona, A., The effect of surface chemistry on the formation of thin films of native fibrillar collagen. *Biomaterials* **2007,** *28*, 576-85.

[18] Elliott, J. T.; Tona, A.; Woodward, J. T.; Jones, P. L.; Plant, A. L., Thin films of collagen affect smooth muscle cell morphology. *Langmuir* **2003,** *19*, 1506-1514.

[19] Keresztes, Z.; Rouxhet, P. G.; Remacle, C.; Dupont-Gillain, C., Supramolecular assemblies of adsorbed collagen affect the adhesion of endothelial cells. *J. Biomed. Mater. Res. Part A* **2006,** *76*, 223-33.

[20] Huang, C.-J.; Chien, Y.-L.; Ling, T.-Y.; Cho, H.-C.; Yu, J.; Chang, Y.-C., The influence of collagen film nanostructure on pulmonary stem cells and collagen–stromal cell interactions. *Biomaterials* **2010,** *31*, 8271-8280.

[21] Arnesen, S.; Mosler, S.; Larsen, N.; Gadegaard, N.; Purslow, P.; Lawson, M., The effects of collagen type I topography on myoblasts in vitro. *Connective tissue research* **2004,** *45*, 238-47.

[22] Dupont-Gillain, C. C.; Alaerts, J. A.; Dewez, J. L.; Rouxhet, P. G., Patterned layers of adsorbed extracellular matrix proteins: influence on mammalian cell adhesion. *Biomed Mater Eng* **2004,** *14*, 281-91.

[23] Zuyderhoff, E. M.; Dupont-Gillain, C. C., Nano-organized collagen layers obtained by adsorption on phase-separated polymer thin films. *Langmuir* **2012,** *28*, 2007-14.

[24] Dewez, J. L.; Berger, V. V.; Schneider, Y. J.; Rouxhet, P. G., Influence of Substrate Hydrophobicity on the Adsorption of Collagen in the Presence of Pluronic F68, Albumin, or Calf Serum. *J Colloid Interface Sci* **1997,** *191*, 1-10.

[25] Keselowsky, B. G.; Collard, D. M.; Garcia, A. J., Surface chemistry modulates fibronectin conformation and directs integrin binding and specificity to control cell adhesion. *J. Biomed. Mater. Res. Part A* **2003,** *66A*, 247-259.

[26] Arima, Y.; Iwata, H., Effect of wettability and surface functional groups on protein adsorption and cell adhesion using well-defined mixed self-assembled monolayers. *Biomaterials* **2007,** *28*, 3074-82.

[27] Tamada, Y.; Ikada, Y., Effect of Preadsorbed Proteins on Cell Adhesion to Polymer Surfaces. *J. Colloid Interface Sci.* **1993,** *155*, 334-339.

[28] Lee, J. H.; Khang, G.; Lee, J. W.; Lee, H. B., Interaction of Different Types of Cells on Polymer Surfaces with Wettability Gradient. *J Colloid Interface Sci* **1998,** *205*, 323-330.

[29] Liu, X.; Lim, J. Y.; Donahue, H. J.; Dhurjati, R.; Mastro, A. M.; Vogler, E. A., Influence of substratum surface chemistry/energy and topography on the human fetal osteoblastic cell line hFOB 1.19: Phenotypic and genotypic responses observed in vitro. *Biomaterials* **2007,** *28*, 4535-4550.

[30] Schweikl, H.; Muller, R.; Englert, C.; Hiller, K. A.; Kujat, R.; Nerlich, M.; Schmalz, G., Proliferation of osteoblasts and fibroblasts on model surfaces of varying roughness and surface chemistry. *Journal of materials science. Materials in medicine* **2007,** *18*, 1895-905.

[31] Dalby, M. J.; Riehle, M. O.; Johnstone, H.; Affrossman, S.; Curtis, A. S., Investigating the limits of filopodial sensing: a brief report using SEM to image the interaction between 10 nm high nano-topography and fibroblast filopodia. *Cell Biol Int* **2004,** *28*, 229-36.

[32] Riehle, M. O.; Dalby, M. J.; Johnstone, H.; MacIntosh, A.; Affrossman, S., Cell behaviour of rat calvaria bone cells on surfaces with random nanometric features. *Materials Science and Engineering: C* **2003,** *23*, 337-340.

[33] Dalby, M. J.; Giannaras, D.; Riehle, M. O.; Gadegaard, N.; Affrossman, S.; Curtis, A. S., Rapid fibroblast adhesion to 27nm high polymer demixed nano-topography. *Biomaterials* **2004,** *25*, 77-83.

[34] Elliott, J. T.; Woodward, J. T.; Langenbach, K. J.; Tona, A.; Jones, P. L.; Plant, A. L., Vascular smooth muscle cell response on thin films of collagen. *Matrix biology : journal of the International Society for Matrix Biology* **2005,** *24*, 489-502.

[35] Shrivastava, A.; Radziejewski, C.; Campbell, E.; Kovac, L.; McGlynn, M.; Ryan, T. E.; Davis, S.; Goldfarb, M. P.; Glass, D. J.; Lemke, G.; Yancopoulos, G. D., An orphan receptor tyrosine kinase family whose members serve as nonintegrin collagen receptors. *Molecular cell* **1997,** *1*, 25-34.

[36] Dupont-Gillain, C. C.; Pamula, E.; Denis, F. A.; Rouxhet, P. G., Nanostructured layers of adsorbed collagen: Conditions, mechanisms and applications. *Prog. Colloid Polym. Sci.* **2004,** *128*, 98-104.

# Appendix 1

# A rough morphology of the adsorbed fibronectin layers favors adhesion of neuronal cells


### *Summary*

range of substrates made of polystyrene (PS) and poly(methyl methacrylate)–poly(methacrylic acid) copolymer (PMMA–PMAA) containing 98 and 80% PMMA (PA98, PA80) and presenting a homogeneous or a patterned surface were used to study fibronectin adsorption and neuronal cell behavior. Fibronectin adsorption showed weak differences regarding the adsorbed amount (evaluated by XPS), but large differences in adsorbed layer morphology as observed by AFM. A fine granular morphology, with dimensions up to 8 nm height and 50–150 nm width, was observed on top of a thin adsorbed layer in the case of PS, PA98, and of a surface made of nanoscale inclusions of the latter in PS. In contrast, the layer adsorbed on PA80, which carries more ionizable groups, showed a higher roughness on the PA80 zones with differences in height up to 30 nm and characteristic lateral dimensions of 400 nm. On substrates of the former category, the cells formed large clusters, revealing poor interactions with the substrate. On PA80, the cells formed large networks with only a few small clusters. The adsorbed layer roughness, resulting from aggregation of fibronectin upon adsorption and from the substrate surface chemical composition, is responsible for neuronal cell spreading and growth. Its effect is not prevented by the presence of inclusions (<30% of the surface)

responsible for smoother areas of adsorbed fibronectin and for protrusions below 40 nm.

# A rough morphology of the adsorbed fibronectin layer favors adhesion of neuronal cells

**C. M. Dekeyser,[1] E. Zuyderhoff,[1] R. E. Giuliano,[2] H. J. Federoff,[2] Ch. C. Dupont-Gillain,[1] P. G. Rouxhet[1]**
[1]*Unité de chimie des interfaces, Université catholique de Louvain, Croix du Sud 2/18, 1348 Louvain-la-Neuve, Belgium*
[2]*Center for Aging and Developmental Biology, University of Rochester School of Medicine and Dentistry, Rochester, New York 14642*

Received 8 May 2007; revised 16 July 2007; accepted 8 August 2007
Published online 17 December 2007 in Wiley InterScience (www.interscience.wiley.com). DOI: 10.1002/jbm.a.31739

**Abstract:** A range of substrates made of polystyrene (PS) and poly(methyl methacrylate)–poly(methacrylic acid) copolymer (PMMA–PMAA) containing 98 and 80% PMMA (PA98, PA80) and presenting a homogeneous or a patterned surface were used to study fibronectin adsorption and neuronal cell behavior. Fibronectin adsorption showed weak differences regarding the adsorbed amount (evaluated by XPS), but large differences in adsorbed layer morphology as observed by AFM. A fine granular morphology, with dimensions up to 8 nm height and 50–150 nm width, was observed on top of a thin adsorbed layer in the case of PS, PA98, and of a surface made of nanoscale inclusions of the latter in PS. In contrast, the layer adsorbed on PA80, which carries more ionizable groups, showed a higher roughness on the PA80 zones with differences in height up to 30 nm and characteristic lateral dimensions of 400 nm. On substrates of the former category, the cells formed large clusters, revealing poor interactions with the substrate. On PA80, the cells formed large networks with only a few small clusters. The adsorbed layer roughness, resulting from aggregation of fibronectin upon adsorption and from the substrate surface chemical composition, is responsible for neuronal cell spreading and growth. Its effect is not prevented by the presence of inclusions ($< 30\%$ of the surface) responsible for smoother areas of adsorbed fibronectin and for protrusions below 40 nm. © 2007 Wiley Periodicals, Inc. J Biomed Mater Res 87A: 116–128, 2008

**Key words:** fibronectin; protein adsorption; neuronal cells; cell adhesion; patterned surfaces

## INTRODUCTION

Protein adsorption is one of the first events to occur when a foreign surface comes into contact with biological systems.[1] Certain proteins, frequently called adhesion proteins, can direct cell attachment, spreading, proliferation, orientation, migration, and differentiation when present at the substrate surface. Chemical or topographical trails on the substrate or heterogeneities in the protein layer itself are used to direct the cell behavior.[2] At the supracellular scale, selective adsorption of proteins (fibronectin or collagen) on lanes of oxidized polystyrene caused selective adhesion of Schwann cells, PC 12 cells and hepatocytes.[3] Grooved poly(methyl methacrylate) (PMMA) preconditioned with collagen caused the orientation of fibroblasts along the grooves.[4] On patterns made by combining topography and chemical contrast, neurites aligned preferentially on vitronectin tracks perpendicular to shallow grooves (50 nm), but aligned increasingly along grooves with increasing depth (up to 6 μm).[5] At the cellular scale, adhesive patterns of different sizes were created in a nonadhesive matrix. Apoptosis was reduced with increasing diameter of fibronectin-coated islands. However, for very small islands (5 μm diameter), the cells were able to grow by creating specific interactions with several islands.[6] At the nanometer scale, the influence of the heterogeneity created in a collagen layer was studied on endothelial cells: discontinuous collagen networks clearly enhanced cell spreading and cytoskeleton organization.[7,8]

Proteins may undergo changes in conformation upon adsorption.[2,9] Fibronectin attaches with a higher affinity to hydrophobic surfaces, and is much more firmly adsorbed.[10] By using antibodies against fibronectin, it was shown[11,12] that the conformation after adsorption was influenced by substrate surface

*Correspondence to:* P. G. Rouxhet; e-mail: rouxhet@cifa.ucl.ac.be

Contract grant sponsors: Foundation for Training in Industrial and Agricultural Research (F.R.I.A.); National Foundation for Scientific Research (F.N.R.S.); Federal Office for Scientific, Technical and Cultural Affairs (Interuniversity Poles of Attraction Program); Research Department of the Communauté Française de Belgique (Concerted Research Action, Travel Fellowship)

hydrophobicity and that the absence of antibody binding was related to the lack of cell attachment. Cell culture experiments showed selective adhesion[11–14] or differentiation[15] on fibronectin-coated hydrophilic surfaces. A study[16] was realized on polysulfone surfaces fabricated with different poly(ethylene glycol) densities, resulting in different water contact angles. After fibronectin conditioning, fibroblasts showed enhanced adhesion and spreading, well expressed focal adhesion and reorganization of the fibronectin layer on surfaces with intermediate contact angles (comprised between 50° and 70°).

A simple method to obtain topographic and/or chemical surface heterogeneity is polymer demixing.[17] Using this technique, different surface morphologies can be obtained.[18–21] The size (50 nm–2 μm wide, 1–50 nm high)[22] and shape of surface features (pits, hills, or even no relief)[23,24] are modulated by carefully choosing the polymers and the conditions used. By demixing of polystyrene (PS) and poly(4-bromostyrene), surfaces were produced with hills of a controlled height (13, 35, and 95 nm) and a homogeneous composition consisting of PS after annealing. The behavior of endothelial cells,[25] fibroblasts,[26,27] and osteoblasts[28,29] differed depending on the hill height and the cell type. Generally, a better cell spreading and cytoskeleton organization was observed on surfaces with the lowest hill height (13 nm height). Fibroblasts grown on a surface produced by poly(*n*-butyl methacrylate)-PS demixing also attached, spread, and developed better on the smooth control and on the surface with the smaller hills (10 nm, compared with 50 nm).[30] A comparison of hills and pits made on surfaces produced by varying the poly(L-lactic acid)/PS ratio[31] showed a stimulation of osteoblast adhesion on nanotextured surfaces, which was more distinct for nanohills, relative to nanopits. Fibroblasts grown on PS–PMMA, differing in hill dimensions, spread more on surfaces with smaller lateral dimensions and on smooth surfaces.[22] However, protein adsorption was not investigated on these surfaces.

Directing the growth of neurons would permit a better understanding of neurite formation and of interactions with the ECM (extracellular matrix) proteins, and would facilitate the study of neuron properties such as cell–cell communication and electrical activity.[32,33] In the field of nerve repair, a better control of neuronal growth could lead to improved implantation of "biomaterial bridging surfaces" with immobilized ECM proteins.[34] Fibronectin is a widely expressed ECM component that may regulate cell migration, neurite outgrowth, and possibly cell proliferation during development, but also nerve regeneration after injury.[35]

The present work concerns the study of cell behavior on demixed polymer surfaces with adsorbed fibronectin. Copolymers containing poly (methacrylic acid) (PMAA) were chosen in order to facilitate chemical grafting in later works. Spin-coating of a random copolymer PMMA–PMAA (98% PMMA) on a PS substrate gave a flat surface with PMMA–PMAA inclusions in a PS surface.[23] Spin-coating of a blend of PS and PMMA–PMAA (80% PMMA) on an inert substrate gave islands of PS in a PMMA–PMAA surface.[24] These two heterogeneous surfaces, with the more hydrophobic polymer covering the largest or the smallest portion of the surface, are examined regarding fibronectin adsorption, and compared with the corresponding flat homogeneous surfaces. Finally, the behavior of mouse cortical neurons is studied on both heterogeneous and homogeneous surfaces.

## MATERIALS AND METHODS

### Substrate preparation

The substrate preparation was described in detail elsewhere[23,24] and is summarized here. Two different types of supports (diameter 12 mm) were used for spin-coating: PS disks (**$PS_f$**) punched from a PS film (Goodfellow, UK) and disks of PMMA punched from homemade films of PMMA ($M_w$ = 996,000, Aldrich), with a high molar mass in order to avoid dissolution during spin-coating. Before use, the disks were cleaned by sonication in isopropanol ($PS_f$) or in water (PMMA). Substrates were prepared by spin-coating 40 μL of a given polymer solution (40 s, acceleration 20,000 rpm/s, speed 5000 rpm) on a given support as follows: **PA98/PS**, spin-coating a $PS_f$ disk with a 10 g/L PMMA–PMAA (98% PMMA; random copolymer, $M_w$ = 34,000, Aldrich) solution in chlorobenzene; **PA98**, spin-coating a PMMA disk with a solution of 10 g/L of PMMA–PMAA (98% PMMA) in chlorobenzene; **PS-PA80**, spin-coating a PMMA disk with a solution of 3 g/L PS ($M_w$ = 230,000, Merck, Germany) and 7 g/L PMMA–PMAA (80% PMMA; random copolymer, $M_w$ of about $10^6$, Polysciences) in dioxane; **PA80**, spin-coating a PMMA disk with a solution of 10 mg/mL PMMA–PMAA (80% PMMA) in dioxane; **$PS_s$**, spin-coating a PMMA disk with a solution of 10 mg/mL PS in dioxane.

### Fibronectin adsorption

#### Procedure

Lyophilized fibronectin from bovine plasma was purchased from Invitrogen (USA). The powder was dissolved in 1 mL Milli-Q water (Millipore, Molsheim, France) in order to achieve a concentration of 1 mg/mL. This stock solution was aliquoted and stored at −20°C. The solutions were prepared just before use by dilution of the stock solution using PBS (phosphate buffered saline at pH 7.2). The substrates were placed in a multiwell plate (1 sample per

well), 1.8 mL of the fibronectin solution was added in each well, and the plate was incubated at 37°C for 24 h. The samples were washed five times using the following procedure: 0.8 mL of the solution was removed, 3 mL Milli-Q water was added, the plate was placed under agitation for 5 min; for the subsequent washes, 3 mL solution was removed and replaced by 3 mL Milli-Q water. The samples were then dried under nitrogen flow.

### Characterization

The samples were imaged by Atomic Force Microscopy (Nanoscope III, Digital instruments, Santa Barbara) at room temperature, in contact mode for the polymer samples and in tapping mode for the samples conditioned with fibronectin. For the contact mode, realized under Milli-Q water, the tip used was made of $Si_3N_4$, had a typical spring constant of 0.01 N/m and a typical radius of curvature of 20 nm (Park Scientific Instruments, Mountain View). The scan rate was about 5 Hz and the applied force was the minimal value allowing to keep the contact between tip and sample. At least four images in height mode (trace and retrace) were recorded per sample. For the tapping mode, realized in air, the tip used was made of silicon, and it had a spring constant comprised between 20 and 80 N/m and a resonance frequency in air between 230 and 410 kHz (Park Scientific Instruments, Mountain View). The images were acquired at a scanning rate of about 1 Hz. Two randomly chosen zones were imaged per sample and for each zone a height image (trace) and a phase image (retrace) were recorded. All obtained images were processed with the Nanoscope software, using either flattening or plane fit according to the relief characteristics, with the minimal polynomial order needed.

XPS analyses were performed using a Kratos Axis Ultra spectrometer (Kratos Analytical, Manchester, UK) equipped with a monochromatized aluminum X-ray source (powered at 10 mA and 15 kV). The samples were fixed on a stainless steel multispecimen holder by using double-sided insulating tape. The pressure in the analysis chamber was about $10^{-6}$ Pa. The angle between the normal to the sample surface and the direction of photoelectron collection was 0°. Analysis was performed in the hybrid lens mode with the slot aperture, the resulting analyzed area being 700 μm × 300 μm. The pass energy was set at 160 eV for the wide scan and 40 eV for narrow scans. In the latter conditions, the full width at half maximum (FWHM) of the $Ag_{3d5/2}$ peak of a standard silver sample was about 0.9 eV. Charge stabilization was achieved by using the Kratos Axis device. The following sequence of spectra was recorded: survey spectrum, $C_{1s}$, $O_{1s}$, $N_{1s}$, and $C_{1s}$ again to check for charge stability as a function of time and the absence of degradation of the sample during the analyses. The *C*—(C,H) component of the $C_{1s}$ peak of carbon was fixed to 284.8 eV to set the binding energy scale. Molar concentration ratios were calculated using peak areas normalized on the basis of acquisition parameters after a linear background subtraction, and experimental sensitivity factors and transmission factors provided by the manufacturer. The results were expressed in element mole fractions, excluding hydrogen which is not detected by XPS.

## Cell culture

### Cell preparation

All animal housing and procedures were performed in compliance with guidelines established by the University Committee of Animal Resources at the University of Rochester. Under a dissecting scope, the brain of an E15 mouse embryo was harvested, from which the cortices were isolated, meninges removed and clean cortices then placed in a conical tube containing cold HBSS (Hank's Balanced Salt Solution, modified without Calcium and Magnesium, Gibco). HBSS was removed and replaced with 2 mL of pre-warmed 0.25% trypsin-EDTA (0.25% Trypsin, 1 m*M* EDTA in HBSS without calcium and magnesium, Gibco). The tube was placed at room temperature and gently agitated every 5 min for up to 20 min. Then the trypsin solution was removed and cold MEM (Minimum Essential Medium, Gibco) was added. The cortices were allowed to sit in MEM at room temperature for 5 min; this exchange was repeated three times. The plating medium was prepared as follows: 100 mL Neurobasal Medium (Gibco), 1 mL L-glutamic acid (2.5 m*M*, Sigma), 250 μL L-glutamine (200 m*M*, Sigma), 2 mL B-27 supplement (Gibco). 20 mL of plating medium was added and the cortices were triturated until most of the tissue was dissociated. The conical tube was allowed to sit for 5 min, then the sediment was removed. The cells were counted and the suspension was diluted with plating medium in order to obtain a concentration of $5 \times 10^4$ cells/well.

### Adhesion tests

A solution of poly(ethyleneimine) (PEI) was prepared by diluting 1 mL of PEI (Sigma, 50% w/v in water) in 500 mL borate buffer (pH 8.5). This solution was filtered into a sterile bottle and 0.4 mL was introduced in each well of a 24-well sterile plate (Corning). After one night in the dark, the PEI solution was removed and the wells were washed three times with 1 mL sterile Milli-Q water, the third wash lasting for 10 min. The plates were allowed to dry overnight. PEI coating of the wells was used in order to avoid migration of the cells from wells to samples, hence increasing excessively the cell concentration on the samples.

The substrates (each disk cut into four pieces) were sterilized in pure ethanol for 30 min in multiwell plates. After ethanol removal, the samples were allowed to dry in the open air. The substrates were conditioned as described for fibronectin adsorption except that the fibronectin solution was prepared with sterile PBS (Invitrogen). After the five washes, they were placed in PEI-coated multiwell plates, then about 1 mL of Neurobasal Medium (Gibco) was added and the plate was warmed up at 37°C. Once the cell suspension was ready, the Neurobasal Medium was removed and 0.8 mL of the cell suspension was added

**TABLE I**
**Characteristics of the Homogeneous Substrates Before and After Fibronectin Adsorption**

| | $PS_f$ | PA98 | $PS_s$ | PA80 |
|---|---|---|---|---|
| Before fibronectin adsorption | | | | |
| (O/C) × 100 | 0.2 | 33 | 1.1 | 33.8 |
| Water contact angle (°) [standard deviation] | 89.0 [0.9] | 71.0 [0.6] | 85.0 [2.9] | 65.5 [1.5] |
| $R_{rms}$ (nm) | 1.7 | 0.8 | 1.8 | 2.3 |
| With adsorbed fibronectin | | | | |
| $R_{rms}$ (nm) | 2.7 | 1.4 | 1.5 | 5.9 |
| Dimension of relief features (nm) | | | | |
| Lateral | 50–150 | 50–150 | 50–150 | 300–500 |
| Vertical | <8 | <8 | <8 | <30 |

per well. The plates were incubated at 37°C for 5 days in an incubator with 7% $CO_2$.

After 5 days, the cells were fixed by replacing the culture medium with a 4% paraformaldehyde solution (PFA, Mallinckrodt Baker Inc.). After 30 min at 4°C, the PFA solution was removed and the samples were stored in PBS at 4°C.

### Immunostaining

The cells were permeabilized with three washes of 10 min with a 0.1% Triton-X solution in PBS. The blocking step was realized by incubating the samples in a 5% nonfat dried milk, 0.05% Triton-X solution in PBS. The cells were then incubated in the blocking solution with a primary antibody, anti-β tubulin (Sigma, mouse IgG2b), or anti-integrin β1 (Chemicon, rat IgG2a) at a dilution of 1:2000. The samples were then washed three times 10 min with a 0.05% Triton-X solution in PBS. The samples were incubated for 45 min in the dark in the blocking solution with a secondary antibody: anti-mouse 488 or anti-rat 594 (Alexa Fluor from Invitrogen), at a dilution of 1:2000. Finally the samples were washed again three times 10 min with a 0.05% Triton-X solution in PBS. In the second wash, a 1:1000 Hoechst solution (Sigma, 5 m*M* in water) was added in order to stain the cell nucleus. For microscopy, the samples were mounted in Mowiol on a glass slide, covered with a glass coverslip, and sealed with nailpolish. The Mowiol solution was made with 6 g glycerol (J.T. Baker), 2.4 g Mowiol (Polyscience), 6 mL Milli-Q water, and 12 mL 0.2*M* Tris buffer (pH 8.5). The mounted samples can be stored at −20°C for several months. They were observed under a fluorescence microscope (Olympus AH-2 microscope) linked to an image processing computer.

### Metabolism measurements

The Alamar Blue assay was used in order to determine the cell activity, which can be related to the amount of living cells. After 5 days of culture, the Alamar Blue reagent (Biosource) was added to the culture medium at a concentration of 1:10. After 7, 23, and 28 h, 100 μL of the solution was removed and placed in a multiwell plate for fluorescence counting. The emitted fluorescence was measured at 590 nm with excitation at 510 nm.

## RESULTS

### Substrate conditioning by fibronectin

The chemical and morphological characteristics of the homogeneous substrates are presented in Table I.[23,24] $PS_f$ and $PS_s$ are very similar, with an O/C ratio measured by XPS close to 0, a water contact angle close to 90° and a rms roughness equal to 1.7–1.8 nm. PA98 and PA80 present higher oxygen surface concentrations and a lower water contact angle. These two substrates are similar regarding surface elemental composition and water contact angle; their surface roughness is slightly lower (PA98) and slightly higher (PA80), compared with $PS_f$ and $PS_s$. To reveal differences of chemical functions between substrates, XPS spectra of PA80, PA98, and PMMA spin-coated following the same procedure were recorded after immersion during 1 h in $10^{-3}M$ KOH followed or not by rinsing during 10 min in water. For PMMA and PA98, no potassium and no change in the shape of $C_{1s}$ and $O_{1s}$ peaks were detected as a result of immersion in KOH solution. As compared with the native state, PA80 submitted to KOH was characterized by the presence of potassium (K/O = 0.04 and 0.15 with and without rinsing, respectively), the presence of an $O_{1s}$ peak component at 530.8 eV typical of carboxylate (fraction of the $O_{1s}$ peak equal to 0.09 and 0.25 with and without rinsing, respectively), and the presence of a $C_{1s}$ component near 288 eV typical of carboxylate. These consistent data, particularly the observation of about 1 potassium ion for 2 oxygen atoms of carboxylate nature, indicate that carboxyl-carboxylate functions are exposed at the surface of PA80, while they are not detected at the surface of PA98.

Fibronectin adsorption isotherms were obtained on the different surfaces in order to determine the concentration to be used. Solution concentrations from 1 to 50 μg/mL were used and the amount of adsorbed fibronectin was evaluated by the nitrogen concentration determined by XPS. The *N* mole fraction

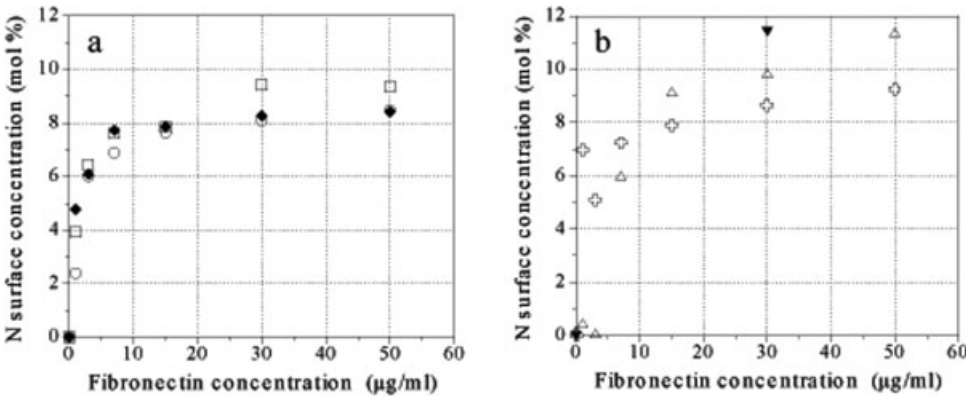


**Figure 1.** Nitrogen surface concentration determined by XPS on (a) $PS_f$ (□), PA98 (○) and PA98/PS (◆); and (b) $PS_s$ (✠), PA80 (Δ) and PS-PA80 (▼) after 24 h fibronectin adsorption from solutions at different concentrations.

increased strongly when the fibronectin concentration rose to about 10 µg/mL and did not increase much at higher concentrations (Fig. 1). In the following experiments, protein adsorption was performed using a solution concentration at the quasi-plateau of adsorption. There was no major difference observed from one kind of substrate to another.

Figure 2 presents AFM images of surfaces before and after fibronectin adsorption (50 µg/mL solution): homogeneous PS film (**$PS_f$**), PMMA–PMAA spin-coated on PMMA (**PA98**), and heterogeneous surface obtained after spin-coating PMMA–PMAA on PS (**PA98/PS**). Cross-sections show that $PS_f$ presents a large lateral scale relief (lateral size of the order of

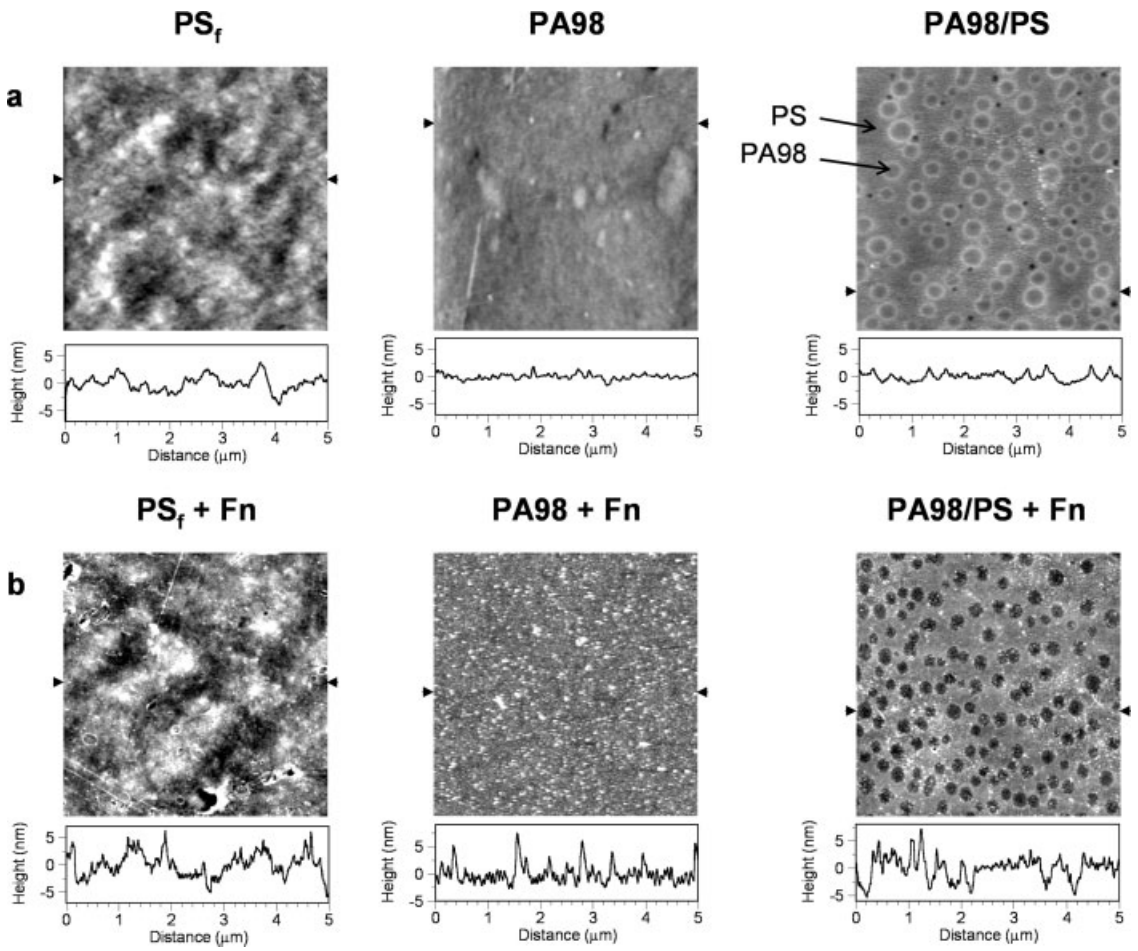


**Figure 2.** AFM images ($5 \times 5$ µm$^2$) and associated cross-sections of surfaces of $PS_f$, PA98, and PA98/PS (a) before and (b) after fibronectin (Fn) adsorption from a 50 µg/mL solution. The z gray scale is 10 nm.

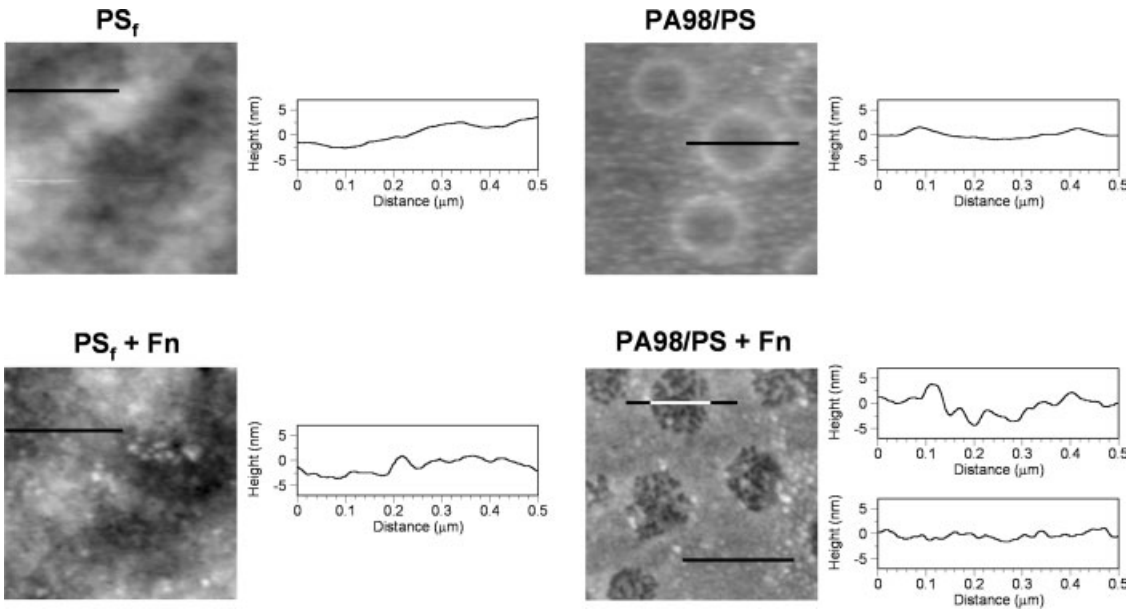


**Figure 3.** AFM images ($1 \times 1$ μm$^2$) of surfaces of $PS_f$ and PA98/PS before and after fibronectin (Fn) adsorption from a 50 μg/mL solution, with cross-sections at the location indicated in the images. The z gray scale is 15 nm.

1 μm) and that fibronectin adsorption adds a fine roughness. This is revealed by the increase of the $R_{rms}$ measured on the AFM images (Table I). The morphology of the fibronectin layer adsorbed on $PS_f$ cannot easily be observed on the 5 μm images because of the polymer surface relief itself. The difference resulting from adsorption is more visible on the 1 μm images and the sections presented in Figure 3. After fibronectin adsorption, relief features with a height below 8 nm are superimposed to the morphology of $PS_f$. Their apparent lateral size is in the range of 50–150 nm. The PA98 surface (Fig. 2) is very smooth. After fibronectin adsorption, particles are regularly distributed on the surface, with dimensions of 3–6 nm height and 50–150 nm width, and $R_{rms}$ increases slightly (Table I). The PA98/PS surface (Fig. 2) presents inclusions of one phase in another phase. Chlorobenzene, the solvent used for spin-coating PMMA–PMAA 98-02, is also a solvent of the PS substrate and causes its dissolution during spin-coating. Polymer demixing when the solvent evaporates leads to a nearly flat surface, with a PS matrix forming characteristic rings around the PMMA–PMAA inclusions.[23] After fibronectin adsorption, the surface of acrylic copolymer inclusions appears to be below the surrounding surface. The fibronectin behavior on the heterogeneous PA98/PS surface can be observed in details in Figure 3. The images and the cross-sections show that adsorbed fibronectin forms many granular structures (up to 8 nm high and 50–150 nm wide) on the PMMA–PMAA inclusions, while the adsorbed layer is smoother on the PS background. This is similar to observations made on the homologous homogeneous surfaces.

Figure 4 presents AFM images of the other surfaces: PS spin-coated on a PMMA film (**$PS_s$**), PMMA–PMAA copolymer spin-coated on a PMMA film (**PA80**), and heterogeneous surface obtained after spin-coating a blend of PS and PMMA–PMAA on a PMMA film (**PS-PA80**). The $PS_s$ is quite smooth, with a few holes spread over the surface. After adsorption, the fibronectin seems to cover the holes while a few positive relief features are observed in the cross-sections; $R_{rms}$ decreases slightly (Table I). The homogeneous PA80 surface contains holes spread all over the surface. After fibronectin adsorption, this surface presents a large-scale relief, with characteristic lateral dimensions in the range of 300–500 nm and differences in height up to 30 nm, but granules are not identified, in contrast with PA98. Finally, the PS-PA80 heterogeneous surface presents a topography with islands. Solvent evaporation during spin-coating induced phase separation, the less concentrated PS forming islands in the PMMA–PMAA, owing to the lower solubility of PS in the solvent used (dioxane).[24] The cross-sections presented in Figure 5 allow the adsorbed layer morphology to be observed in details. Whereas the islands and the baseline are extremely smooth before protein adsorption, the surface becomes much rougher after fibronectin adsorption. Two observations can be made: (i) fibronectin seems to accumulate at the edges of the islands, and (ii) besides the edges, fibronectin forms a much smoother layer on

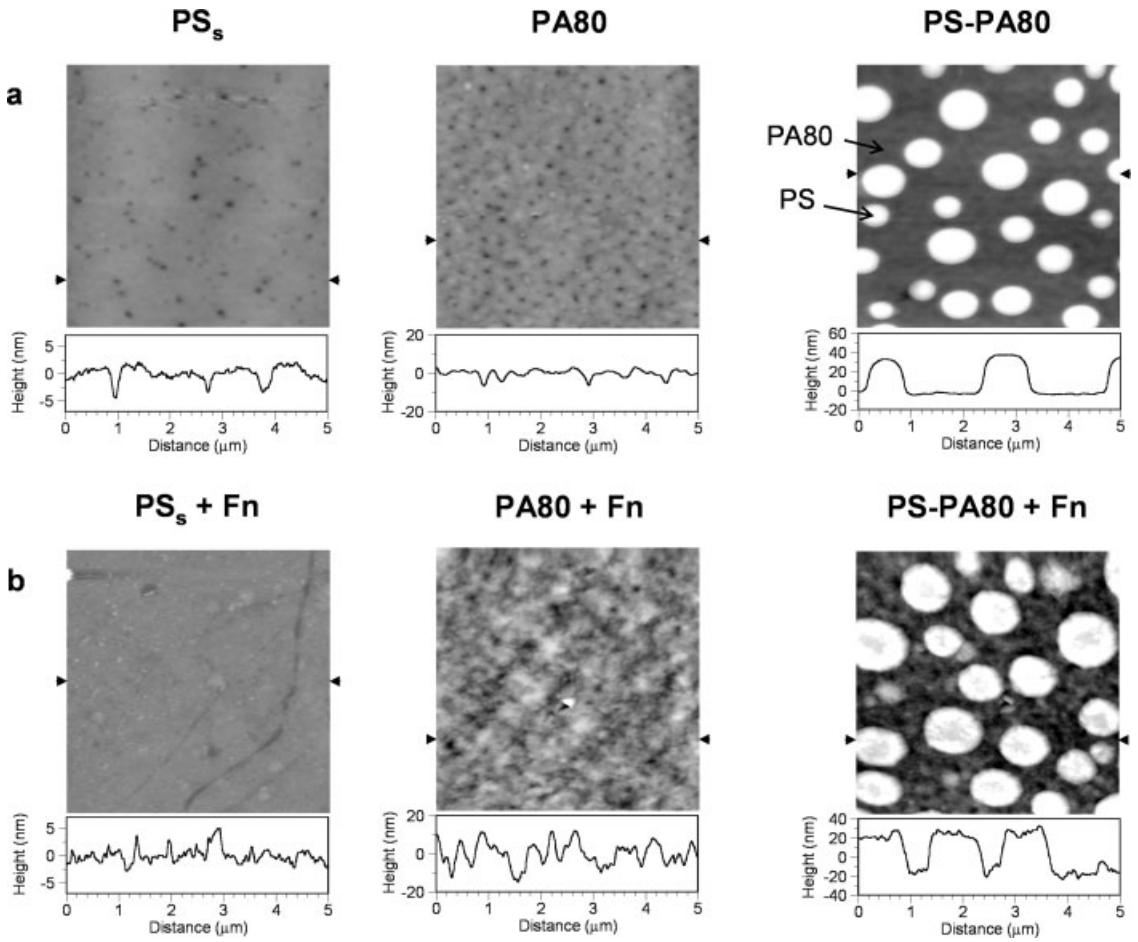


**Figure 4.** AFM images ($5 \times 5$ μm$^2$) and associated cross-sections of surfaces of PS$_s$, PA80, and PS-PA80 (a) before and (b) after fibronectin (Fn) adsorption from a 50 μg/mL solution (except PS-PA80, 30 μg/mL). The z gray scale is 50 nm.

the PS islands (differences in height below 8 nm) than on the PMMA–PMAA surface (differences in height up to 30 nm). Except the edge effect, the observations are again very similar to those made on the homologous homogeneous surfaces.

### Mouse cortical cell cultures

The substrates were conditioned by fibronectin adsorption from a 30 μg/mL solution and used in cell adhesion tests. Figure 6 presents representative pictures obtained in a first set of experiments, showing whole cells (a,c, staining for β-tubulin) and nuclei (b,d, Hoechst staining). For the first group, i.e. PS$_f$, PA98, and PA98/PS, large clusters were found, with some processes (outward projections). The number of cells per cluster, evaluated on images stained for the nucleus, was comprised between 15 and 50. For the second group of surfaces (PA80 and PS-PA80), large networks were observed with many processes over the surface. A few aggregates were present, with a size not exceeding 5–10 cells. Staining for integrin β1 was also realized and showed a co-localization with the β-tubulin. Note that no focal contacts are found on neuronal cells, which rather exhibit point contacts consisting in smaller integrin aggregates without any characteristic shape.[36]

Quantitative approaches were used in order to possibly discriminate the substrates regarding the cell behavior. The density of adhering cells was determined. The density of cells that were alive before fixation was also evaluated on images obtained by Hoechst staining: a dead cell has a very small and bright nucleus, while a living cell has a larger and unevenly stained nucleus. These results were not accurate since certain cells were washed during fixation and staining. However, the number of living cells was proportional to the total number of cells (results not shown). The cell activity was evaluated by Alamar Blue measurements before fixation, after 5 days in culture, but the results (not shown) were similar for all the substrates. Although the two classes of surfaces differed according to the formation of a net of processes, they did not differ

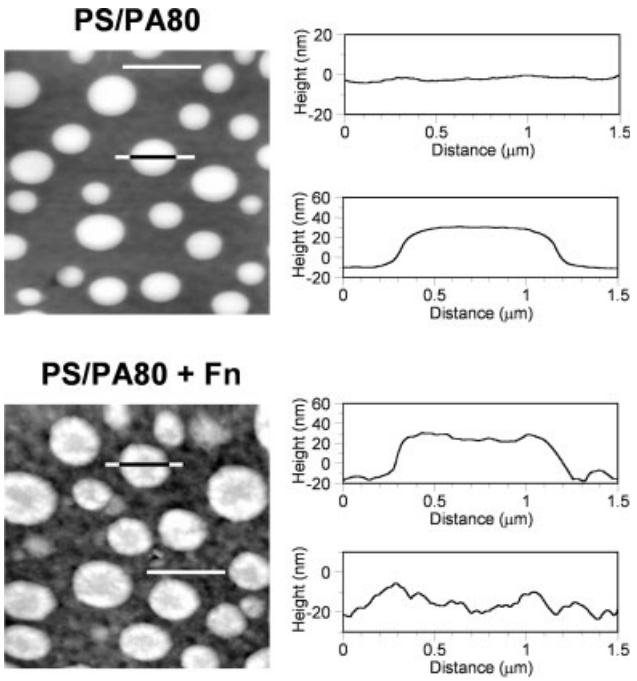


**Figure 5.** AFM images ($5 \times 5$ μm$^2$) of surfaces of PS-PA80 before and after fibronectin (Fn) adsorption from a 30 μg/mL solution, with cross-sections at the locations indicated in the images. The z gray scale is 50 nm.

significantly regarding the average length of processes. Signs of poor adhesion are clumping of neuronal cell bodies and fasciculation of processes.[37] Thus cell clustering (number of cells per cluster) was tentatively used to discriminate the surfaces. The ratio of cells in clusters over the total cell number is presented in Figure 7. The replicates refer to different substrate specimens in the first set of experiments. Two groups can be distinguished: on the one hand, PS, PA98, and PA98/PS, where most of the cells are in clusters (about 70%, except on PA98, where this ratio is lower), and on the other hand, PA80 and PS-PA80, on which only 10–20% of the cells are found in clusters.

The results of the first set of experiments were ranked according to the proportion of cells in aggregated form (majority of aggregated cells or majority of individual cells), and the cluster size (small, medium, or large corresponding to $<10$, 10–30, or $>30$ cells/cluster). The results are presented in Table II (set 1). Their significance was further established by other experiments involving a more rapid evaluation that was designed to avoid bias regarding cell culture or substrate preparation. In set 2, two randomly chosen pictures, representing 1% of the sample surface, were examined and evaluated by eye according to the same criteria. In set 3, pictures were taken systematically at four places of the sample using a lower magnification, in order to cover about 8% of the sample surface. The edges of the samples were avoided as they could have been damaged during sample manipulation. The polymer samples for the three culture experiments were prepared at the same time, except set 3B, for which new samples were prepared and $PS_f$ was replaced by $PS_s$. Table II shows a constant distinction between two groups of samples; moreover the proportion of cells in aggregated form was correlated with the cluster size. On the samples containing PA80 (PA80 and PS-PA80), the majority of the cells were individual and the clusters formed were small. On the other samples ($PS_f$, PA98, PA98/PS, and $PS_s$), the cells were mainly found in an aggregated state and large clusters were formed.

## DISCUSSION

### Substrate conditioning by fibronectin

On $PS_f$ and $PS_s$ (Figs. 2 and 4), fibronectin forms a rather smooth layer, with relief features below 5 nm height and a width comprised between 50 and 80 nm. Knowing that fibronectin is a fibrilar protein with dimensions of about $6 \times 6 \times 60$ nm$^3$, it may be concluded that the relief thickness corresponds to about a single layer of slightly flattened molecules. According to the ratio between the thickness and the AFM probe radius (about 5–10 nm) and to the apparent lateral size, the latter is not much larger than the real lateral size. After fibronectin adsorption, the PA98 surface presents surface features similar to PS with some granules which are thicker and better resolved. The surface morphology obtained on PA98/PS (Figs. 2 and 3) confirms that fibronectin adsorption tends to produce a more regular layer on PS and a more granular structure on PA98. In contrast fibronectin adsorbed on PA80 forms thicker (about 20 nm) and broader relief features, as observed both on the homogeneous PA80 surface and on PS-PA80 (Figs. 4 and 5).

The nitrogen molar fraction given by XPS does not significantly differ between the different surfaces. However, as the substrate surfaces have a different chemical composition, a comparison must be based on a more detailed analysis of the results. The N/C molar concentration ratio given by XPS may be compared with ratios computed using models of the adsorbed layers in which $\gamma$ and $(1 - \gamma)$ represent the fractions of the surface covered by a protein layer with a constant thickness $t_1$ and $t_2$, respectively (note that $t$ is a cumulated thickness, neglecting voids):

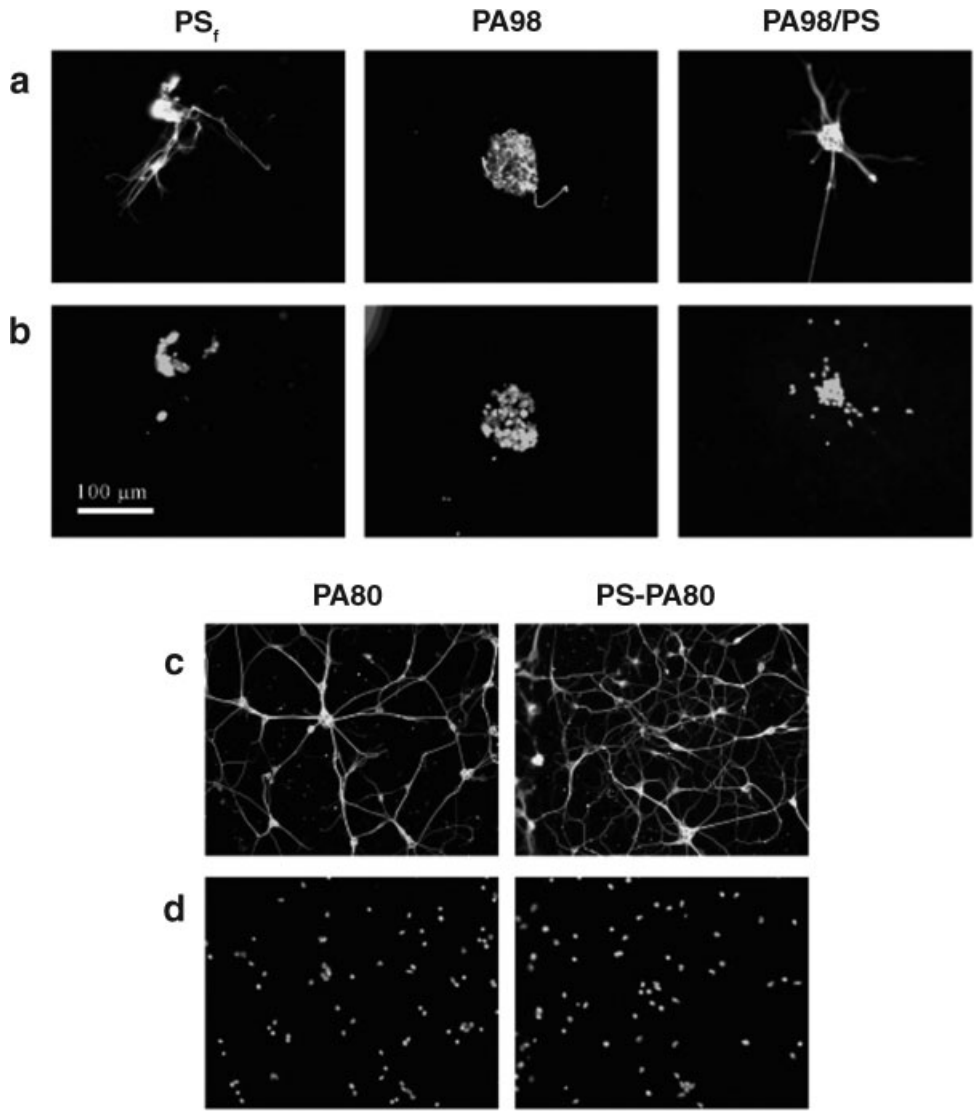


**Figure 6.** Images obtained by fluorescence microscopy of mouse cortical neurons cultured on substrates conditioned with fibronectin, $PS_f$, PA98, PA98/PS, PA80, and PS-PA80: (a,c) staining of the whole cell (β-tubulin), (b,d) nucleus staining (Hoechst).

$$\frac{N}{C}=\frac{i_C}{i_N}\cdot\frac{\sigma_N}{\sigma_C}\times\frac{\gamma\lambda_N^{prot}C_N^{prot}\left[1-\exp\frac{-t_1}{\lambda_N^{prot}\cos\theta}\right]+(1-\gamma)\lambda_N^{prot}C_N^{prot}\left[1-\exp\frac{-t_2}{\lambda_N^{prot}\cos\theta}\right]}{\gamma\left\{\lambda_C^{prot}C_C^{prot}\left[1-\exp\frac{-t_1}{\lambda_C^{prot}\cos\theta}\right]+\lambda_C^{poly}C_C^{poly}\exp\frac{-t_1}{\lambda_C^{prot}\cos\theta}\right\}+(1-\gamma)\left\{\lambda_C^{prot}C_C^{prot}\left[1-\exp\frac{-t_2}{\lambda_C^{prot}\cos\theta}\right]+\lambda_C^{poly}C_C^{poly}\exp\frac{-t_2}{\lambda_C^{prot}\cos\theta}\right\}} \quad (1)$$

where $i_C$ and $i_N$ are the sensitivity factors provided by the instrument manufacturer for carbon (0.278) and nitrogen (0.477); $\sigma_C$ and $\sigma_N$ are the photoionization cross-sections for carbon (1.0) and nitrogen (1.8)[38]; θ is the angle made by the direction of photoelectron collection with respect to the normal to the sample surface (here θ = 0); $C$ and λ represent the concentration and the electron mean free path in the protein layer (superscript prot) or in the polymer substrate (superscript poly, PS or PMMA): $C_C^{prot}$ = 61.21 and $C_N^{prot}$ = 17.15 mmol/cm$^3$ (calculated from the fibronectin sequence[39] and considering a density of 1.4 g/cm$^3$),[40] $C_C^{PS}$ = 80.8 mmol/cm$^3$, $C_C^{PMMA}$ = 59.5 mmol/cm$^3$,[41] $\lambda_C^{prot}$ = 3.5 nm and $\lambda_N^{prot}$ = 3.2 nm

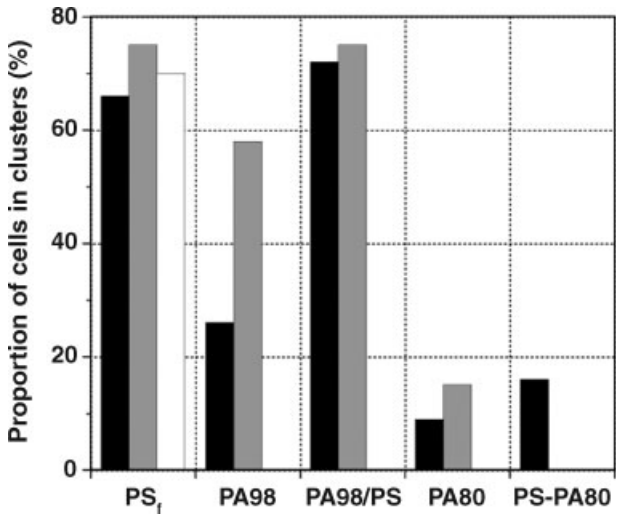


**Figure 7.** Proportion of mouse cortical neurons in clusters after culture on different substrates conditioned with fibronectin.

(values calculated for albumin[42]), $\lambda_C^{PS} = 3.8$ nm, $\lambda_C^{PMMA} = 3.25$ nm.[41]

Figure 8 presents parameters that are compatible with the N/C molar ratios measured by XPS, on the basis of Eq. (1). Two different models were considered, in order to determine whether fibronectin was adsorbed besides the structures observed by AFM: a first one involving a discontinuous adsorbed protein layer and a second one involving a continuous layer with two different adsorbed layer thicknesses. The two models merge if the adsorbed layer is continuous ($\gamma = 1$) with a uniform thickness $t_1$. In this case, the thickness could be in the range of 1.7–2.8 nm depending on the substrate. If the surface coverage by the protein is lower (discontinuous layer), the minimal surface coverage that could fit the measured N/C ratio is in the range of 50–60%, depending on the substrate. This is much higher than the degree of surface coverage by relief features, which was observed by AFM on PA98 (Fig. 2), $PS_f$ (Fig. 3), and $PS_s$ (Fig. 4), indicating that fibronectin is adsorbed in the space between these features. If it is considered that the granules observed by AFM ($t_2 = 5$ nm) cover 10 to 30% ($1 - \gamma$) of the surface, the thickness $t_1$ of fibronectin adsorbed besides the granules is comprised between 1.5 and 1.0 nm on PA98 and around 2 nm on PS. Figure 9 schematizes the layer adsorbed on the heterogeneous PA98/PS surface, according to the combination of XPS and AFM data, with a thinner fibronectin background and larger granular features on the PA98 inclusions compared with the PS matrix.

In the case of PA 80, AFM shows the presence of a rough adsorbed layer with differences in height up to 20 nm ($R_{rms} = 5.9$ nm). The XPS data are compatible with a degree of surface coverage $\gamma$ of about 60%

**TABLE II**
**Qualitative Observation of Mouse Cortical Neurons Cultured on Different Substrates Preconditioned With Fibronectin, for 3 Independent Cell Culture Series**

| | | $PS_f$ | | PA98 | | PA98/PS | | $PS_s$ | | PA80 | | PS-PA80 | |
|---|---|---|---|---|---|---|---|---|---|---|---|---|---|
| Set* | Observ.** | State*** | Cluster Size | State*** | Cluster Size | State*** | Cluster Size | State*** | Cluster Size | State*** | Cluster Size | State*** | Cluster Size |
| 1 | Quant. | Aggr. | Large | Aggr. | Large | Aggr. | Large | | | Indiv. | Small | Indiv. | Small |
| 2 | Qual. | Aggr. | Large | Aggr. | Large | Indiv. | Large | | | Indiv. | Small | Indiv. | Small |
| 3A | Qual., syst. | Aggr. | Large | Aggr. | Large | Aggr. | Medium | | | Indiv. | Small | Indiv. | Medium |
| 3B | Qual., syst. | | | | | | | Aggr. | Large | Indiv. | Small | Indiv. | Medium |

*The polymer samples come from the same batch, except those from experiment 3B.
**Observ. = observations; quant. = quantitative; qual. = qualitative; syst. = systematic (see text for details).
***Aggr. = aggregated form; indiv. = individual cells.

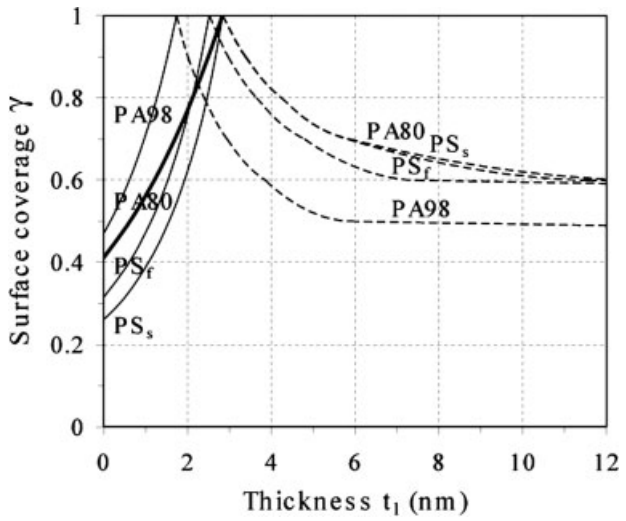


**Figure 8.** Plot of surface coverage γ versus thickness $t_1$ showing the pairs of values compatible with the N/C molar ratio measured by XPS after adsorption of fibronectin on the homogeneous supports $PS_f$, $PS_s$, PA98, and PA80. The dashed lines correspond to a discontinuous coverage ($t_2 = 0$); the plain lines correspond to a continuous layer for which the fraction $(1 - \gamma)$ of the surface is covered by a layer of thickness $t_2 = 5$ nm (thin line) or $t_2 = 20$ nm (thick line, PA80).

(discontinuous layer, $t_2 = 0$; cf. Fig. 8). Owing to the small depth analyzed by XPS, the same results are obtained for any thickness above about 8 nm. Alternately, a model with a portion $(1 - \gamma)$ of the surface covered by a layer of thickness $t_2 = 20$ nm was considered. It appears then in Figure 8 (PA80, plain line) that the XPS data are compatible with a surface coverage by fibronectin aggregates lower than 60% $(1 - \gamma)$ provided the rest of the surface is covered by a thinner (up to 3 nm) layer. It appears thus that all substrates provide a high degree of surface coverage by fibronectin but differ according to the size of fibronectin aggregates. This is much larger on PA80 compared with PA98 and PS. The state of aggregation may not be related to marked differences of oxygen surface concentration, apparent hydrophilicity or surface roughness. However it is related to a higher surface density of carboxyl-carboxylate functions conferred by the PMAA segments.

### Mouse cortical cell cultures

Among the investigated substrates, two were favorable for cell spreading and growth, as the cells were individual and their processes formed an organized network. These two surfaces have in common the presence of the PA80 copolymer, while one of them is homogeneous, and the other one is heterogeneous with PS islands. In contrast, homogeneous $PS_f$, $PS_s$, and PA98, and heterogeneous PA98/PS induced cell aggregation, an evidence of poor interactions with the substrate. Adsorbed fibronectin, as observed by AFM, showed different morphologies according to the polymer, with the PA80 surface inducing a much rougher adsorbed layer. The presence of PA80 and the resulting aggregation of fibronectin in the adsorbed phase thus appear to be critical factors for cell spreading and growth.

The PA98/PS sample (topography showing rings of 0.15–1.5 μm diameter and up to 8 nm height) affects the cells in the same way as homogeneous $PS_f$, $PS_s$, or PA98 samples. The PS-PA80 sample, with its particular topography (protruding islands of 0.5–1 μm diameter and about 40 nm height) induced by the PS inclusions in PA80, does not affect the cells differently from the flat and homogeneous PA80 sample. The cell network formation observed here thus seems to be exclusively linked to the fact that a high proportion of the surface is covered by strongly aggregated fibronectin. It does not seem to be influenced by inclusions characterized by a lower fibronectin aggregation and responsible for surface protrusions in the range examined here (surface coverage below 30%, height below 40 nm, and lateral size below 1.0 μm).

The influence of the substrate wettability deserves consideration. The tendency of cells to adhere,[11–14] spread[11,14] or differentiate[15] on hydrophilic supports conditioned with fibronectin has been observed for other cell types cultured on fibronectin. In the present study, there is no general link between fibronectin adsorption or cell behavior and apparent surface hydrophilicity. PA98 and PA80 have only slightly different water contact angles (71° and 66°, respectively), but induce different fibronectin and cell behaviors; on the other hand PA98 and PS show a larger difference of water contact angles with similar behaviors. The global hydrophilicity as evaluated by the static water contact angle may be too raw to discriminate surface properties. The acidic functions and the surface electrical charge appear to play a role by influencing fibronectin aggregation. As the isoelectric point of fibronectin is 5.6,[39] aggregation would be favored by a repulsive electrostatic contribution. Surface charge effects on protein adsorption or on cell behavior have been reported,[2] but no general tendency could be established, the cell response

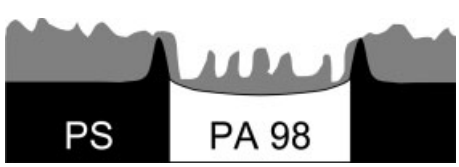


**Figure 9.** Model describing fibronectin adsorption on the heterogeneous PA98/PS surface (fibronectin is in gray).

depending on cell type, surface chemistry as well as surface charge. Miller and Boettiger[43] reported an increase in spread area for fibrosarcoma cells grown on negatively charged PS compared with the uncharged polymer substrate, whereas the same amount of fibronectin was bound to both surfaces.

The cell culture media used here contained proteins (albumin, catalase, insulin, superoxide dismutase, transferrin). None of these proteins is an adhesion protein; on the other hand they may displace fibronectin and have an adverse effect on cell attachment. Moreover, during the culture, the cells secrete different proteins, including their own adhesion proteins.[44] The exchange between fibronectin and albumin has been studied several times. Albumin is the major competing protein since it is present at high concentration in serum-containing culture media.[10] For pure PS and tissue culture PS (surface oxidized), Grinnell and Feld[11] found that only a small amount (10–20%) of fibronectin could be desorbed by sequential incubations. Klebe et al.[45] observed a similar cell behavior, whether the substrate was conditioned with fibronectin alone or with fibronectin and subsequently albumin, on a series of substrates with different wettabilities. Finally, Renner et al.[10] found that preadsorbed fluorescent dye labeled fibronectin was more readily displaced when exposed to a solution of fibronectin, compared with a solution of albumin or with pure PBS. It appears thus that adsorbed fibronectin is not easily displaced from the surfaces.

Antibody binding assays allowed a comparison to be made between the exposure of different ligands towards the solution.[12] The exposure of ligands involved in cell adhesion was relatively enhanced for fibronectin adsorbed on tissue culture PS compared with PS. The difference was observed in a wide range of the amount of adsorbed fibronectin (average thickness from below 1 to about 7 nm). Labeling of the sulfhydryl group located near the cell binding domain[14] showed different fluorescence emission spectra for fibronectin adsorbed on glass and on silanized glass, indicating a different environment for these sulfhydryl groups and hence different fibronectin conformation on these substrates. The influence of PA80 on neuron cell behavior through the morphology of the adsorbed fibronectin layer may tentatively be attributed to the exposure of ligands. This could possibly be due to a change of conformation induced by aggregation; however aggregation may also be itself a result of a change of conformation upon adsorption. Furthermore Altankov et al.[16,46] observed that, if the interaction of fibronectin with the surface is too strong, the cells are not able to reorganize their matrix. Accordingly the rougher morphology of the fibronectin layer adsorbed on PA80 might be more favorable to cell adhesion because of easier remodeling by the cells, owing to a weaker interaction with the surface.

## CONCLUSION

Whereas fibronectin is adsorbed in similar amounts on the surfaces studied, the adsorbed layer morphology was found to be dependent on the substrate nature. In comparison with $PS_f$, $PS_s$, and PA98, the layer formed on PA80 was much rougher, with relief features up to 30 nm in height. The neuronal cells cultured on these surfaces were found to form large clusters on substrates of the first category including PS with PA98 inclusions, which indicates poor interactions with the substrate. In contrast, the cells cultured on PA80-containing surfaces formed large networks with only a few small aggregates. The fibronectin morphology observed on PA80 is thus more favorable for the formation of neural networks, possibly because of a better exposure of ligands or an easier remodeling by the cells.

The influence of the chemical functions at the substrate surface (anionic groups) on fibronectin aggregation and thereby on cell adhesion appears to be a dominating factor compared with global differences of elemental composition or apparent hydrophilicity. It is not prevented by defects due to heterogeneities in the range examined here, i.e. surface coverage of weakly aggregated fibronectin below 30%, topographic heterogeneities with height below 40 nm and lateral size below 1.0 μm.

## References


1. Williams DF. Tissue-biomaterial interactions. J Mater Sci 1987;22:3421–3445.
2. Wilson CJ, Clegg RE, Leavesley DI, Pearcy MJ. Mediation of biomaterial-cell interactions by adsorbed proteins: A review. Tissue Eng 2005;11:1–18.
3. Dewez J-L, Lhoest J-B, Detrait E, Berger V, Dupont-Gillain CC, Vincent L-M, Schneider Y-J, Bertrand P, Rouxhet PG. Adhesion of mammalian cells to polymer surfaces: From physical chemistry of surfaces to selective adhesion on defined patterns. Biomaterials 1998;19:1441–1445.
4. Alaerts JA, De Cupere VM, Moser S, Van den Bosh de Aguilar, Rouxhet PG. Surface characterization of poly(methyl methacrylate) microgrooved for contact guidance of mammalian cells. Biomaterials 2001;22:1635–1642.
5. Britland S, Perridge C, Denyer M, Morgan H, Curtis A, Wilkinson C. Morphogenetic guidance cues can interact synergistically and hierarchically in steering nerve cell growth. Exp Biol Online 1997;V1:1–15.
6. Chen CS, Mrksich M, Huang S, Whitesides GM, Ingber DE. Geometric control of cell life and death. Science (Washington, DC) 1997;276:1425–1428.
7. Keresztes Z, Rouxhet PG, Remacle C, Dupont-Gillain C Supramolecular assemblies of adsorbed collagen affect the adhesion of endothelial cells. J Biomed Mater Res A 2006;76: 223–233.
8. Dupont-Gillain CC, Alaerts JA, Dewez JL, Rouxhet PG. Patterned layers of adsorbed extracellular matrix proteins: Influence on mammalian cell adhesion. Biomed Mater Eng 2004; 14:281–291.

9. Norde W, Giacomelli CE. Conformational changes in proteins at interfaces. From solution to the interface, and back. Macromol Symp 1999;145:125–136.
10. Renner L, Pompe T, Salchert K, Werner C. Dynamic alterations of fibronectin layers on copolymer substrates with graded physicochemical characteristics. Langmuir 2004;20: 2928–2933.
11. Grinnell F, Feld MK. Fibronectin adsorption on hydrophilic and hydrophobic surfaces detected by antibody binding and analyzed during cell adhesion in serum-containing medium. J Biol Chem 1982;257:4888–4893.
12. Underwood PA, Steele JG, Dalton BA. Effects of polystyrene surface chemistry on the biological activity of solid phase fibronectin and vitronectin, analysed with monoclonal antibodies. J Cell Sci 1993;104:793–803.
13. Grinnell F, Feld MK. Adsorption characteristics of plasma fibronectin in relationship to biological activity. J Biomed Mater Res 1981;15:363–381.
14. Iuliano DJ, Saavedra SS, Truskey GA. Effect of the conformation and orientation of adsorbed fibronectin on endothelial cell spreading and the strength of adhesion. J Biomed Mater Res 1993;27:1103–1113.
15. Stephansson SN, Byers BA, Garcia AJ. Enhanced expression of the osteoblastic phenotype on substrates that modulate fibronectin conformation and integrin receptor binding. Biomaterials 2002;23:2527–2534.
16. Altankov G, Thom V, Groth T, Jankova K, Jonsson G, Ulbricht M. Modulating the biocompatibility of polymer surfaces with poly(ethylene glycol): Effect of fibronectin. J Biomed Mater Res 2000;52:219–230.
17. Walheim S, Boeltau M, Mlynek J, Krausch G, Steiner U. Structure formation via polymer demixing in spin-cast films. Macromolecules 1997;30:4995–5003.
18. Tanaka K, Takahara A, Kajiyama T. Film thickness dependence of the surface structure of immiscible polystyrene/poly (methyl methacrylate) blends. Macromolecules 1996;29:3232–3239.
19. Affrossman S, Jerome R, O'Neill SA, Schmitt T, Stamm M. Surface structure of thin film blends of polystyrene and poly (*n*-butyl methacrylate). Colloid Polym Sci 2000;278:993–999.
20. Ton-That C, Shard AG, Teare DOH, Bradley RH. XPS and AFM surface studies of solvent-cast PS/PMMA blends. Polymer 2001;42:1121–1129.
21. Li X, Han Y, An L. Surface morphology control of immiscible polymer-blend thin films. Polymer 2003;44:8155–8165.
22. Tsai IY, Kimura M, Stockton R, Green JA, Puig R, Jacobson B, Russell TP. Fibroblast adhesion to micro- and nano-heterogeneous topography using diblock copolymers and homopolymers. J Biomed Mater Res A 2004;71:462–469.
23. Dekeyser CM, Biltresse S, Marchand-Brynaert J, Rouxhet PG, Dupont-Gillain C. Submicrometer-scale heterogeneous surfaces by PS-PMMA demixing. Polymer 2004;45:2211–2219.
24. Zuyderhoff E, Dekeyser CM, Rouxhet PG, Dupont-Gillain ChC. An AFM, XPS and wettability study of the surface heterogeneity of thin films of PS/PMMA-PMAA blends. Submitted for publication.
25. Dalby MJ, Riehle MO, Johnstone H, Affrossman S, Curtis ASG. In vitro reaction of endothelial cells to polymer demixed nanotopography. Biomaterials 2002;23:2945–2954.
26. Dalby MJ, Riehle MO, Johnstone HJH, Affrossman S, Curtis ASG. Polymer-demixed nanotopography: Control of fibroblast spreading and proliferation. Tissue Eng 2002;8:1099–1108.
27. Dalby MJ, Giannaras D, Riehle MO, Gadegaard N, Affrossman S, Curtis ASG. Rapid fibroblast adhesion to 27 nm high polymer demixed nano-topography. Biomaterials 2004;25:77–83.
28. Riehle MO, Dalby MJ, Johnstone H, MacIntosh A, Affrossman S. Cell behaviour of rat calvaria bone cells on surfaces with random nanometric features. Mater Sci Eng C 2003; 23:337–340.
29. Lim JY, Hansen JC, Siedlecki CA, Runt J, Donahue HJ. Human foetal osteoblastic cell response to polymer-demixed nanotopographic interfaces. J R Soc Interface 2005;2:97–108.
30. Dalby MJ, Riehle MO, Johnstone HJH, Affrossman S, Curtis ASG Nonadhesive nanotopography: Fibroblast response to poly(*n*-butyl methacrylate)-poly(styrene) demixed surface features. J Biomed Mater Res A 2003;67:1025–1032.
31. Lim JY, Hansen JC, Siedlecki CA, Hengstebeck RW, Cheng J, Winograd N, Donahue HJ. Osteoblast adhesion on poly(L-lactic acid)/polystyrene demixed thin film blends: Effect of nanotopography, surface chemistry and wettability. Biomacromolecules 2005;6:3319–3327.
32. Ravenscroft MS, Bateman KE, Shaffer KM, Schessler HM, Jung DR, Schneider TW, Montgomery CB, Custer TL, Schaffner AE, Liu QY, Li YX, Barker JL, Hickman JJ. Developmental neurobiology implications from fabrication and analysis of hippocampal neuronal networks on patterned silane-modified surfaces. J Am Chem Soc 1998;120:12169–12177.
33. Zhang J, Venkataramani S, Xu H, Song YK, Song HK, Palmore GT, Fallon J, Nurmikko AV. Combined topographical and chemical micropatterns for templating neuronal networks. Biomaterials 2006;27:5734–5739.
34. Zhang Z, Yoo R, Wells M, Beebe TP Jr, Biran R, Tresco P. Neurite outgrowth on well-characterized surfaces: Preparation and characterization of chemically and spatially controlled fibronectin and RGD substrates with good bioactivity. Biomaterials 2005;26:47–61.
35. Venstrom KA, Reichardt LF. Extracellular matrix 2: Role of extracellular matrix molecules and their receptors in the nervous system. FASEB J 1993;7:996–1003.
36. Tawil N, Wilson P, Carbonetto S. Integrins in point contacts mediate cell spreading: Factors that regulate integrin accumulation in point contacts vs. focal contacts. J Cell Biol 1993; 120:261–271.
37. Banker G, Goslin K. Culturing Nerve Cells, 2nd ed. Cambridge, MA: MIT Press; 580 p.
38. Scofield JH. Hartree-Slater subshell photoionization cross-sections at 1254 and 1487 eV. J Electron Spectrosc 1976;8:129–137.
39. http://us.expasy.org/cgi-bin/protparam1?P07589@noft@
40. Paynter RW, Ratner BD. The study of interfacial proteins and biomolecules by X-ray photoelectron spectroscopy. In: Andrade JD, editor. Surface and Interfacial Aspects of Biomedical Polymers, Vol. 2: Protein Adsorption. New York: Plenum Press; 1985. p 189–216.
41. Ashley JC. Inelastic interactions of low-energy electrons with organic solids: Simple formulas for mean free paths and stopping powers. IEEE T Nucl Sci 1980;NS27:1454–1458.
42. Andrade JD. X-ray photoelectron spectroscopy (XPS). In: Andrade JD, editor. Surface and Interfacial Aspects of Biomedical Polymers, Vol. 1: Surface Chemistry and Physics. New York: Plenum Press; 1985. p 105–195.
43. Miller T, Boettiger D. Control of intracellular signaling by modulation of fibronectin conformation at the cell-materials interface. Langmuir 2003;19:1723–1729.
44. Dewez JL, Doren A, Schneider YJ, Rouxhet PG. Competitive adsorption of proteins: Key of the relationship between substratum surface properties and adhesion of epithelial cells. Biomaterials 1999;20:547–559.
45. Klebe RJ, Bentley KL, Schoen RC. Adhesive substrates for fibronectin. J Cell Physiol 1981;109:481–488.
46. Altankov G, Grinnell F, Groth T. Studies on the biocompatibility of materials: Fibroblast reorganization of substratum-bound fibronectin on surfaces varying in wettability. J Biomed Mater Res 1996;30:385–391.